School of Engineering and Science
Department of Electrical and Computer Engineering

Modeling and Simulation of Protective Relay for Short Circuits in AC Micro-grids using Fuzzy Logic

Aminu Maruf Asumo

This thesis is presented for the Degree of
Doctor of Philosophy
of

Curtin University

October 2016

DECLARATION

To the best of my knowledge and belief this thesis contains no material previously published by any other person except where due acknowledgment has been made.

This thesis contains no material which has been accepted for the award of any other degree or diploma in any university.

Signature:

Date: October 2016

ABSTRACT

The duo of high human appetite for electricity in the 21st century and high human population growth rate entail inadequacy of contemporary electric power protective systems for the emerging micro-grid. Proposed solutions reported in literature have not been adequate in overcoming some of the drawbacks of contemporary protective systems. This thesis presents results of a research which seeks to propose a new model of protective device for short circuits in ac micro-grids. An index test bed is developed using first principle and data-driven modeling in SimPowerSystems. The index test bed has *Type 3 wind turbines* using doubly-fed induction generators as micro-sources. It is capable of grid-connected and islanded modes of operation under voltage and reactive power control strategies. Short circuits are simulated and the test bed's response is validated. Using requisite equations and fuzzy logic, a multivariable relay is developed. The relay model is embedded in the index test bed and its response to short circuits is investigated and found reliable. Three alternative test beds are further developed and the proposed relay model is embedded in each. Response of the proposed relay to short circuits in each of the alternative test beds is further investigated and found satisfactory. Finally, the proposed relay model is further embedded in 24 (twenty-four) standard test beds, including The CERTs/AEP micro-grid test bed and The IEEE European Low Voltage Test Feeders. Response of the proposed relay in each of the standard test beds is consistent with a reliable protective system which overcomes the drawbacks associated with proposals reported in literature. Consequently, a protective relay for short circuits in ac micro-grids is proposed.

ACKNOWLEDGMENTS

The conception and commencement of this work without the contribution of Late Prof. Ravindra Mukerjee would have been daunting. His contribution is therefore highly appreciated. It is with delight that I recognize the contributions of Prof. Zhu Quan Zang, Dr. Lenin Gopal, Dr. Law Kah Haw and Prof. Marcus Lee for providing the impetus for the success of this work. Similarly, I thank Prof. Chinnasamy Palanichamy and Dr. Ahmed Abu-Siada for the role they played at the early stage of the project.

For the lean support offered me by the Faculty of Engineering and Science, I remain very grateful. I must appreciate my wife, Madinat, my sons, Adam and Saleem, for the enabling mind to endure the demand of this work and for the understanding without which this work would have been abortive.

Without its support which turned out to be partial, this study would probably not have been initiated. So, I thank the Tertiary Education Trust Fund of Nigeria.

TABLE OF CONTENTS

LIST OF FIGURES

LIST OF TABLES

GLOSSARY

AC	Alternating Current
AC/DC/AC	AC to DC to AC converter
AEP	American Electric Power
CB	Circuit Breaker
C-C	Cross-Country
CERTS	Consortium for Electric Reliability Technology Solutions
DC	Direct Current
DFIG	Doubly-Fed Induction Generator
DG	Distributed Generation
DSP	Digital Signal Processor
D-STATCOM	Distribution-level Static Compensator
FCL	Fault Current Limiter
FCS	Fault Current Source
FLC	Fuzzy Logic Controller
IDMT	Inverse Definite Minimum Time
IGBT	Insulated Gate Bipolar Transistor
K-map	Karnaugh map
L-G	Line-to-Ground
L-L	Line-to-Line
LVRT	Low Voltage Ride-Through
MFR	Multivariable Fuzzy Rule-based
MF	Membership Function
MGCC	Micro-Grid Control Center
MS1	Micro-source 1
MS2	Micro-source 2
PCC	Point of Common Coupling
PI	Proportional-Integral
PLC	Power Line Carrier
PQ	Active-Reactive power
PSM	Plug Setting Multiplier
PV	Active Power-Voltage
Q control	Reactive Power Control
RC4S	Reliable, Cost-effective, Sensitive, Selective, Speedy and Safe
SC	Short Circuit
SSFCL	Solid-State Fault Current Limiter
STATCOM	Static Compensator
TDS	Time Dial Setting
UFCL	Unidirectional Fault Current Limiter
V control	Voltage Control
VSI	Voltage-Sourced Inverter
WT3	Type 3 Wind Turbine

NOMENCLATURES

LVRT = Low Voltage Ride-Through

$\rightarrow$ = Steady

$\uparrow_V$ = Rise under V control

$\uparrow_Q$ = Rise under Q control

$\downarrow\sim$= Drop with oscillation

$\uparrow\sim$= Rise with oscillation

Chapter 1: Introduction

1.1 Research Motivations

When humans commenced farming in 8000 B.C., human population was only 5 million. In 2016 (2000 years after Christ), human population is estimated at 7.4 billion. It is estimated that human population would hit 10 billion in year 2050 [1]. In 10,000 years, human population grew from 5 million to 7.4 billion, forming average population growth ratio of 1480. In the history of humans, the 21st century human has the highest appetite for electricity, as marked by the increasing electrification of many human activities, such as medical electrification and transportation electrification. The duo of high human population and high appetite for electricity push operation of existing power system beyond its nominal boundaries. As a result, the emerging power system cannot guarantee quality protection, particularly when power flow inevitably becomes bidirectional in the emerging power system (micro-grid) [2, 3].

A micro-grid is a robust distributed generation (DG) system which mainly seeks to provide quality, reliable and sustainable power to a load center. It is a building block of smart grid which necessarily operates using advanced control architecture and quality protection, but may include energy storage system and runs autonomously or in grid-connected mode [4-6]. While the benefits, topology and control of micro-grids are well established, a proper design of protection scheme remains a challenging area due to the nature of the DG micro-sources within the grid that may be of two-way power flow such as energy storage or plug-in electric vehicles [7-9]. The change of DG micro-source between passive and active modes which results in loss of radial nature of the distribution system requires a new evaluation for relay settings and coordination. This comes with a number of challenges on over-current protective devices, including blinding of protection, false tripping, loss of fuse-recloser coordination, non-synchronized reclosing and disabling of automatic reclosing [10-13].

While the proposed protective schemes in literature provide partial solutions to the mentioned challenges associated with overcurrent devices, they fail to meet some requirements of micro-grid protection. Although *current differential* does not exhibit same drawbacks of overcurrent devices, its implementation calls for a sophisticated communication architecture, making it vulnerable to communication failures in addition to failing to satisfy the plug-and-play requirement of micro-grid [14-16]. Dewadasa et al. [17] proposed a current differential which is capable of providing protection for the micro-grid in both islanded and grid-connected modes. However, this scheme requires communication link which makes it less reliable especially when

the number of DGs increases. While the emerging smart grids are communication-intensive in operation, it is expected that only non-critical operations will be driven by communication architecture. This is because systems that are based entirely on technologies such as wired and wireless communication are less reliable due to failure of communication links in the case of wired communication and transient obstructions in line-of-sight in the case of terrestrial wireless communication. Non-terrestrial communication systems are usually more expensive to develop. Also, because communication-based micro-grids have relatively high vulnerability to failure, they often require back-up protocols to improve their reliability [18]. This increases development and maintenance costs. The bandwidth requirement of communication-assisted micro-grids or smart grids results in high running cost of such systems. This increased cost translates to relatively high cost of electrical energy generated from such communication-assisted power infrastructure [19]. While use of external devices does not suffer from overcurrent drawbacks, it potentially compromises the safety of the system and personnel during short circuit. The proposed fault current limiter (FCL) by Ustun et al. [20] requires communication link and thereby vulnerable to link failure. It also suffers from unreliable magnitude of FCL impedance value due to the changes in impedance as a result of proliferation of DG connection to the distribution network. This is in addition to the error introduced by the transient response of the added FCL impedance. Thus, full deployment of micro-grids makes it necessary to have a new, reliable and cost-effective protective device which does not suffer from the drawbacks of overcurrent and other protective schemes reported in literature [14, 21, 22].

In 2011, Y. L. Goh et al. [23] proposed a Digital Signal Processor-based over-current relay using fuzzy logic. The proposed relay is developed for medium-voltage distribution feeder of 11kV. The relay is simple and cost-effective, since it uses inexpensive solid state devices for implementation. It also satisfies the peer-to-peer requirement of micro-grid. However, one of its major deficiencies is the fact that it is a component-based protective system. Operation of the micro-grid requires system-wide protection in order to ensure reliable, cost-effective, speedy, selective and sensitive operation in addition to component-based protection provided by existing systems.

Another major drawback with the protective schemes in literature is that they have been investigated without simulating the effect of control on the micro-grid during short circuit. Control strategy is critical for reliable operation of a power system. When the micro-grid is grid-connected, its control is dictated by the utility. However, when it is islanded, its control is determined by a number of variables including net capacity and type of micro-sources, available energy storage capacity, load type and ownership [24]. Control strategy affects the values of

system's primary and derived parameters which are used for measurement. In practice therefore, governing control strategy determines the response of protective devices and hence their reliability under short circuit condition in micro-grids.

From the simulation results of this study and as published in [25], it is obvious that in a micro-grid capable of grid-connection, the difference between normal operating parameters and abnormal operating parameters is not crisp. Typically, a short circuit current magnitude in a grid-connected micro-grid could be so small that it is a normal condition in the utility and the utility protection becomes blinded [26]. On the other hand, a utility short circuit could be a normal operating condition in a grid-connected micro-grid due to the limiting effect of the converters in the micro-grid. This lack of clear separation of normal and abnormal operating boundaries in a micro-grid capable of utility connection is better described using fuzzy logic theory. Therefore, variation of the critical parameters to short circuits under different conditions (islanded or grid-connected, voltage or reactive power control) is not crisp but fuzzy. This fuzziness in the boundaries of these parameters challenges use of existing protection such as over-current devices as published by Ustun et al. in [20].

Consequently, safe and reliable operation of the micro-grid necessitates proposing new protective system which overcomes the drawbacks associated with the proposals in literature. It is necessary that the proposal is investigated and operates satisfactorily under various control strategies, facilitates the plug-and-play requirement and meets the peer-to-peer requirement of micro-grid protection. Such system is the multivariable fuzzy rule-based (MFR) protective relay developed and proposed in this report. Its implementation does not require communication protocol (this makes it satisfy the peer-to-peer requirement). Also, it is simple, cost-effective and its operation is devoid of external devices. Thus, the MFR protective relay presented in this report does not suffer from the drawbacks associated with use of over-current devices in micro-grid as well as drawbacks associated with other proposals in literature. Finally, it has been investigated under voltage and reactive power control strategies and it facilitates the plug-and-play requirement of micro-grid protection. Through extensive simulation of the rules which engage the critical parameters of micro-grids and utility, this report therefore presents a new relay based on fuzzy combination of multiple input variables.

1.2 Research Objectives

The fulcrum of this research is protection of micro-grid in islanded and grid-connected modes via control strategies. The research objectives are:

a. To perform modeling and simulation of a micro-grid and then investigate its steady-state and dynamic behaviors in grid-connected and islanded modes under various control strategies.
b. To perform stability and small signal analyses of a micro-grid in grid-connected and islanded modes under various control strategies with different short circuit conditions such as single line-to-ground, double line-to-ground, three phase-to-ground, line-to-line, and cross-country short circuit.
c. To propose a new protective device devoid of differential relaying, telecommunication links, fault current source and other deficiencies associated with existing proposals for micro-grids using low-cost combinational components. The hardware implementation of this device is realized using software, i.e. SimPowerSystems®.
d. Proposing a new protection scheme based on the new device and evaluating its effectiveness under different control regimes such as constant PQ, constant V, both under islanded and grid-connected operations.

1.3 Research Methodology

Fig. 1.1 presents a pseudo flow chart which summarizes the major activities carried out in this research. An RC4S device is defined as a Reliable, Cost-effective, Sensitive, Selective, Speedy and Safe system. The diagram also depicts the methods and order of these activities.

The research is split into three phases, namely; project conception, project implementation, and critical analysis and documentation. In project conception phase, literature review is carried out to identify research gap and conceive a tentative research methodology via test bed development and comparative evaluation of computer software. In this phase PSCAD, MATLAB and Simulink (SimPowerSystems, Control Design, PID Tuner, Fuzzy Logic Toolbox), PSSE (NEVA and GMB) and PowerWorld are used to develop the index test bed for a micro-grid capable of grid-connection and islanding. After comparative evaluation of the software, a decision is taken to undertake the project in MATLAB and its auxiliaries. This brings the project to the end of first phase.

The second phase is the project implementation where the test bed is enhanced in SimPowerSystems, time series objects are constructed in MATLAB, small signal analyses are performed using Simulink Control Designer, controllers are designed using PID Tuner and dynamic short circuit analyses are performed in SimPowerSystems as technical validation of the test bed. Two mutually exclusive control strategies are implemented – the active power-voltage (PV or V) control and the active-reactive power (PQ or Q) control. When the micro-grid is

operated in V control, the voltage controller keeps the grid voltage constant with a 4% droop. When it is operated in Q control, the var controller keeps the reactive power at the grid constant by injecting or absorbing reactive power.

Then, the logical rules governing the critical parameters are framed, and the proposed protective relay is implemented using Fuzzy Logic Toolbox. Offline tests are then performed on the new relay to validate adequacy of the framed fuzzy rules. The proposed relay is then embedded in the test bed to evaluate its feasibility. The new relay is then embedded in three alternative test beds to review its wider applicability. The proposed relay is further embedded in each of 24 standard test beds for further evaluation. The standard test beds include the CERTS/AEP Test Bed and The IEEE European Low Voltage Test Feeders. The CERTS/AEP micro-grid test bed sought to enhance micro-sources into a micro-grid. In collaboration with AEP the project accomplished this objective through development and demonstration of three advanced techniques called the CERTS micro-grid concepts. The techniques are: (1) a method for effecting automatic and seamless transitions between grid-connected and islanded modes of operation; (2) a scheme of protection within the micro-grid that is devoid of high fault current; and (3) a method for micro-grid control which seeks to achieve voltage and frequency control in islanded mode without use of high-speed communication. The techniques were demonstrated at a full-scale test bed built near Columbus, Ohio and operated by AEP. Other participants in the project included University of Wisconsin-Madison, Sandia National Laboratories, Woodward, Princeton Power Systems, Northern Power Systems, Tecogen, and Lawrence Berkeley National Laboratory. The demonstration was sponsored by the California Energy Commission.

Upon establishing satisfactory response of the proposed relay, further literature review is performed to keep the project abreast of the state-of-the-art by other researchers in related discipline. This brings the project to the end of the second phase.

Upon completion of this phase, the research proceeds to the critical analysis and documentation phase for thesis production. In this phase, further literature review is performed and the thesis is developed. In each of the three phases of the project, literature is reviewed to keep up with recent proposals and contributions in related fields. The major merit of this method over those reported in literature is that it results in cost-effective protective device with a potential to operate reliably and safely without use of communication link. This is in addition to the fact that proposed relay is evaluated under two control strategies, since protection cannot be isolated from control in practical micro-grids.

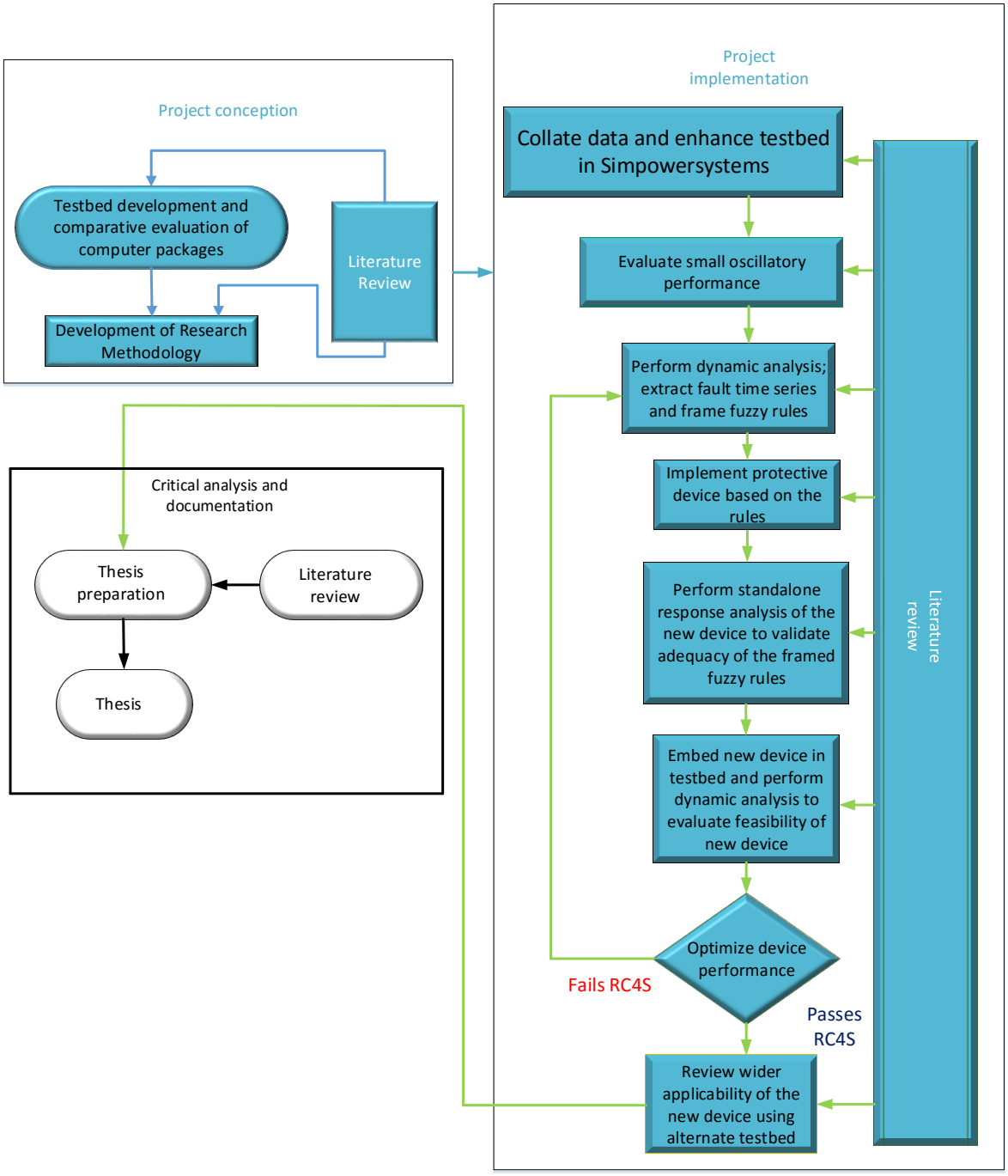

Fig. 1.1. A summary of research activities

1.4 Report Outline

This report is presented in seven chapters:

- Chapter 2 (Literature Review) presents survey of published literary materials which have proposed solutions to solving the problem of inadequacy of contemporary protective devices for the micro-grid. The review is presented on the basis of the fundamental working principles of the various proposals reported in literature. The chapter also discusses the main strengths and weaknesses associated with each proposal.

- Chapter 3 (Machine Modeling and Design of Control Systems) presents first principle modeling of the various components which constitute the utility and the micro-grid. The mathematical equations which describe the physical properties of these components are used to model both the steady-state and dynamic behaviors of the components. It also covers design of active power, reactive power, voltage and current management systems for a converter-interfaced ac micro-grid using data-driven modeling.

- Chapter 4 (Short Circuit Dynamic Analysis in Grid-connected Mode) presents grid-connected short circuit dynamic analysis of the test bed developed in the previous chapter. The short circuits simulated are single line-to-ground, line-to-line, three phase and three phase cross-country at requisite element (generator, transformer, micro-source and feeder).

- Chapter 5 (Short Circuit Dynamic Analysis in Islanded Mode) presents dynamic short circuit analysis of the test bed as a technical validation in islanded mode. While the micro-grid is islanded by disconnecting the Point of Common Coupling (PCC), single line-to-ground short circuit, line-to-line short circuit, three phase short circuit and three phase cross-country short circuit are applied to the micro-grid and the response of the network is investigated and presented in this chapter.

- Chapter 6 (Proposed Micro-Grid Protection) presents the new multivariable fuzzy rule-based relay (MFR) for short circuits in ac micro-grids. Using requisite equations, the rules which govern the interaction of four parameters in the system are framed. Using the framed rules, fuzzy logic controllers are designed for micro-source and feeder sub-relays. Offline and online response tests of the relay show that it provides reliable detection and

protection of the micro-grid against different short circuits in both islanded and grid-connected modes under both control regimes.

- Chapter 7 (Summary and Conclusion) presents main conclusion of the research and some activities necessary to complement this work and to establish reliability of the proposed relay. The contribution of the research to existing literature in related field has also been highlighted.

1.5 Conclusion

In conclusion, this chapter introduces the report on a new protective relay for short circuits in ac micro-grids. The motivations for embarking on the study as well as its objectives have been presented. The methodology of the study and at-a-glance outline of this chapter have also been articulated in this chapter. In order to pluck out the gap in contemporary literature and to keep pace with developments with respect to protective devices for micro-grids, a literary review has been undertaken and presented in the succeeding chapter.

Chapter 2: Literature Review

This chapter presents a survey of published literary materials which have proposed solutions to solving the problem of inadequacy of contemporary protective devices for the micro-grid. The review is presented on the basis of the fundamental working principles of the various proposals reported in literature. The working principles are based on measurement and requisite combination of primary quantities (such as current) and derived quantities (such as impedance), as depicted in Fig. 2.1. The chapter also discusses the main strengths and weaknesses associated with each proposal within the framework of its class of devices based on its evaluation by the author of this report.

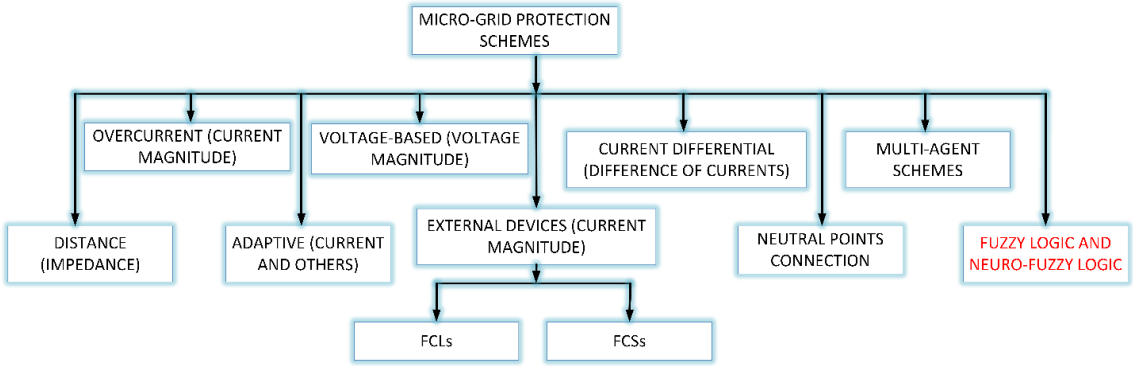

Fig. 2.1. Overview of proposed protective schemes for micro-grids based on operational principles

In a micro-grid capable of grid-connection, the difference between normal operating parameters and abnormal operating parameters is not crisp. Typically, a short circuit current magnitude in a grid-connected micro-grid could be so small that it is a normal condition in the utility and the utility protection becomes blinded [27]. On the other hand, a utility short circuit could be a normal operating condition in a grid-connected micro-grid due to the limiting effect of the converters in the micro-grid. This lack of clear separation of normal and abnormal operating boundaries in a micro-grid capable of utility connection is better described using fuzzy logic theory. Therefore, variation of the critical parameters to short circuit under different conditions (islanded or grid-connected, V or Q control) is not crisp but fuzzy. This fuzziness in the boundaries of these parameters challenges use of existing protection such as overcurrent devices as published by Ustun et al. in [20].

2.1 Overcurrent Protection Schemes

Proposals for micro-grid protection based on current magnitudes evolved from the well-established overcurrent protection in the utility industry [28]. Such proposals attempt to solve the problem of relay blinding caused by increased penetration of power converter-interfaced micro-sources in grid-connected mode by making modified measurement of current magnitude or by adding measurement of other quantities to improve device's reliability. A typical example is the approach proposed by Nikkhajoei and Lasseter [29, 30] in 2006. Their proposed technique is based on measurement of zero and negative sequence quantities to distinguish between line-to-ground and line-to-line faults respectively. The advantage of this proposal is that it provides detection and protection against balanced and unbalanced short circuit faults. However, it suffers from the drawbacks of overcurrent devices such as blinding and sympathetic (false) tripping of protection. In 2008, Best et al. [31] implemented a 3-stage selectivity scheme. In their technique, stage 1 detects the fault event in accordance with local measurements; stage 2 deploys inter-breaker communication; and stage 3 adapts relay settings via a supervisory controller. The major merit of this technique in comparison with the proposal by Nikkhajoei and Lasseter [29, 30] is that it does not suffer from drawbacks associated with use of overcurrent devices. However, its implementation is expensive and its operation is vulnerable to communication failure.

In 2012, Zamani et al. [32] developed a novel protection scheme using microprocessor-based relays for low-voltage micro-grids protection against types of faults in both grid-connected and islanded modes of operation. Its operation is based on definite-time grading of all relays within the micro-grid, requiring use of communication links.

These proposals based on overcurrent protection suffer from either blinding or vulnerability to communication failures, rendering them unreliable. The major strength of the proposals based on measurement of current magnitude is that they are effective for both short-circuit and high impedance faults. The major weaknesses associated with these proposals include blinding of protection, false tripping, loss of fuse-recloser coordination, non-synchronized reclosing and disabling of automatic reclosing [10-13].

2.2 Voltage-based Protection Schemes

Voltage-based protection schemes basically employ voltage measurements in protecting the micro-grids against different kinds of faults. In 2006, Al-Nasseri et al. [33] proposed a scheme that could monitor and transform output voltages of micro-sources into dc quantities using the *dq* reference frame such that the scheme could be employed in protecting the micro-grids against both in-zone and out-of-zone faults. A major strength of this method is that it is able to detect both

balanced and unbalanced faults using minimal resources. However, its operation measures only output voltage of the micro-sources thereby limiting it to only the low current faults which occur within the micro-grid in islanded mode. This implies it is unable to detect utility faults when the micro-grid is grid-connected and is thereby only complementary to the utility protective system which detects high current faults.

In 2009, a novel protection scheme was proposed by Loix et al. [34]. The scheme is based on the effect of different fault types on Park's components of voltage and it is capable of protecting micro-grids against three phase, two phase and one phase-to-earth faults. Its primary operation is independent of communication links, but requires communication links for optimal protection. The most prominent feature of this scheme compared to the one proposed by Al-Nasseri et al. is its versatility – it could be used in the protection of micro-grids of various configurations. Its major improvement over proposals based on current magnitudes (overcurrent devices) is that it does not suffer from blinding effect and other drawbacks of overcurrent devices. It is also effective for in-zone and out-of-zone faults. However, since its optimal operation requires communication link, it is vulnerable to communication failure in addition to being expensive to implement and maintain.

2.3 Current Differential Protection Schemes

A form of protection for apparatus such as transformers, generators, busses and power lines and feeders is current differential. A differential relay works on the basic theory of Kirchhoff's current law, which states that the sum of the currents entering and exiting a node equals zero [35]. It operates only when the differential between these currents exceeds a pre-determined magnitude. A major strength of this scheme is its insensitivity to bidirectional power flows and reduction in fault current magnitudes in islanded micro-grids.

In 2006, Nikkhajoei and Lasseter [30] proposed a dual technique scheme for micro-grid protection by differential protection and symmetrical components calculations. They employed zero sequence and negative sequence currents within the micro-grid to detect single line-to-ground and line-to-line faults, respectively. This proposal helps provide protection for the micro-grid in grid-connected and islanded modes. However, it is unable to provide protection for balanced short circuit fault since it employs only zero- and negative-sequence components for measurement.

In 2006, Zeineldin et al. [36] published a paper on the micro-grids future and were concerned on two major challenges, voltage/frequency control and protection. Consequently, they proposed a scheme where they had employed differential relays in both ends of each line. These relays which

were designed to operate in 50ms were capable of protecting the micro-grid in islanded mode of operation. This proposal provides protection for balanced and unbalanced short circuit fault. However, its operation is limited to islanded mode of operation, expensive to implement and maintain.

In 2009, Conti et al. [37] detailed out a scheme based on three protection strategies in detection of multi-phase and phase-to-ground faults in isolated micro-grids. This proposal protects the micro-grid from balanced and unbalanced faults using minimal components which makes it cost-effective. However, its operation is limited to islanded mode of the micro-grid. This leads to emergency islanding in the event of utility fault if the micro-grid is grid-connected during the fault. Emergency islanding portends unnecessary load-shedding if the micro-grid imports power from the utility to meet its local demand and lacks expensive energy storage for long-term operation. The consequence of this is a potential to compromise the primary purpose of the micro-grid which is to enhance reliability and resilience of the distribution network in order to minimize service disruption.

In 2010, Sortomme et al. [38] proposed a novel protection scheme based on the principle of synchronized phasor measurements and microprocessor relays in order to recognize all kinds of faults including high impedance faults. They showed that installing the relays at the end of each micro-grid line will provide a robust protection. This is a significant contribution since it is able to protect the micro-grid from both high- and low-impedance faults under balanced and unbalanced conditions, for both grid-connected and islanded modes of operation. However, it is capital-intensive to implement and maintain, and vulnerable to communication failures.

In 2010, Parsai et al. [39] proposed a communication-based scheme called power line carrier (PLC) with multiple levels of protection offering effective protection for meshed micro-grids. It is a significant contribution over devices in its class since it provides multi-layer protection for meshed micro-grid. This is considering the change in natively radial nature of distribution network due to increased penetration of distributed generators. However, its operation relies on communication protocol, decreasing its reliability due to heightened vulnerability to failure. This is in addition to its high implementation and maintenance costs.

In 2011, a novel scheme was proposed by Dewadasa et al. [40] using differential protection. This scheme takes into account all the protection challenges such as bidirectional power flow and reduction of fault current level in the islanded operation mode and it is capable of protecting the micro-grids in both grid-connected and islanded modes of operation. A major contribution of this scheme is that it could potentially satisfactorily protect feeders and micro-sources within the

micro-grid. However, it is very expensive to implement and vulnerable to communication failures. It is also prone to failures as a result of increased penetration of distributed generators.

2.4 Distance (Impedance) Protection Schemes

A distance relay (also called impedance relay) differs in principle from other forms of protection because its performance is not governed by the magnitude of the current or voltage in the protected circuit but rather on the ratio of these two quantities. Such relays are actually double actuating quantity relays with one coil energized by voltage and other coil by current. The current element produces a positive or pick up torque while the voltage element produces a negative or reset torque. The relay operates only when the V/I (impedance) ratio falls below a predetermined value (or set value). In 2008, Celli et al. [41] proposed a distance relay scheme to detect grounded faults in distribution systems with high penetration of distributed generation. This method uses wavelet coefficients of the transient fault current at critical points of the network. The scheme works without communication link or synchronized measures. However, if link is used to permit communication among the relays, the scheme could be used to satisfactorily protect the network against ungrounded faults. An obvious strength of this technique is that its operation is not entirely dependent on communication protocol but could be enhanced with communication protocol. However, its operation is vulnerable to measurement error because intermediate in-feed of micro-sources has impact on the measurement of the fault impedance.

2.5 Adaptive Protection Schemes

Adaptive protection scheme could solve problems arising from both modes of grid-connected and islanded operations. In adaptive protection, automatic readjustment of relay settings triggers when the micro-grid changes from the grid-connected mode to the islanded mode or vice versa [42]. It is an online system that could modify the preferred protective response to change under system conditions or requirements in a timely manner using signals or control actions that are generated externally.

In 2006, Tumilty et al. [43] suggested an adaptive protection scheme without the requirement of a communication system. They used a voltage based fault detection method in discriminating the voltage drop in short-circuit incidents and over-load events. The proposal is capable of protecting the micro-grid from balanced and unbalanced faults. It is also devoid of use of communication protocol and therefore potentially cost-effective. Though it is capable of adapting to load changes, its operation is limited to islanded mode of operation and it requires reconfiguration as penetration of micro-sources increases. Another drawback is the fact that adaptation is not instantaneous and

the time delay is sufficient to cause severe consequences in power converter-interfaced micro-grids, since in such micro-grids the fault envelop is short-lived.

In 2009, Oudalov and Fidigatti [44] proposed a novel adaptive micro-grid scheme using digital relaying and advanced communication. The system is based on a centralized architecture which determines the micro-grid state and adapts protection settings accordingly. Its major strength is the fact that it adapts to network changes, in both grid-connected and islanded modes. It also provides protection for balanced and unbalanced faults. However, because it uses a micro-grid control center (MGCC), its reliability is relatively low since the MGCC is a single master failure point. In addition, its requirement for advanced communication protocol makes it capital-intensive to implement and maintain.

In 2011, Dang et al. [45] employed energy storage system and isolation transformers to detect the operating mode of micro-grid. Therefore, identification of the fault could be executed by comparing between the zero sequence current and a pre-determined value. This proposal does not require communication protocol, making it cost-effective. Also, it protects the micro-grid from balanced and unbalanced faults in grid-connected and islanded modes. However, adaptation is not instantaneous and slow adjustment of settings portends severe damage to equipment and harm to personnel.

In 2012, Khederzadeh [46] published a proposal in which the potential of the numerical relays was efficiently used to protect the micro-grids. In this scheme, settings of the relays are adapted to the status of the micro-grid in grid-connected and islanded operating modes. Its major strengths include capability to operate in grid-connected and islanded modes and protection of the micro-grid from balanced and unbalanced faults. However, its operation relies on communication link which makes it vulnerable to link failure. This also makes its implementation and maintenance capital-intensive. Most importantly, it does not facilitate the plug-and-play and peer-to-peer requirements of micro-grid protection.

In 2016, Lien et al. [47] proposed an adaptive fault protection system using communication-assisted digital relays for ac micro-grids having multiple grounding system. The proposed scheme has two parts, one part provides protection for the micro-grid in islanded mode while the other provides protection for the micro-grid in grid-connected mode of operation. The grid-connected protection is based on existing conventional protective devices but supported by communication system. The proposed islanded mode protection scheme is based on a fast-dependable-adaptable module. The module includes combination of under/over voltage relay, under/over frequency relay and instantaneous and time-delay over-current relays. These relays are well established in the contemporary protection schemes. The proposed protection scheme is able to provide reliable

protection for the micro-grid in both modes and for both balanced and unbalanced faults. However, it is defective since it does not satisfy the plug-and-play and peer-to-peer requirements of micro-grids. Because it fails the peer-to-peer requirement, it is capital intensive to maintain and unreliable. It is further unreliable since settings adaptation is not instantaneous.

2.6 Protection Schemes Driven by External Devices

The main challenge faced in micro-grid protection is associated with the huge difference between the fault current levels in the grid-connected and islanded modes of operation [48]. Consequently, it becomes challenging to implement an adequate protection scheme which is able to operate suitably in both grid-connected and islanded modes. Some approaches in literature propose a modification of the short-circuit level when the micro-grid operating mode changes from grid-connected to islanded, or vice versa. These devices can be classified into fault current limiters and fault current sources, as presented in the next subsection.

2.6.1 Fault current limiters (FCLs)

FCLs are employed to reduce the aggregated contribution of all micro-sources, and it is capable of adequately reducing the short circuit current level to a predetermined value on the onset of short circuit fault. In 2011, Ustun et al. [49] proposed a conceptual design of a micro-grid protection scheme using current limiters in fault current estimation. The strengths of this proposal include the fact that it does not suffer from drawbacks associated with use of over current protection and it protects the micro-grid in both grid-connected and islanded modes. However, the proposed scheme requires communication link to monitor the micro-grid and update relay fault currents according to the variations in the system. It is designed such that it responds to dynamic changes in the system such as connection or disconnection of micro-sources. It is therefore susceptible to link failure. It also suffers from unreliable magnitude of FCL impedance value due to the changes in impedance as a result of proliferation of micro-source connection to the distribution network. In addition, it is vulnerable to the error introduced by the transient response of the added FCL impedance.

In 2012, Ghanbari and Farjah [50] proposed a novel FCL scheme using resonant type solid-state fault current limiter (SSFCL) which exhibits very low impedance through a series resonant circuit under normal condition. Under fault condition, the fault current limiter offers a very high impedance through a parallel resonant circuit.

In 2013, Ghanbari and Farjah [51] proposed a unidirectional fault current limiter (UFCL). The proposed UFCL is installed between the upstream and downstream network, such that it only limits the current contribution of the downstream network during a fault in the upstream.

Inversely, during a fault in downstream, the UFCL is inactive and allows a full contribution of the upstream network. It was shown that by this strategy, the proposed UFCL can preserve the coordination protection of the upstream overcurrent relays. These two proposals by Ghanbari and Farjah provide protection for the micro-grid in both grid-connected and islanded modes. Its operation can be enhanced with communication link. However, as a result of proliferation of micro-source connection to the distribution network, it suffers from unreliable magnitude of FCL impedance value due to the changes in impedance. In addition, it is susceptible to the error introduced by the dynamic response of the added FCL impedance.

2.6.2 Fault current sources (FCSs)

The short circuit current level in the micro-grid is limited to approximately 2-3 times of the rated current because of the existence of converter-based micro-sources. Fault current sources in the form of energy storage devices (flywheels or batteries) can be used to provide supplementary short-circuit level to the network [48]. In 2013, Oudalov et al. [13] proposed a FCS for micro-grid protection. During normal operation, the FCS power circuit remains idle. Upon fault occurrence, the network voltage drops, activating the FCS. The FCS attempts to restore the original network voltage by injecting a fault current into the network. The injected fault current is sufficiently high to trigger overcurrent relay trip logic, energizing a circuit breaker. This proposal provides adequate protection for the micro-grid in both grid-connected and islanded modes. It also does not suffer from the drawbacks associated with traditional use of overcurrent devices such as blinding and sympathetic (false) tripping. However, it is expensive to implement, maintain and could be counter-productive since the injected short circuit current could be sufficiently high to harm the micro-grid's components and working personnel.

While the proposals articulated provide partial solution such as overcoming the drawbacks associated with use of overcurrent devices and protection for the micro-grid in grid-connected and islanded modes of operation, they do not provide full solution. This is because some of them are based on methods where main operation is based on vulnerable communication protocols while others are potentially harmful to the system and personnel. Also, they do not facilitate the plug-and-play requirement of micro-grid protective system. Another major drawback with the protective schemes in literature is that they have been investigated without simulating the effect of control on the micro-grid during fault. Control strategy is critical for reliable operation of a power system. When the micro-grid is grid-connected, its control is dictated by the utility. However, when it is islanded, its control is determined by a number of variables including net capacity and type of micro-sources, available energy storage capacity, load type and ownership.

Control strategy affects the values of system's primary and derived parameters which are used for measurement. Therefore, governing control strategy determines the response of protective devices and hence their accuracy under fault condition in practical micro-grid.

Consequently, safe and reliable operation of the micro-grid necessitates proposing new protective system which overcomes the drawbacks associated with the proposals in literature. It is necessary that the proposal is investigated and operated satisfactorily under various control strategies, facilitates the plug-and-play requirement and meets the peer-to-peer requirement of micro-grid protection. The multivariable fuzzy rule-based protective relay presented in this report does not suffer from the drawbacks associated with use of overcurrent in micro-grid as well as drawbacks associated with other proposals in literature. Its implementation does not require communication protocol (this makes it satisfy the peer-to-peer requirement), it is simple, cost-effective and is devoid of external devices. Finally, it has been investigated under voltage and reactive power control strategies and it facilitates the plug-and-play requirement of micro-grid protection.

2.7 Protection Based on Multi-agent Schemes

In 2016, Hussain et al. [52] proposed an N-version programming-based protection scheme for micro-grids using multi-agent approach. The scheme was developed in MATLAB Simulink with three protection versions namely, Clarke's transformation-based current protection, positive sequence phase differential-based protection and conventional over-current-based protection. In their proposal, the software makes the final decision about the fault and which of the three protection versions to activate through a polling process. The polling process relies on a truth table and a K-map for voting and making of decision. Their proposal is applicable to both balanced and unbalanced faults in both modes of operation. However, its drawbacks include its reliance on inter-agent communication which makes the system vulnerable to communication failure and highly expensive to operate. In addition, the entire proposal is capital intensive since it uses three different hardware for fault detection and fault clearance. It includes two non-over-current networks in addition to the over-current protection found in conventional schemes, this results in over-redundancy of hardware and increased failure points.

2.8 Protection Based on Neutral Points Connection

In 2016, Kamel, Alsaffar and Habib [53] proposed a simple and novel protection scheme for islanded micro-grids. Their proposal simply increases the magnitude of fault current in islanded mode of operation such that the fault current from the inverter is sufficiently large and sustained for detection using conventional over-current devices for protection. The proposed scheme

achieves this by connecting the neutral points of all micro-grid loads to the neutral line of the micro-grid's earth. By providing a path of least resistance, this increases the short circuit current during short circuit fault. The proposed scheme is simple, cost-effective and reliable. It also satisfies the peer-to-peer requirement of micro-grid. However, it fails the plug-and-play requirement of micro-grid. Its applicability is also limited to micro-grids in islanded mode of operation. For a micro-grid that is capable of grid connection, the proposed scheme is unreliable and inappropriate. This is because, under utility short circuit the proposed protection could become counter-productive and hazardous to other equipment and personnel when subjected to utility short circuit MVA.

2.9 Protection Based on Fuzzy Logic and Neuro-Fuzzy Logic

In 1997, Abyane, Faez and Karegar [54] proposed a new method for determining and improving the Time Dial Setting (TDS) and operating time of an overcurrent relay. The proposed method uses neural network and fuzzy logic. The improved TDS is found using a full "counterpropagation" neural network while the improved operating time is found using fuzzy logic. The inputs to the fuzzy logic processor are TDS, Plug Setting Multiplier (PSM) and the existing overcurrent relay characteristic. The proposed method simply improves the operating time of the test relay. The proposal does not propose a new relay suitable for micro-grid application.

In 2004, Erenturk and Altas [55] proposed an over-current relay for fault identification in a radial power system using fuzzy logic. The proposed protective relay is based on measurement of rms current magnitude of each phase in a three phase power system and measurement of bus voltages. The bus voltages are used for distinguishing between normal and abnormal operating conditions of the power system. The sum of the current in the three phases is also obtained and used for neutral based faults. The proposed relay is used to identify both balanced and unbalanced faults. The rms values of current are utilized to form inputs to the proposed fuzzy processor. The fuzzy processor fuzzifies its inputs, produces inference based on its rule set and de-fuzzifies the inference to produce crisp output for fault identification. The fuzzy processor is based on 11 "If-Then" rules. Its de-fuzzification is based on the Center of Area method proposed by mamdani. The proposed relay is simple, inexpensive and satisfies the peer-to-peer requirement of micro-grid. It is also suitable for both balanced and unbalanced faults in a radial feeder. However, its applicability is limited to only fault detection without ability to make a relaying decision to clear the fault by isolating faulted circuit. It also fails to satisfy the plug-and-play requirement of micro-grid.

In 2011, Goh et al. [23] proposed a Digital Signal Processor-based over-current relay using fuzzy logic. The Digital Signal Processor (DSP) is used to handle computation and generation of data in real time. The DSP is implemented using the Texas Instrument's TMS320F2812 microprocessor. The relay is based on measurement of current and voltage, though called over-current relay. The naming follows the fact that primary protection is based on current magnitude measurement while voltage measurement is added to improve the performance of the current element. The characteristics of the current element of the relay is based on the Inverse Definite Minimum Time (IDMT) curve so that the element's response to short circuit is inversely proportional to the magnitude of short circuit current. The inputs to the Fuzzy Logic Controller (FLC) are the ratio of currents and voltages. The ratio of currents and voltages are fuzzified according to a set of membership functions. There are three linguistic characteristics for current ratio and four linguistic characteristics for voltage ratio. The inputs consist of triangular and trapezoidal membership functions. The membership function for the current ratio is between 0 and 6, while that of voltage is between 0 and 1.2. After fuzzification the fuzzified values are matched to their controllers. The controller outputs are de-fuzzified, obtaining the crisp values which represent the operation time for the over-current relay.

The proposed relay is developed for medium-voltage distribution feeder of 11kV. The relay is simple and cost-effective, since it uses inexpensive solid state devices for implementation. It also satisfies the peer-to-peer requirement of micro-grid. However, one of its major deficiencies is the fact that it is a component-based protective system. Operation of the micro-grid requires system-wide protection in order to ensure reliable, cost-effective, speedy, selective and sensitive operation in addition to component-based protection provided by existing systems. The proposed relay cannot be used to provide protection for micro-sources which are requisite sub-systems of micro-grids. The proposed relay is essentially a modification of existing protection and it fails to satisfy the plug-and-play requirement of micro-grids, since addition of micro-sources entails reconfiguration of the proposed relay.

2.10 Conclusion

In conclusion, a review of reported literature has been discussed in this chapter. The proposed methods of micro-grid protection have been thoroughly diagnosed within the framework of class of protection such that each class is presented on the basis of fundamental operating principles. A total of 9 (nine) major classes have been discussed. The crucial merits and demerits associated with each proposal have also been highlighted. The inadequacies in existing proposals necessitate

a new proposal which satisfies the requirements of protective systems for micro-grids, justifying the motivation to undertake this research.

The index test bed used for this study has been developed using a combination of first principle and data-driven modeling. In order to establish the response and stability of the test bed, small-signal analysis and design of closed-loop feedback regulators have been performed. The succeeding chapter presents modeling of the machines in the test bed and design of control systems.

Chapter 3: Machine Modeling and Design of Control Systems

This chapter presents first principle modeling of the various components which constitute the utility and the micro-grid. The mathematical equations which describe the physical properties of these components are used to model both components' steady-state and dynamic behaviors. In the utility, the components are steam turbine, synchronous generator, excitation system, power system stabilizer, transformer, transmission lines, static loads and STATCOM. In the micro-grid, the components are reactive var source, wind turbine, doubly-fed induction generator, transformer, feeders and static loads.

Also presented in this chapter is design of pitch regulator, active power regulator, reactive power regulator, grid ac voltage regulator, dc bus voltage regulator, grid-side converter current regulator and rotor-side converter current regulator. Each regulator is designed using small signal frequency response analysis, resulting in stable systems with satisfactory response. The regulators are combined to implement two mutually exclusive control regimes: the active power-voltage (PV or V) control and the active-reactive power (PQ or Q) control.

3.1 System Under Study

The index test bed developed for this study is shown in Fig. 3.1. The section in green rectangle is the utility. In the system, the synchronous generator included in the utility is rated 100MVA, 13.8kV, 50Hz. A 20MVA STATCOM is modeled and linked to the utility side at the Point of Common Coupling. The utility services a local inductive load of 3.6MVA and a remote inductive load of 89.44MVA. In this report, MS1 is Microsource1; MS2 is Microsource2; feeder-a is feeder connected to MS1; and feeder-b is feeder connected to MS2.

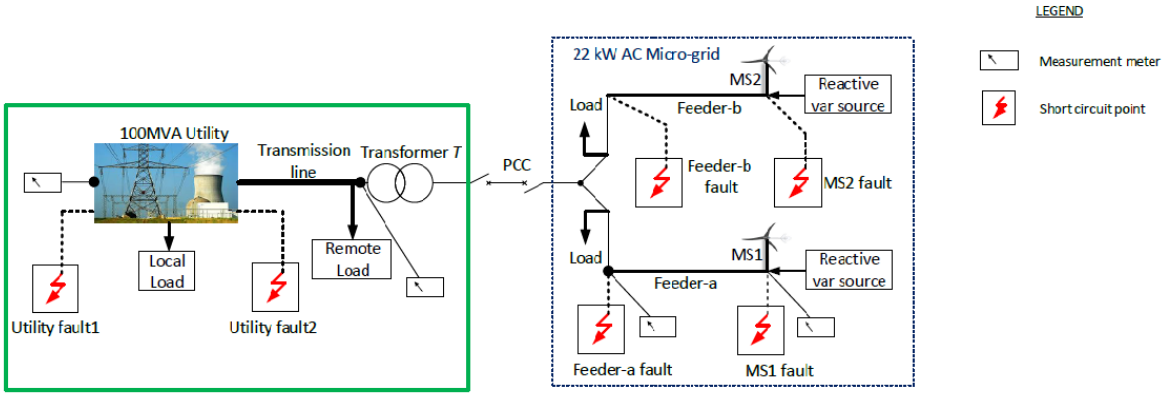

Fig. 3.1. A diagram showing the basic elements of the index system under study

3.2 Models of Utility Components

Fig. 3.2 shows a functional diagram of steam turbine, speed governor and major constituents of the utility system. The time span of the stability study is relatively short in comparison with time required for significant load change. Thus, load changing equipment is neglected.

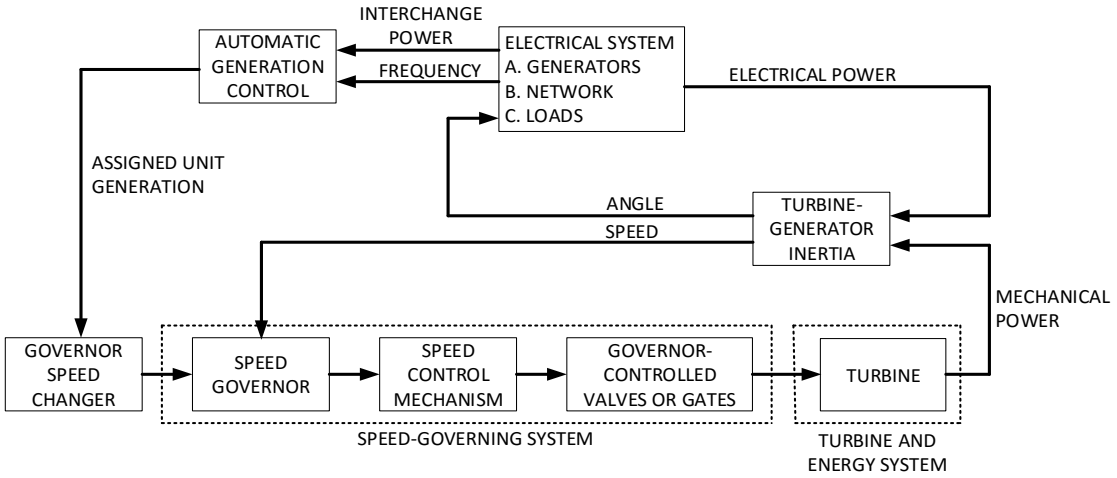

Fig. 3.2. Functional block diagram showing steam turbine and associated equipment

3.2.1 Steam turbine and speed governor

A complete tandem compound steam prime mover which incorporates a speed governing system, a four-stage steam turbine, and a four-mass shaft is modeled in the steam turbine and governor system as presented in Fig. 3.3 and Fig. 3.4 [56]. Primarily, the speed-governing system serves to perform the following:

i. To start, maintain and adjust speed of turbine-generator unit for synchronizing with the running units/grid.
ii. To maintain system frequency after synchronization by adjusting turbine output to load changes.
iii. To share load changes with the other units in a planned manner in response to system frequency error.
iv. To adjust output of the unit in response to operator or other supervisory commands.
v. To perform normal shut down or emergency over speed shut down for protection.

In the electro-hydraulic system shown, the generator speed is sensed by a tachometer mounted on the generator rotor shaft. It converts the speed to electrical signal and delivers it to the governor circuits. Also, it is a source of an output to operate speed relays for various sequence controls and of power to drive the transistor amplifiers which is fed to the load controller. The load controller compares its input with a reference load and delivers the error signal to the position controller.

The output of the position controller is passed to the servo-system and steam valves. The valve opening and closing controls the amount of steam available to the steam turbine thereby increasing or decreasing its speed. In comparison to the mechanical-hydraulic-controlled system, the feedback loops of steam flow and servomotor provide improved system linearity [57]. Additional notes on Fig. 3.3 and Fig. 3.4 can be found from [56].

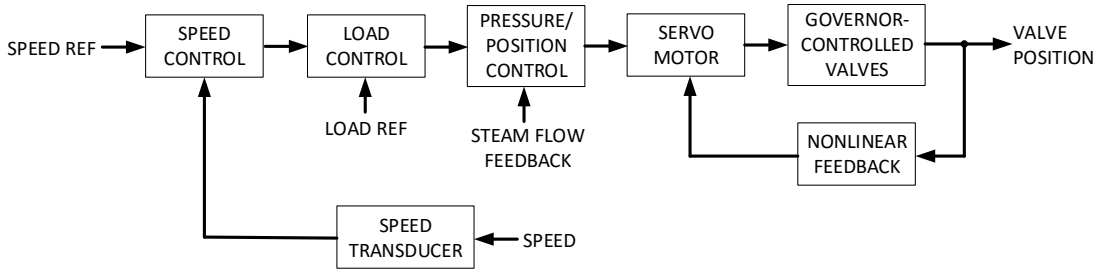

Fig. 3.3. Functional block diagram of electro-hydraulic speed-governing system for steam turbines

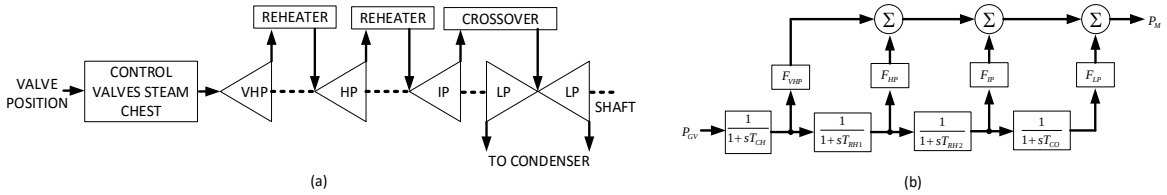

Fig. 3.4. (a) Tandem compound double reheat steam system configuration; (b) approximate linear model

A compound steam turbine uses governor-controlled valves at the inlet to the very high pressure (VHP) or high pressure (HP) to control flow of steam. Delays are introduced between valve movements and corresponding changes in flow of steam by the steam chest, inlet piping to the first turbine cylinder, re-heaters and crossover piping. Thus, for power system stability studies, the modeling objective is to determine these delays. A simple time constant relates flows into and out of any steam vessel [56]. Fig. 3.5 depicts a simplified steam vessel.

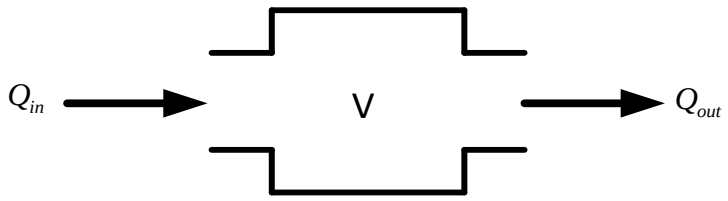

Fig. 3.5. A simplified steam vessel

With reference to Fig. 3.5, the continuity equation is given in (3.1).

$$\frac{dW}{dt} = Q_{in} - Q_{out} \tag{3.1}$$

Where, W is the weight of steam in kg in a volume m^3, t is time in seconds, Q_{in} is inflow in kg and Q_{out} is outflow in kg. Assuming the weight of the outflow is proportional to the pressure in the vessel, it can be shown that the steam vessel time constant, T , is given by (3.2) [56].

$$\frac{Q_{out}}{Q_{in}} = \frac{1}{1+sT} \tag{3.2}$$

$$\text{Where, } s = \frac{d}{dt} \tag{3.3}$$

3.2.2 Excitation system

The excitation system is the *IEEE Type DC1A Excitation System Model* proposed in [58-60] and presented in Fig. 3.6. Its basic elements are voltage regulator and exciter. The exciter is represented by the transfer function between the regulator's output, E_f, and the exciter's output, V_f, as modeled by the transfer function in (3.4).

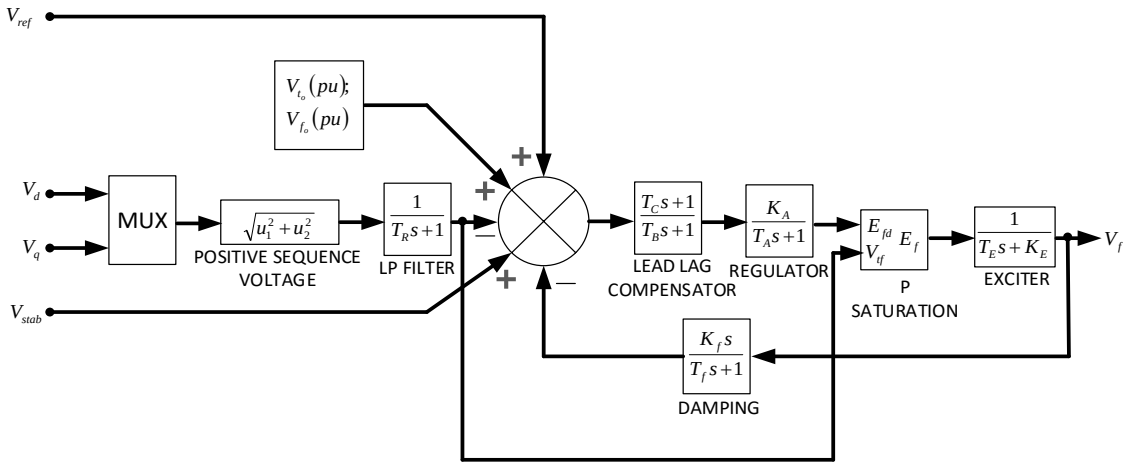

Fig. 3.6. Simplified DC commutator exciter

$$\frac{V_f}{E_f} = \frac{1}{T_E s + K_E} \tag{3.4}$$

This block models a field controlled dc-commutator exciter with continuously acting voltage regulator. It uses self-excited shunt fields with a voltage regulator operating in a buck-boost mode. LP filter and P saturation are low-pass filter and proportional saturation, respectively. The inputs to this model are the desired reference voltage, V_{ref}, terminal voltage, V_{ta}, and field voltage, V_{fa}.

Other inputs are low-pass filtered positive-sequence direct and quadrature axes components from the terminal voltage transducer, output voltage of power system stabilizer, V_{stab} and exciter's output voltage, V_f as a feedback. At the summing junction, the exciter's output voltage and transducer's terminal voltages are subtracted from the other voltages. The resulting signal is compensated and amplified by the voltage regulator. The major time constants, T_A, and gain, K_A, associated with the voltage regulator are shown. The resulting signal is passed through a saturation block and used to control the exciter. V_{stab} is connected to the power system stabilizer for additional stabilization of power system oscillations [56, 58, 61].
Other variables are described in Appendix A1.

3.2.3 Synchronous generator

A) Generator mechanical system

The mechanical part of the synchronous generator implements a model described by (3.5).

$$\left.\begin{aligned} \Delta\omega(t) &= \tfrac{1}{2H}\int_0^t (T_m - T_e)dt - Kd\Delta\omega(t) \\ \omega(t) &= \Delta\omega(t) + \omega_0 \end{aligned}\right\} \tag{3.5}$$

where,

$\Delta\omega$ is change in speed of operation.
H is constant of inertia.
T_m is mechanical torque.
T_e is electromagnetic torque.
K_d is damping factor which represents the effect of damper windings.
$\omega(t)$ is mechanical speed of the rotor.
ω_0 is per unit speed of operation.

The implementation of the model is shown in Fig. 3.7. The damper windings normally included in synchronous machines is simulated by the coefficient K_d . When the generator is connected to an infinite bus (zero impedance), the change in mechanical power, P_m, results in change of machine power angle which can be approximated by the second-order transfer function given in (3.6). The model in (3.6) assumes the power angle is sufficiently small such that (3.7) is valid [61].

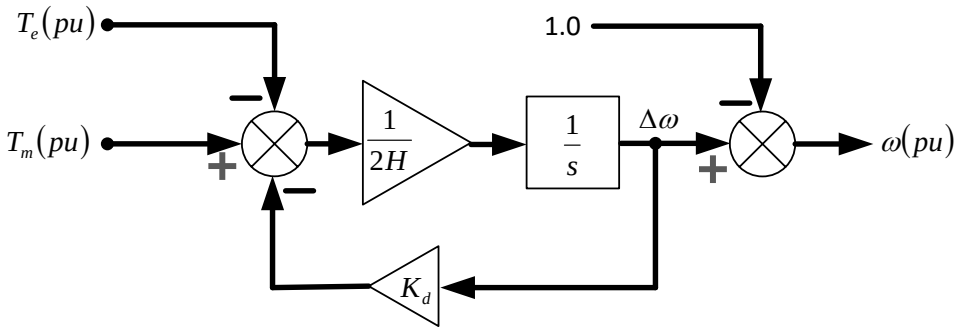

Fig. 3.7. Implementation of mechanical part of the synchronous generator

$$\left.\begin{aligned} \frac{\delta}{P} &= \frac{1}{2H}\frac{\omega_e}{s^2 + 2\xi\omega_n s + \omega_n^2} \\ \xi &= (K_d/4)\sqrt{2/(\omega_s H P_{\max})} \\ \omega_n &= \sqrt{\omega_s P_{\max}/(2H)} \\ P_{\max} &= \frac{V_t E}{Z} \end{aligned}\right\} \tag{3.6}$$

$$\sin(\delta) = \delta \tag{3.7}$$

where,

δ is power angle in radians (angle of internal voltage *E* with respect to terminal voltage).

P_m is per unit mechanical power.

ω_n is frequency of electromechanical oscillations in rads^{-1}.

ξ is damping ratio.

ω_e is electrical frequency in rads^{-1}.

$P_{\max}$ is per unit maximum power transmitted through impedance Z at a terminal voltage V_t and internal voltage E .V_t, E and Z are in p.u..

H is constant of inertia.

K_d is damping factor.

Appendix A2 provides parameters of the synchronous generator.

B) Generator electrical system

The electrical part of the synchronous generator which accounts for dynamics of the stator, field and damper windings is represented by a sixth-order state-space model in the rotor reference

frame (*dq* frame), as shown in Fig. 3.8. The per phase electrical system consists of a voltage source with a resistive-inductive (RL) impedance in series. The internal impedance of the generator is implemented by RL . The resistance, *R* (in Ohms), can be zero but the inductance, *L* (in Henry), must be greater than zero.

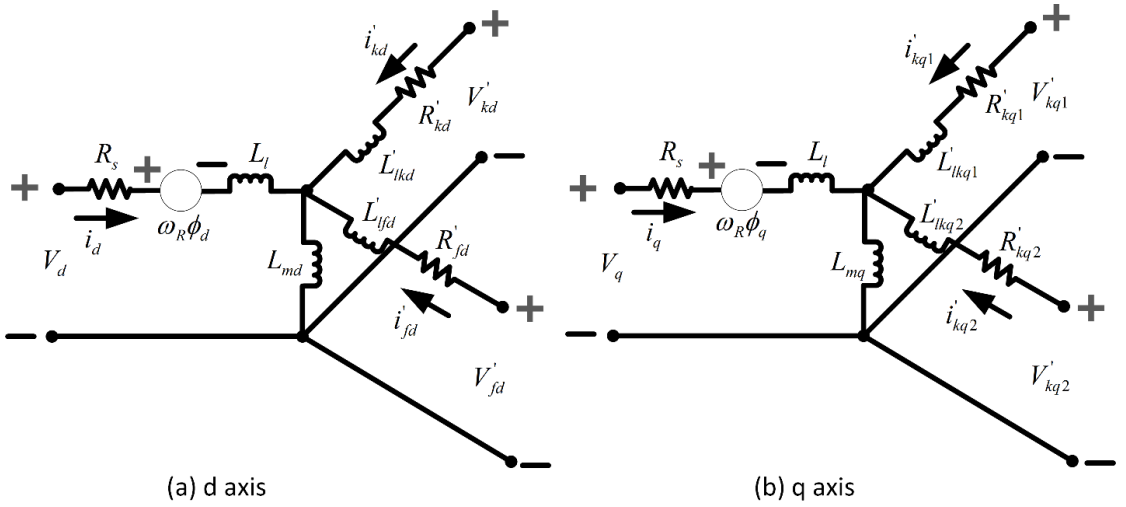

Fig. 3.8. Dynamic model of three phase synchronous generator

The mathematical equations describing the equivalent circuit shown in Fig. 3.8 are provided in (3.8) – (3.10). All rotor parameters are primed and viewed from the stator [62, 63].

$$\left.\begin{aligned} V_d &= R_s i_d + \tfrac{d}{dt}\phi_d - \omega_R\phi_q \\ V_q &= R_s i_q + \tfrac{d}{dt}\phi_q + \omega_R\phi_d \\ \phi_d &= L_d i_d + L_{md}\left(i'_{fd} + i'_{kd}\right) \\ \phi_q &= L_q i_q + L_{mq} i'_{kq} \end{aligned}\right\} \tag{3.8}$$

$$\left.\begin{aligned} V'_{fd} &= R'_{fd} i'_{fd} + \tfrac{d}{dt}\phi'_{fd} \\ V'_{kd} &= R'_{kd} i'_{kd} + \tfrac{d}{dt}\phi'_{kd} \\ \phi'_{fd} &= L'_{fd} i'_{fd} + L_{md}\left(i_d + i'_{kd}\right) \\ \phi'_{kd} &= L'_{kd} i'_{kd} + L_{md}\left(i_d + i'_{fd}\right) \end{aligned}\right\} \tag{3.9}$$

$$\left.\begin{aligned} V'_{kq1} &= R'_{kq1} i'_{kq1} + \tfrac{d}{dt}\phi'_{kq1} \\ V'_{kq2} &= R'_{kq2} i'_{kq2} + \tfrac{d}{dt}\phi'_{kq2} \\ \phi'_{kq1} &= L'_{kq1} i'_{kq1} + L_{mq} i_q \\ \phi'_{kq2} &= L'_{kq2} i'_{kq2} + L_{mq} i_q \end{aligned}\right\} \tag{3.10}$$

The subscripts are defined as follows:

- *d, q: d axis, q axis quantity.*
- *R, s: Rotor quantity, stator quantity.*
- *l, m: Leakage inductance, magnetizing inductance.*
- *f, k: Field quantity, damper winding quantity.*

where,

R_s is stator resistance per phase in Ohm.

L_l is stator leakage inductance in Henry.

L_{md} is direct axis magnetizing inductance viewed from stator in Henry.

L_{mq} is quadrature axis magnetizing inductance viewed from stator in Henry.

The base values of the stator parameters, represented with subscript $sbase$, are given in (3.11).

$$\left.\begin{aligned} V_{sbase} &= \frac{V_n\sqrt{2}}{\sqrt{3}} \\ I_{sbase} &= \frac{S_n\sqrt{2}}{V_n\sqrt{3}} \\ Z_{sbase} &= \frac{V_{sbase}}{I_{sbase}} = \frac{V_n^2}{S_n} \\ L_{sbase} &= \frac{Z_{sbase}}{\omega_{base}} \end{aligned}\right\} \tag{3.11}$$

where,

S_n is three phase nominal power (VA).

V_n is nominal line-to-line voltage (V_{rms}).

f_n is nominal frequency (Hz).

The base angular frequency in rads^{-1} is given in (3.12).

$$\omega_{base} = 2\pi f_n \tag{3.12}$$

Appendix A3 provides electrical parameters of the synchronous generator.

Requisite models of power system stabilizer, three phase power transformer and STATCOM are included in the test bed depicted in Fig. 3.1.

3.3 Models of Micro-grid Components

The micro-grid consists of two micro-sources modeled using the Type 3 Wind Turbine Generator (WTG3) based on doubly-fed induction generator (DFIG). Either DFIG is nominally rated 11kW, 575V and interconnected to 2.5km highly resistive feeders (a and b) such that each

feeder is linked to the utility radially at the PCC as shown in Fig. 3.1. The micro-grid services a total inductive local load of 12.42kVA and operates at a frequency of 50Hz, with cut-in and cut-out wind speeds of $3ms^{-1}$ and $6ms^{-1}$, respectively. The micro-grid is islanded by disconnecting the PCC.

3.3.1 Reactive power source

The reactive power source of the micro-grid consists of a three-phase source, transformer and a reactive load connected to the wind energy generator (DFIG) as shown in Fig. 3.9.

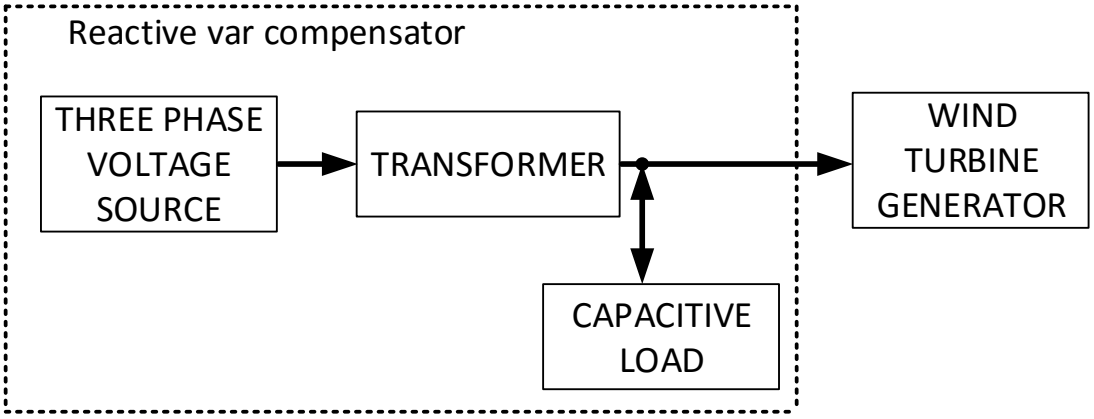

Fig. 3.9. Block diagram showing three phase reactive var compensator and WTG3

A) Three-phase source

The three-phase source implements a balanced three-phase voltage source with an internal resistive-inductance (*R-L)* impedance [64]. The three voltage sources are connected in Y with a grounded neutral. The source internal resistance and inductance are modeled by specifying source inductive short circuit level and X/R ratio. The source inductance *L* (in H) is obtained using the inductive three-phase short circuit power S_{sc} (in VA), base voltage V_{base} (in V_{rms} phase-to-phase), and source frequency *f* (in Hz) as provided in (3.13) [65, 66].

$$L = \frac{V_{base}^2}{S_{sc}} . \frac{1}{2\pi f} \tag{3.13}$$

The source internal resistance *R* (in Ohms) is modeled using (3.14).

$$R = \frac{2\pi f L}{X/R} \tag{3.14}$$

Appendix B1 provides data for parameters associated with the reactive power source.

B) Three-phase transformer

The three-phase transformer is implemented using linear transformer model, as shown in Fig. 3.10.

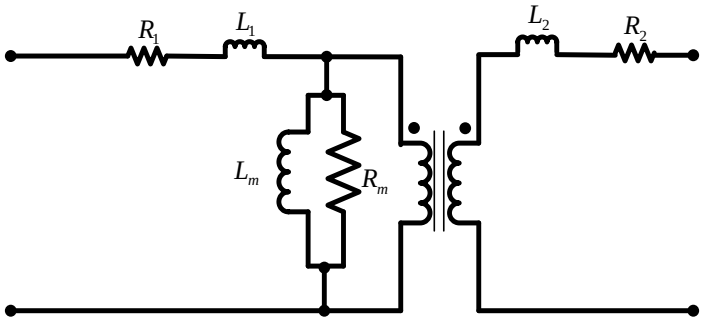

Fig. 3.10. Linear transformer model

Neglecting transformer saturation so that simulation starts from steady state, the model accounts for the winding resistances (R_1 and R_2), leakage inductances (L_1 and L_2) and magnetizing (R_m and L_m) characteristics of the core, modeled with a linear branch as shown. Resistance and inductance of the windings are specified in per unit (p.u.). Each p.u. quantity is based on transformer rated power S_n (in VA), nominal voltage V_n (in V_{rms} of corresponding winding) and nominal frequency f_n (in Hz) as defined in (3.15). In order to specify magnetizing current (resistive and inductive) of 0.2%, a value (1/0.002 = 500) is used for the resistance and inductance of the magnetizing branch. The transformer neutral is grounded through a 66 Ohms resistor [65, 66].

$$\left.\begin{aligned} R_{p.u.} &= \frac{R(\Omega)}{R_{base}} \\ L_{p.u.} &= \frac{L(H)}{L_{base}} \\ Z_{base} &= R_{base} = X_{base} = \frac{V_n^2}{S_n} \\ L_{base} &= \frac{X_{base}}{2\pi f_n} \end{aligned}\right\} \qquad (3.15)$$

Appendix B1 provides data for parameters associated with the transformer.

C) Three-phase capacitive load

Three-phase capacitive load provides reactive power at the terminals of the wind turbine generator by increasing or decreasing reactive power absorption. The load is modeled such that its

impedance is kept constant during bus initialization by the load flow solution process [67]. The capacitive reactive power Q_c (in var) it absorbs is proportional to the square of the nominal line-to-line voltage V_n (in V_{rms}) at the terminals of the generator, as given by (3.16) [65, 66].

$$Q_c = 2\pi f_n C V_n^2 \tag{3.16}$$

where,

f_n is the nominal frequency in Hz.

C is the load capacitance in Farad.

Appendix B1 provides data for parameters associated with the capacitive load.

3.3.2 Wind turbine-generator system

The wind turbine-generator system consists of wind turbine, induction generator, ac-ac converter and controller.

A) Wind Turbine

The wind turbine model presented is a variable pitch type based on the steady-state power characteristics of the turbine. The mechanical output power P_m (in Watts) of the wind turbine is given in (3.17) [68, 69]. The model assumes the stiffness of the drive train is infinite. It also assumes the inertia and friction factor represent those of the turbine and generator coupled together.

$$P_m = c_p(\lambda, \beta)\frac{\rho A}{2} v_w^3 \tag{3.17}$$

where,

c_p is performance coefficient of the turbine.

ρ is air density in kgm^{-3}.

A is turbine swept area in m^2.

v_w is wind speed in ms^{-1}.

λ is tip speed ratio (rotor blade tip speed to wind speed).

β is blade pitch angle in degree.

The electric power-speed characteristic is used to specify a series of speed-power pairs for the tracking characteristic. The power is in p.u. based on nominal generator power, while the speed is in p.u. based on synchronous speed. It specifies speeds of point A to point D, as shown in Fig. 3.11. Speed_B is greater than speed_A and speed_D is greater than speed_C. The power at point C is the maximum turbine output power for the specified wind speed at point C [70].

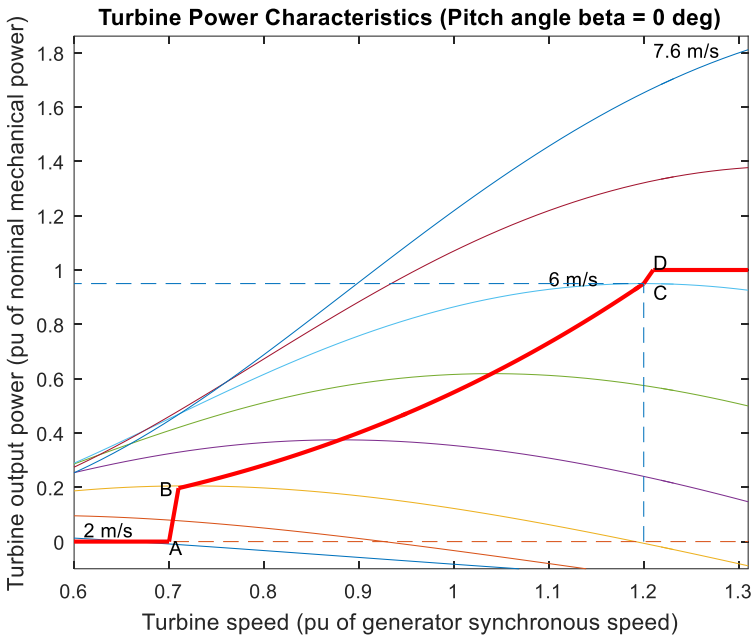

Fig. 3.11. Wind turbine power characteristic

Appendix B2 provides data for parameters associated with the wind turbine.

B) Induction generator

The induction machine presented models the dynamics of three-phase single squirrel-cage asynchronous generator. Its mechanical part is represented by a second-order system in (3.18). Its electrical part is represented by a set of fourth-order systems in (3.19) and (3.20), while Fig. 3.12 depicts its electrical equivalent circuit in *d* and *q* axes [68, 71, 72]. All electrical parameters are modeled in the rotating (*dq*) reference frame and all rotor parameters are referred to the stator (indicated with primed parameters). Core saturation is neglected.

$$\left.\begin{aligned} \tfrac{d}{dt}\omega_m &= \tfrac{1}{2H}\left(T_e - F\omega_m - T_m\right) \\ \tfrac{d}{dt}\theta_m &= \omega_m \end{aligned}\right\} \tag{3.18}$$

where,

ω_m is rotor angular velocity in rads^{-1}.

H is combined inertia constant of rotor and load.

T_e is electromagnetic torque in N.m.

F is combined rotor and load viscous friction coefficient.

T_m is mechanical torque of shaft in N.m.

θ_m is rotor angular position in radian.

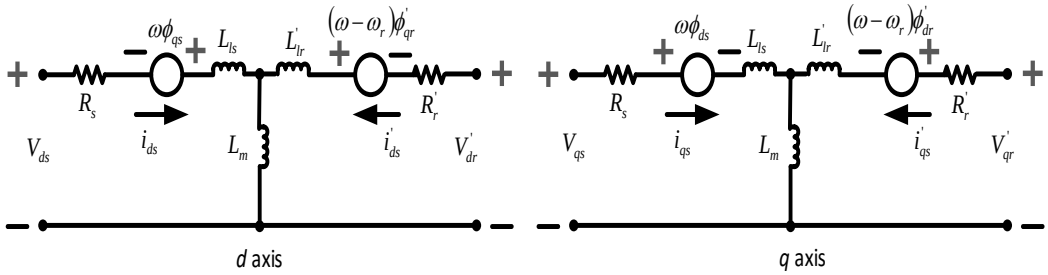

Fig. 3.12. Electrical circuit of induction generator

$$\left.\begin{aligned}
V_{qs} &= R_s i_{qs} + \frac{d\phi_{qs}}{dt} + \omega\phi_{ds} \\
V_{ds} &= R_s i_{ds} + \frac{d\phi_{ds}}{dt} - \omega\phi_{qs} \\
V'_{qr} &= R'_r i'_{qr} + \frac{d\phi'_{qr}}{dt} + (\omega-\omega_r)\phi'_{dr} \\
V'_{dr} &= R'_r i'_{dr} + \frac{d\phi'_{dr}}{dt} - (\omega-\omega_r)\phi'_{qr} \\
T_e &= 1.5p(\phi_{ds} i_{qs} - \phi_{qs} i_{ds})
\end{aligned}\right\} \tag{3.19}$$

$$\left.\begin{aligned}
\phi_{qs} &= L_s i_{qs} + L_m i'_{qr} \\
\phi_{ds} &= L_s i_{ds} + L_m i'_{dr} \\
\phi'_{qr} &= L'_r i'_{qr} + L_m i_{qs} \\
\phi'_{dr} &= L'_r i'_{dr} + L_m i_{ds} \\
L_s &= L_{ls} + L_m \\
L'_r &= L'_{lr} + L_m
\end{aligned}\right\} \tag{3.20}$$

Machine parameters are defined in Table 3.1.

Table 3.1. Definition of machine parameters

Quantity	Definition
R_s, L_{ls}	Stator resistance, leakage inductance.
L_m, L_s	Magnetizing inductance, total stator inductance.
V_{qs}, i_{qs}	*q* axis stator voltage, *q* axis stator current.
V_{ds}, i_{ds}	*d* axis stator voltage, *d* axis stator current.
ϕ_{qs}, ϕ_{ds}	Stator *q* axis flux, stator *d* axis flux.
ω, ω_r	Reference frame angular velocity, electrical angular velocity.
$R_r^{'}, L_{lr}^{'}, L_r^{'}$	Rotor resistance, leakage inductance, total rotor inductance.
$V_{qr}^{'}, i_{qr}^{'}$	*q* axis rotor voltage, *q* axis rotor current.
$V_{dr}^{'}, i_{dr}^{'}$	*d* axis rotor voltage, *d* axis rotor current.
$\phi_{qr}^{'}, \phi_{dr}^{'}$	Rotor *q* axis flux, rotor *d* axis flux.
T_e, p	Electromagnetic torque, pole pair.

C) AC-AC converter

The ac-ac converter consists of a rectifier and an inverter. The rectifier is a three-phase $575V_{dc}$ controlled converter with 1% ripple which feeds the inverter. The inverter is a three-phase six-step Voltage Sourced Inverter (VSI) modeled in SimPowerSystems. The rectifier is modeled in SimPowerSystems using (3.21) [73].

$$\left.\begin{aligned} V_{dc} &= \frac{3V_{LLpeak}\cos\alpha}{\pi} \\ V_{dc} &= \frac{3\sqrt{3}V_{peak}\cos\alpha}{\pi} \\ V_{rms} &= \frac{V_{peak}}{\sqrt{2}} \end{aligned}\right\} \tag{3.21}$$

where,

α is IGBT firing angle

Three-phase Voltage Sourced Inverter

A functional block diagram of the VSI is shown in Fig. 3.13. The inverter is implemented using classical full bridge 2-level power switch topology.

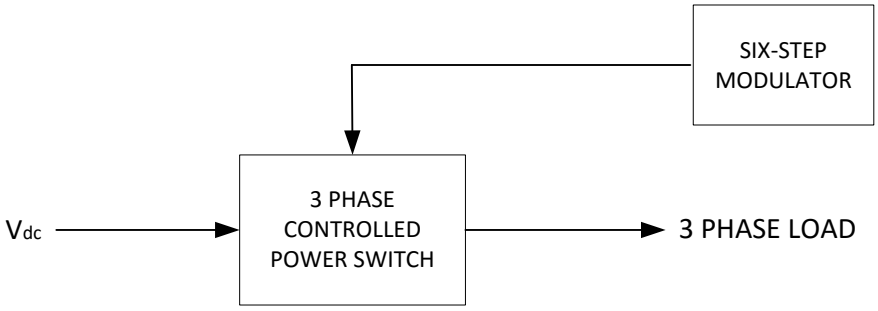

Fig. 3.13. Three-phase voltage sourced inverter based on six-step modulation

The inverter's power switches are based on Insulated Gate Bipolar Transistors (IGBTs). The full bridge inverter module consists of six power switches and six clamping diodes, as shown in Fig. 3.14. Each leg has its own binary control signal as described in (3.22).

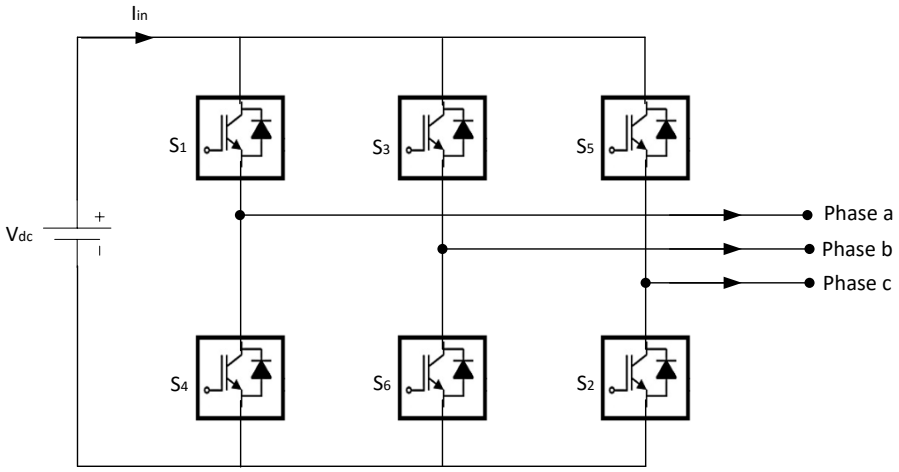

Fig. 3.14. Three-phase six-step inverter circuit

$$S_x \in \{1,0\}\begin{cases} 1 \Longrightarrow ONstate \\ 0 \Longrightarrow OFFstate \end{cases}, x = a,b,c \tag{3.22}$$

The semiconductor switches in one leg are controlled with complementary signals to avoid both conducting at the same time and short circuit the dc link. This also prevents both switches from simultaneous opening, preventing undefined output voltages. When $S_x = 1$, phase *x* output node is connected to the positive bar, generating a phase output voltage $v_{xn} = V_{dc}$. With $S_x = 0$, phase *x* output node is connected to the negative bar, generating a phase output voltage $v_{xn} = 0$. The inverter phase output voltage, in Volts, is given by (3.23) [74].

$$v_{xn} = \frac{S_x}{2(1-D_c)} V_{dc}, \forall S_x \in \{0,1\}, x = a,b,c; n = neutral\ terminal \tag{3.23}$$

where,

V_{dc} is dc voltage from rectifier.

D_c is duty cycle of modulator.

Since the inverter is controlled with three binary signals, it is sequenced by $2^3 = 8$ different switching states (S_a, S_b, S_c), presented in Table 3.2.

Table 3.2. Switch states for three phase VSI

Switching States	**Gating Signals**			**Output Voltage**		
	S_a	S_b	S_c	v_{an}	v_{bn}	v_{cn}
1	0	0	0	0	0	0
2	1	0	0	V_{dc}	0	0
3	1	1	0	V_{dc}	V_{dc}	0
4	0	1	0	0	V_{dc}	0
5	0	1	1	0	V_{dc}	V_{dc}
6	0	0	1	0	0	V_{dc}
7	1	0	1	V_{dc}	0	V_{dc}
8	1	1	1	V_{dc}	V_{dc}	V_{dc}

Pulse width modulation

The modulator is a non-carrier-based pulse width modulator modeled to turn on the IGBTs in a manner that they operate in the 180^o conduction mode. The conduction mode diagram is shown in Fig. 3.15. The modulator's duty cycle and frequency are given in (3.24) [74, 75].

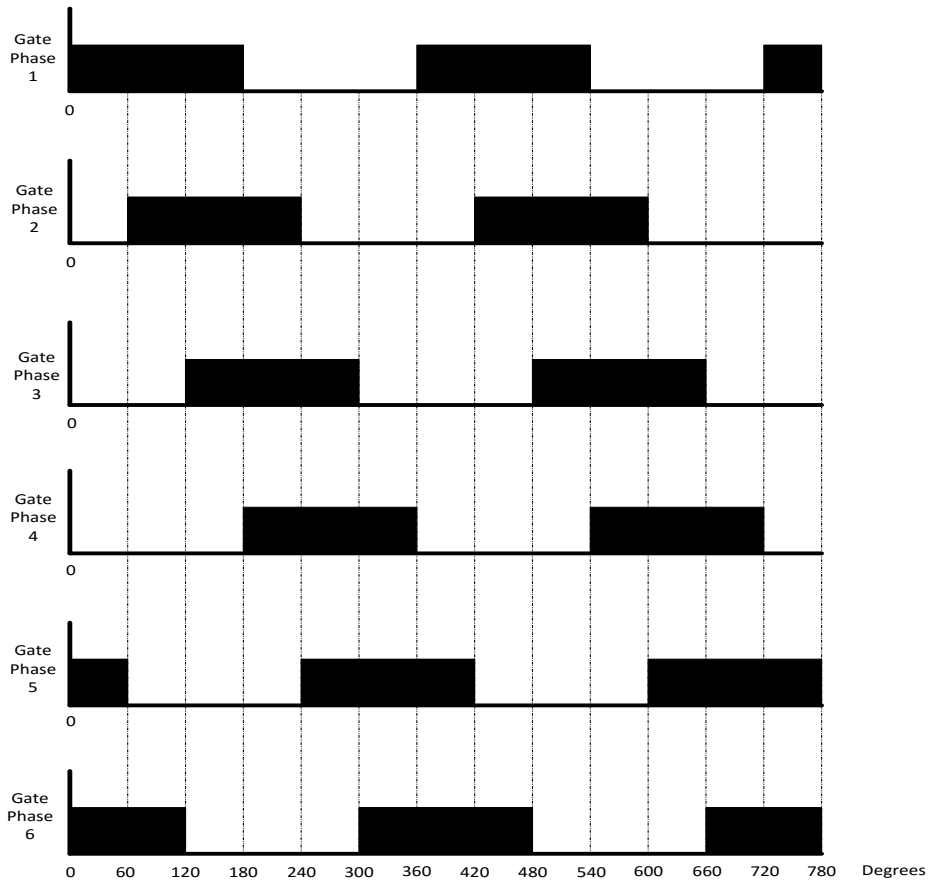

Fig. 3.15. 180° conduction mode diagram

$$\left.\begin{aligned} D_c &= \frac{T_{ON}}{T_{ON}+T_{OFF}} \\ f &= \frac{1}{T} \end{aligned}\right\} \tag{3.24}$$

where,

T_{ON} is active duration of the pulse in second.

T_{OFF} is inactive duration of the pulse in second.

f is frequency of gate pulse.

The phase delay, firing angle and frequency of gate pulse are given in (3.25) [76].

$$\Delta t = \frac{\alpha}{360f} \tag{3.25}$$

where,

Δt is phase delay in second.

$\propto$ is electrical firing angle in degree.

In SimPowerSystems, modeling of gate firing angle is done in time. Conversion of firing angle (degrees) to phase delay (second) is done using (3.25), and presented in Table 3.3.

Table 3.3. Phase delay of power switches

Switch	**Firing Angle**	**Phase Delay (second)**
S_1	0º	0.0000
S_2	60º	0.0033
S_3	120º	0.0067
S_4	180º	0.0100
S_5	240º	0.0133
S_6	300º	0.0167

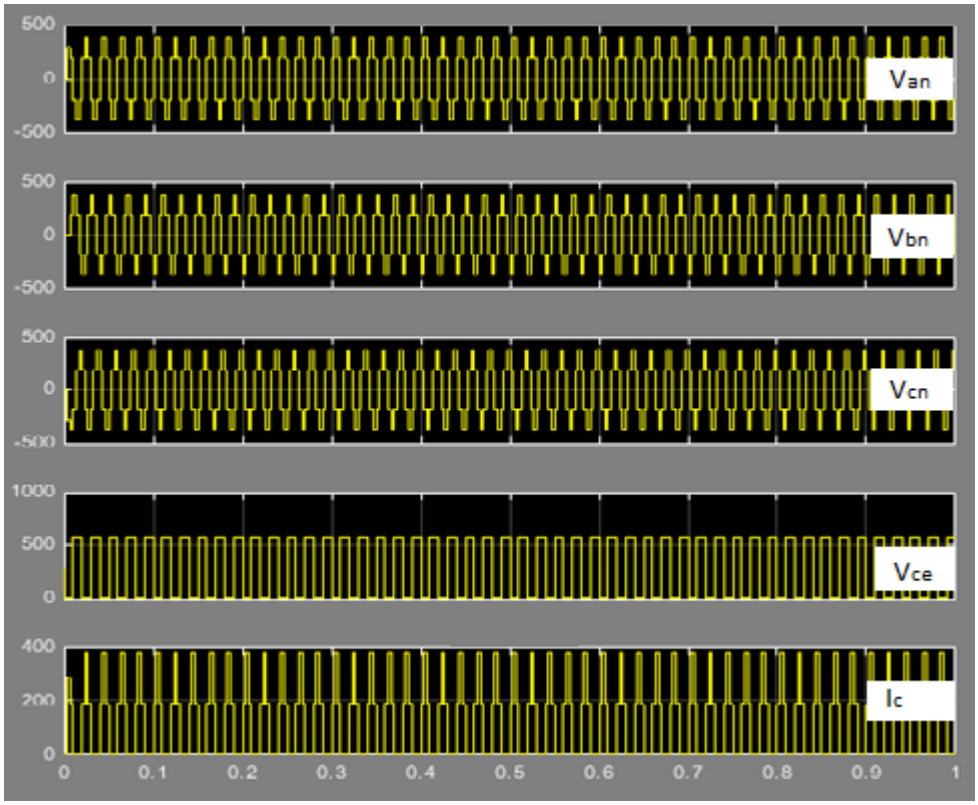

Fig. 3.16. Plots showing outputs quantities of the VSI and S_1

Other requisite parameters of the inverter are presented in Appendix B3.

Fig. 3.16 shows plots of the output quantities of the voltage sourced inverter. In the plots, V_{an}, V_{bn} and V_{cn} are respectively phase-a voltage, phase-b voltage and phase-c voltage. V_{ce} and I_c are the collector-emitter voltage and collector current of the IGBT associated with S_1, respectively.

Requisite models of transformers, distribution feeders and static *RL* loads in the micro-grid are implemented and incorporated in the test bed presented in Fig. 3.1.

3.4 Design of Control Systems

This section presents small signal stability analysis of the components in the micro-grid and design of requisite control systems using closed-loop feedback architecture. Fig. 3.17 shows a simplified arrangement of the components which make up the DFIG.

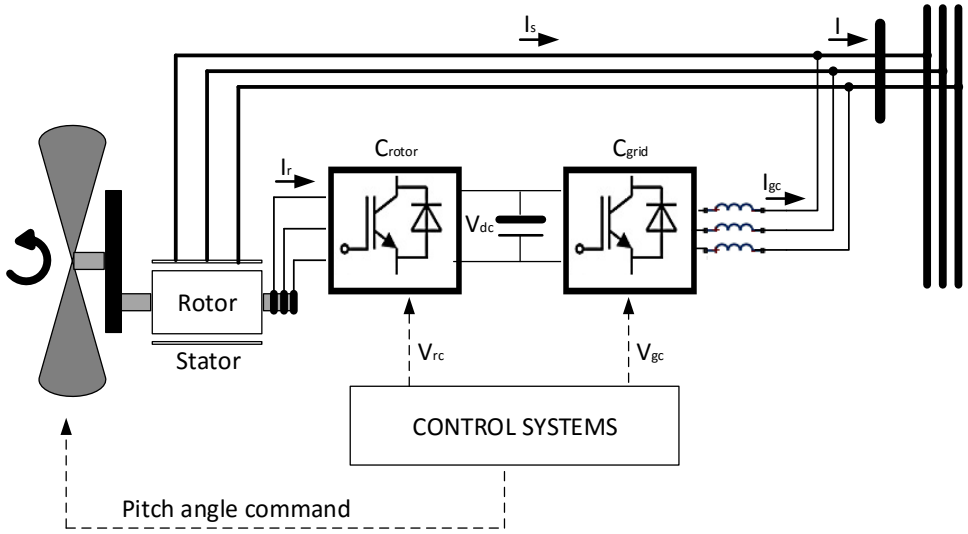

Fig. 3.17. A simplified DFIG and its connection to the grid

In Fig. 3.13, C_{rotor} is rotor-side converter; C_{grid} is grid-side converter; I_s is stator current; I_r is rotor current; I is supply current; and I_{gc} is grid-side converter current.

Table 3.4. Required system specifications

Initial value	0	Final value	1
Rise time	5.00 s	% Rise	90
Settling time	15.00 s	% Settling	1.0
% Overshoot	10.00	% Undershoot	0

3.4.1 Active power management systems

A) Pitch regulator

The open-loop transfer function of the wind turbine is provided in (3.26).

$$G(s) = \frac{K_p}{1 + T_p s} \tag{3.26}$$

where,

$K_p = 2200, T_p = 0.22375.$

Its step response is shown in Fig. 3.18. It fails to meet the required specifications set in Table 3.2. A proportional (P) compensator (C) is therefore implemented.

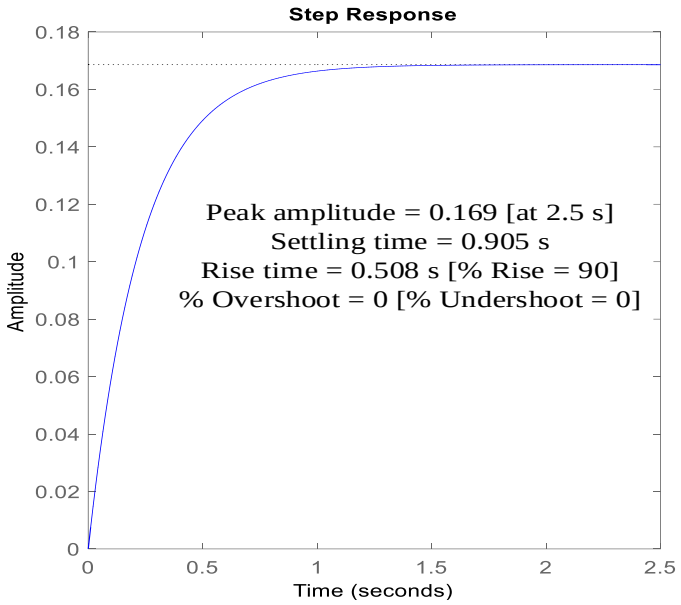

Fig. 3.18. Wind turbine rotor pitch open-loop unit step response

The transfer function of the P compensator is provided in (3.27).

$$C = K_p \tag{3.27}$$

where,

$K_p = 450.00.$

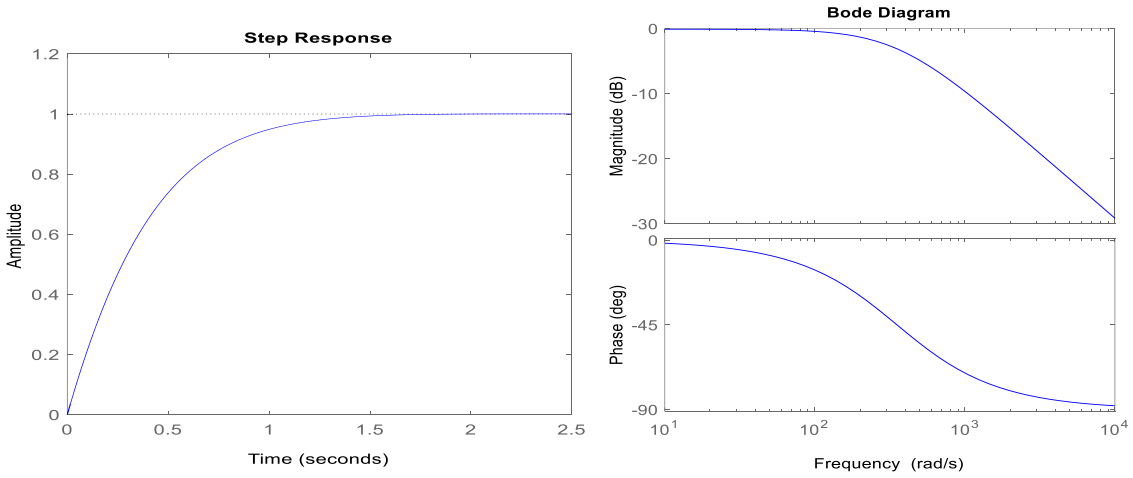

(a) Step response in time domain (b) Bode diagram

Fig. 3.19. Closed-loop response of pitch control system in frequency domain

Fig. 3.19 shows the closed-loop response of the implemented pitch control system. It is a stable loop with infinite gain and phase margins. The system meets the required specifications provided in Table 3.2.

B) Active power regulator

The open-loop transfer function of the generator is provided in (3.28).

$$G(s) = \frac{K_p}{(1+T_{p1}s)(1+T_{p2}s)} \tag{3.28}$$

where,

$$K_p = 2000, T_{p1} = 7.7814x10^{-5}, T_{p2} = 3.4536x10^{+5}.$$

Its step response is shown in Fig. 3.20. It fails to meet the required specifications set in Table 3.2. A proportional-integral (PI) compensator is therefore implemented as shown in Fig. 3.21.

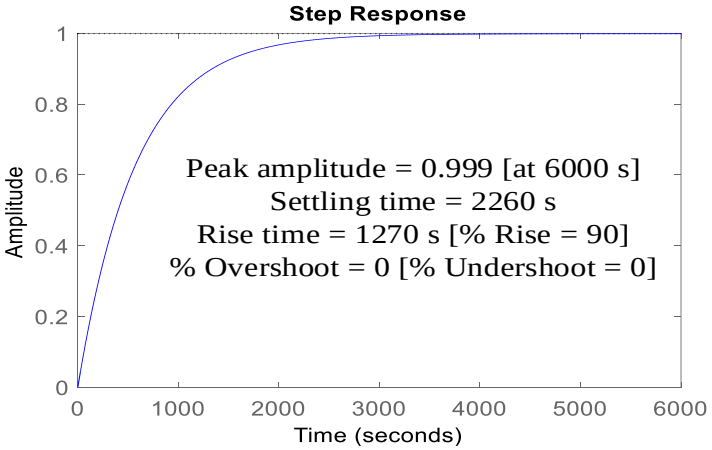

Fig. 3.20. Generator open-loop unit step response

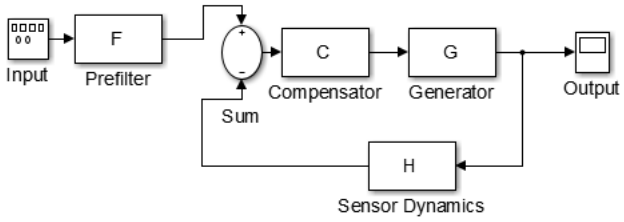

Fig. 3.21. Architecture of active power regulator

The transfer function of the PI compensator is provided in (3.29).

$$C = K_p + \frac{K_i}{s} \tag{3.29}$$

where,

$K_p = 107.42, K_i = 0.0010742.$

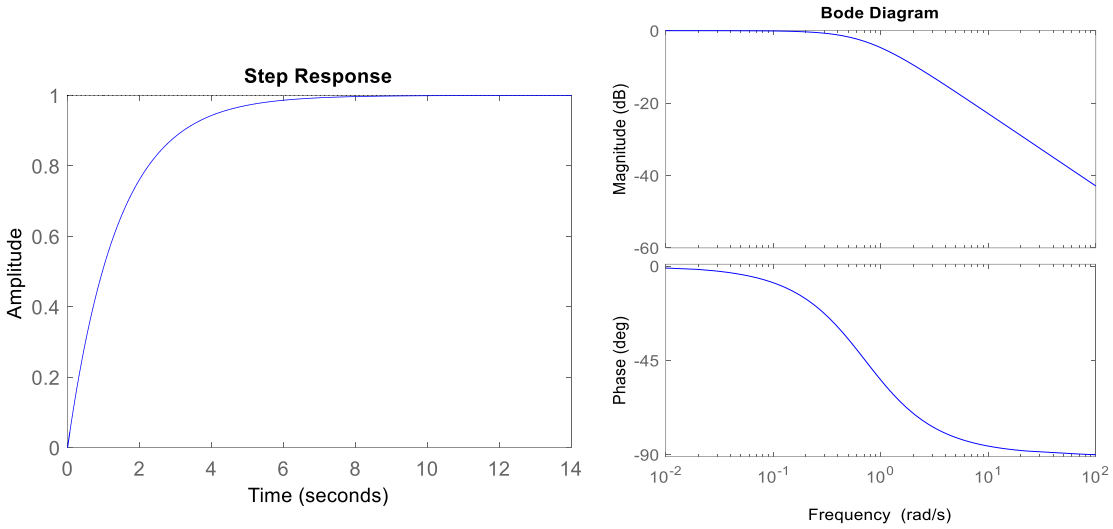

(a) Step response in time domain (b) Bode diagram

Fig. 3.22. Closed-loop response of active power regulator in frequency domain

Fig. 3.22 shows the closed-loop response of the tuned PI compensator and generator system. It is a stable loop with infinite gain margin and phase margin of 90° at $5.79x10^{-3}$ rads^{-1}. The system meets the required specifications provided in Table 3.2.

3.4.2 Reactive power management system

The open-loop transfer function of the reactive var source is provided in (3.30).

$$G(s) = \frac{K_p}{1 + T_p s} \tag{3.30}$$

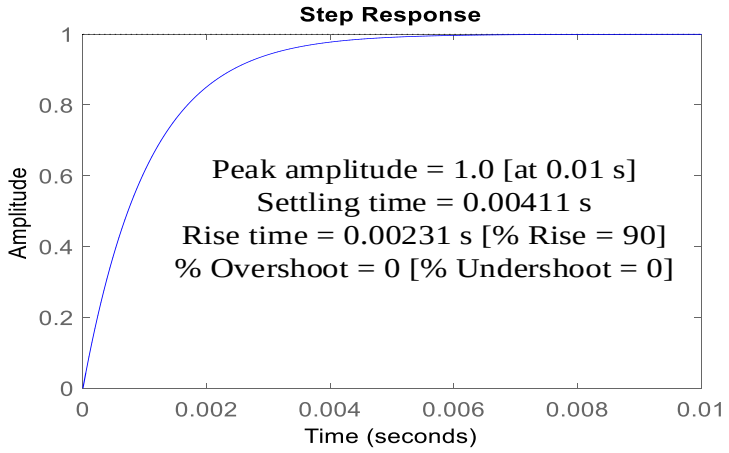

Fig. 3.23. Var source open-loop unit step response

where,

$$K_p = 26817, T_p = 22668.$$

Its step response is shown in Fig. 3.23.

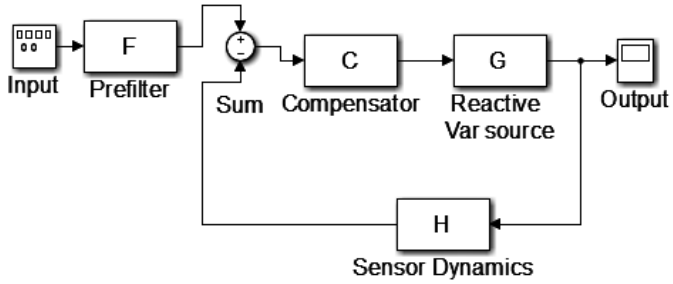

Fig. 3.24. Architecture of reactive power management system

A PI compensator is implemented. Its transfer function is provided in (3.26).

$$C = K_p + \frac{K_i}{s} \tag{3.31}$$

where,

$$K_p = 0.48287, K_i = 3.3057x10^{-7}.$$

Fig. 3.25 shows the closed-loop response of the designed reactive power management system. It is a stable loop with infinite gain margin and phase margin of 180° at 0 rads^{-1}. The system meets the required system specifications provided in Table 3.2.

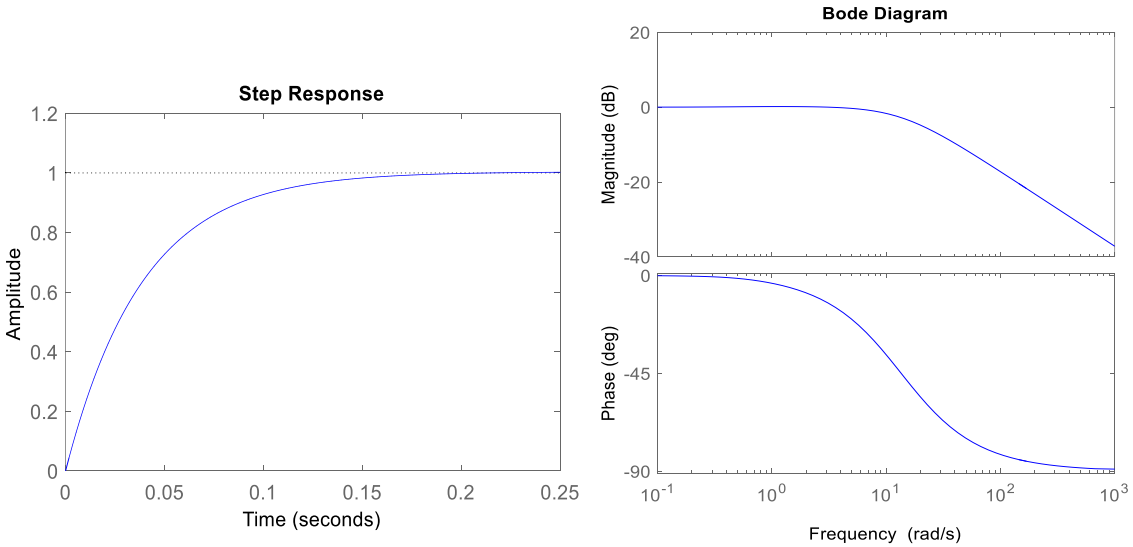

(a) Step response in time domain (b) Bode diagram

Fig. 3.25. Closed-loop response of reactive power management system in frequency domain

3.4.3 Voltage management systems

A) Grid ac voltage regulator

The open-loop transfer function of the voltage source is provided in (3.32).

$$G(s) = \frac{K_p}{1 + T_p s} \tag{3.32}$$

where,

$$K_p = 1.0, T_p = 50000.$$

Its step response is shown in Fig. 3.26.

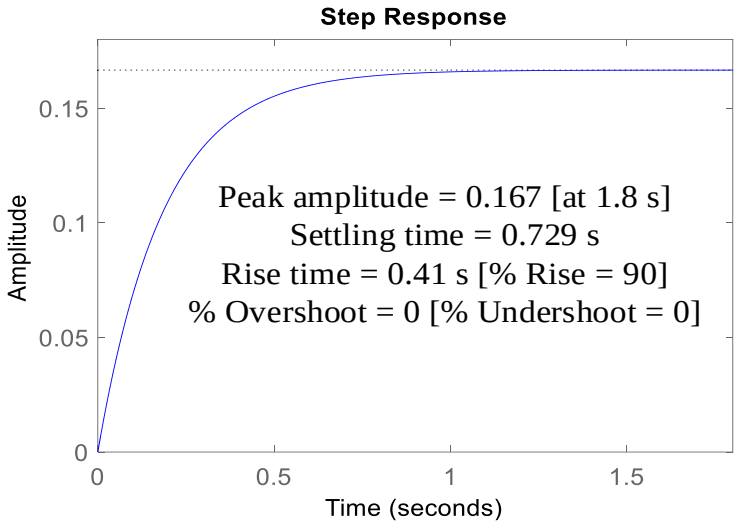

Fig. 3.26. Voltage source open-loop unit step response

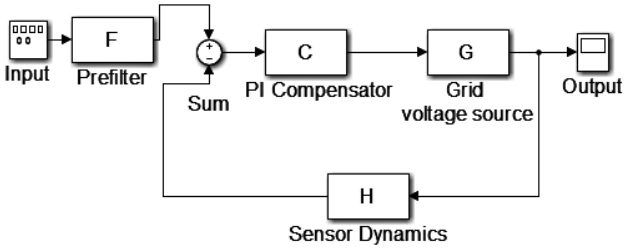

Fig. 3.27. Architecture of grid voltage regulator

A PI compensator is implemented. Its transfer function is provided in (3.33).

$$C = K_p + \frac{K_i}{s} \tag{3.33}$$

where,

$$K_p = 65933, K_i = 1.7973.$$

Fig. 3.28 shows the closed-loop response of the tuned grid voltage regulator. It is a stable loop with infinite gain margin and phase margin of 180° at $4.37x10^{-3}$ rads^{-1}. The system meets the required system specifications provided in Table 3.2.

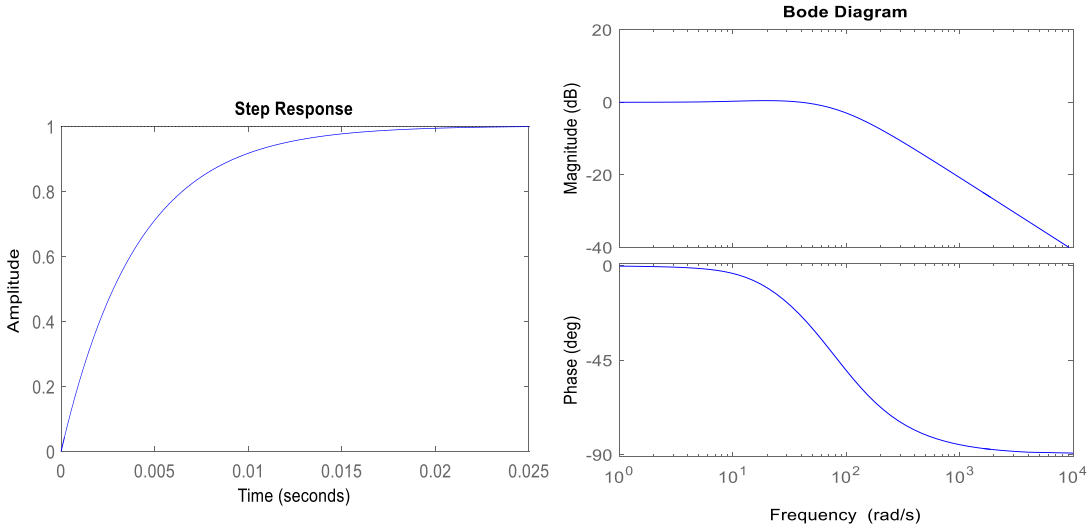

(a) Step response in time domain (b) Bode diagram

Fig. 3.28. Closed-loop response of grid voltage regulator in frequency domain

B) DC bus voltage regulator

The open-loop transfer function representing the dc voltage of the rotor-side converter is provided in (3.34). Its open-loop unit step response is provided in Fig. 3.29. A PI compensator whose transfer function is presented in (3.35) is implemented such that the converter closed loop meets the requirements in Table 3.2. Fig. 3.30 shows the closed-loop response of the tuned dc bus voltage regulator. It is a stable loop with infinitely large gain and phase margins.

$$G(s) = \frac{K_p}{1 + T_p s} \tag{3.34}$$

where,

$K_p = 178.63, T_p = 40000.$

$$C = K_p + \frac{K_i}{s} \tag{3.35}$$

where,

$K_p = 197.0, K_i = 0.00648.$

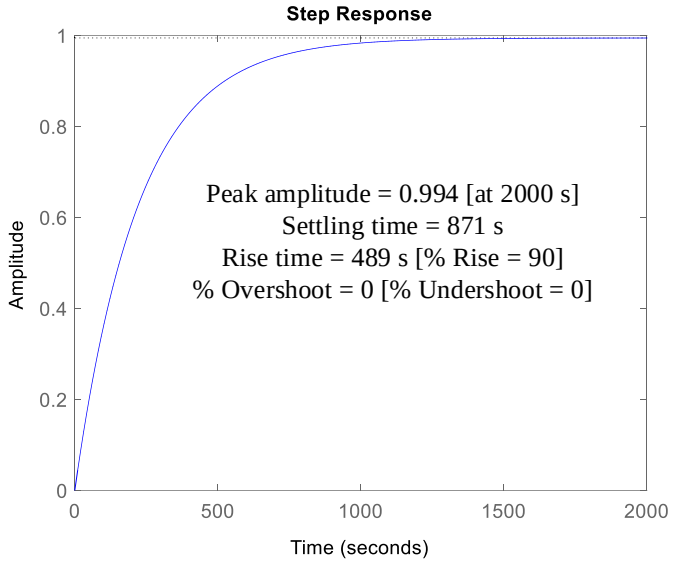

Fig. 3.29. DC bus voltage open-loop unit step response

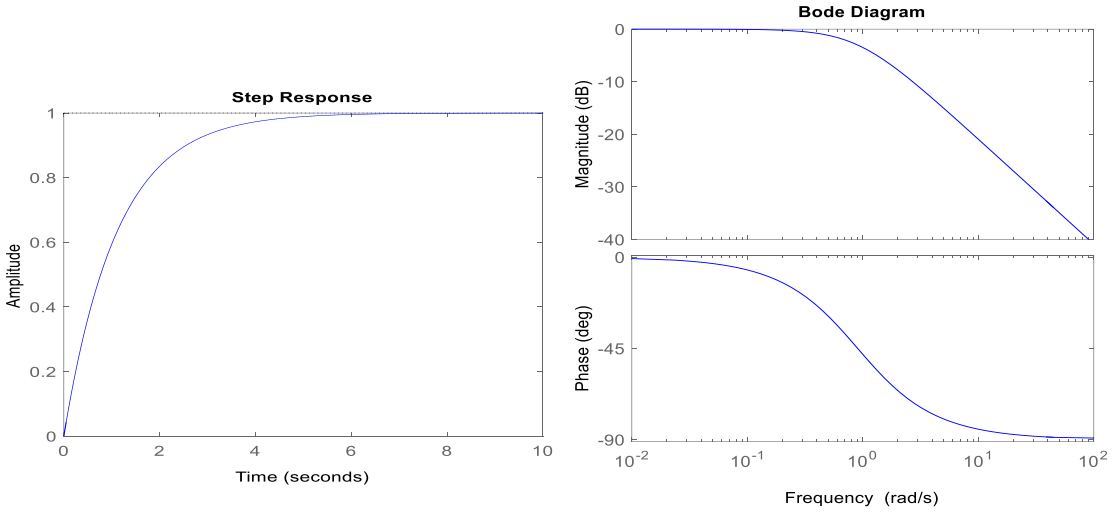

(a) Step response in time domain (b) Bode diagram

Fig. 3.30. Closed-loop response of dc bus voltage regulator in frequency domain

3.4.4 Converter current management systems

A) Grid-side converter current regulator

The unit step response of the grid-side converter is shown in Fig. 3.31. Its open-loop transfer function is provided in (3.36).

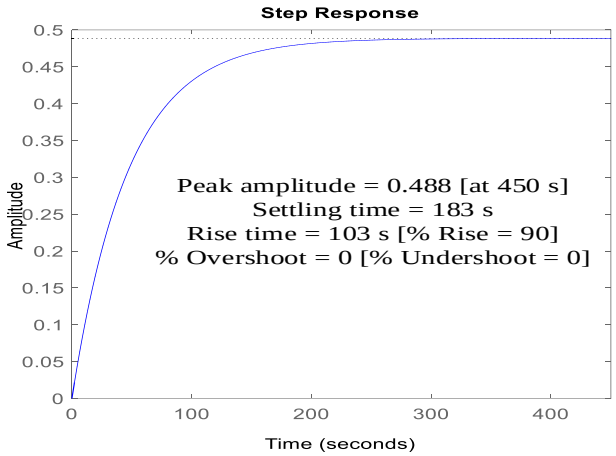

Fig. 3.31. Grid-side converter open-loop unit step response

$$G(s)=\frac{K_p}{1+T_p s} \tag{3.36}$$

where,

$$K_p = 0.95516, T_p = 91.698.$$

A PI compensator whose transfer function is presented in (3.37) is implemented such that the controller-converter closed loop meets the requirements in Table 3.2.

$$C = K_p + \frac{K_i}{s} \tag{3.37}$$

where,

$$K_p = 76.1112, K_i = 1.2276.$$

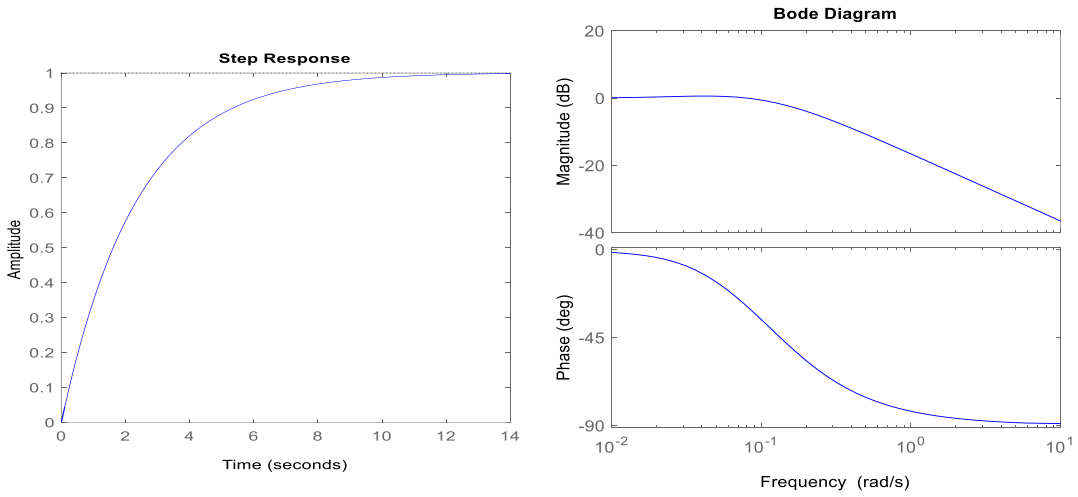

(a) Step response in time domain (b) Bode diagram

Fig. 3.32. Closed-loop response of grid-side current regulator in frequency domain

Fig. 3.32 shows the closed-loop response of the tuned grid-side converter current regulator. It is a stable loop with infinite gain margin and phase margin of 180° at 0 rads^{-1}. The closed-loop system meets the required system specifications provided in Table 3.2.

B) Rotor-side converter current regulator

The unit step response of the rotor-side converter is shown in Fig. 3.33. Its open-loop transfer function is provided in (3.38).

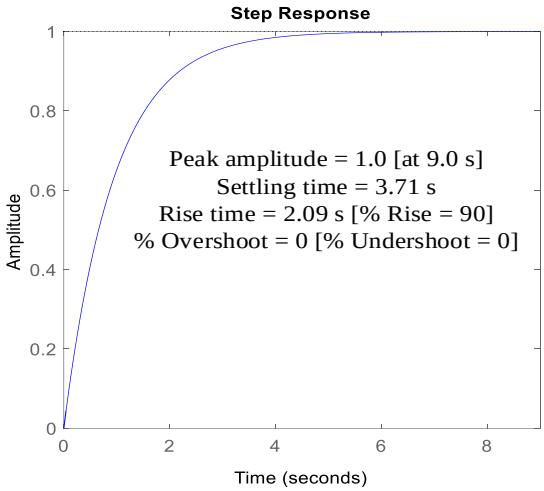

Fig. 3.33. Rotor-side converter open-loop unit step response

$$G(s) = \frac{K_p}{1 + T_p s} \tag{3.38}$$

where,

$K_p = 3.8315x10^5, T_p = 3.6368x10^5$.

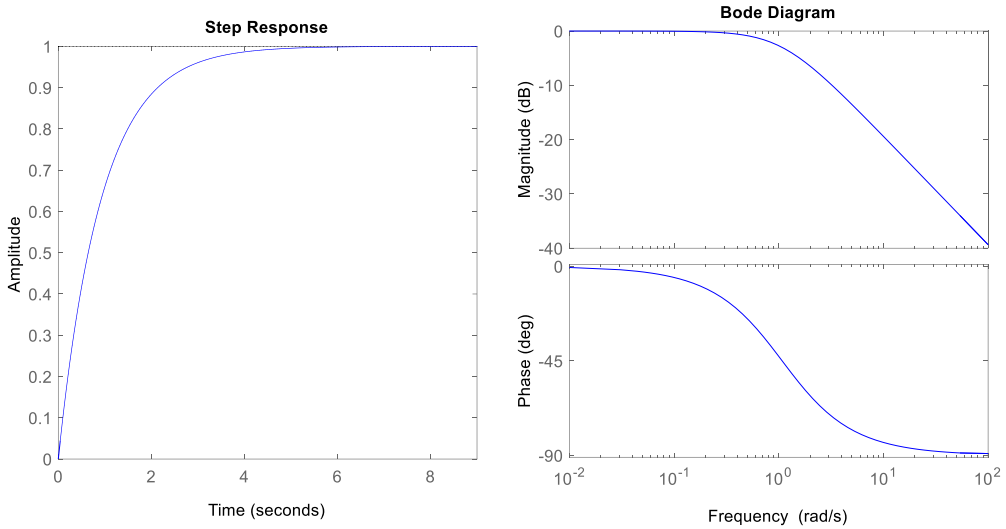

(b) Step response in time domain (b) Bode diagram

Fig. 3.34. Closed-loop response of rotor-side current regulator in frequency domain

A PI compensator whose transfer function is presented in (3.39) is implemented such that the controller-converter closed loop meets the requirements in Table 3.2.

$$C = K_p + \frac{K_i}{s} \tag{3.39}$$

where,

$K_p = 0.69473, K_i = 3.4514x10^{-6}$.

Fig. 3.34 shows the closed-loop response of the tuned rotor-side converter current regulator. It is a stable loop with infinite gain margin and phase margin of 180^o at 0 rads^{-1}.

As shown in Table 3.5, the closed-loop systems meet the required specifications provided in Table 3.4. The percent improvement in peak response ($\%A_{p,imp}$) is given by (3.40).

$$\%A_{p,imp} = \frac{(A_{pc} - A_{po})}{A_{pc}} x100 \tag{3.40}$$

where,

A_{pc} is closed-loop step response.

A_{po} is open-loop step response.

Table 3.5. Summary of system response to unit step signal

	Without regulator			**With regulator**			
Plant	A_{po} (Peak amplitude)	$t_{set}(s)$ (Settling time)	$t_{ris}(s)$ (Rise time)	A_{pc} (Peak amplitude)	$t_{set}(s)$ (Settling time)	$t_{ris}(s)$ (Rise time)	% $A_{p,imp}$ (Improvement in A_p)
Wind turbine	0.169 at 2.5s	0.905	0.508	1.0 at 2.5s	1.51	0.748	83.10
Active power source (generator)	0.999 at 6000s	2260	1270.00	1.0 at 14s	9.55	2.45	0.10
Capacitive reactive power source	1.0 at 0.01s	0.00411	0.00231	1.0 at 0.25s	0.233	0.0761	0.00
Grid AC voltage source (generator)	0.167 at 1.8s	0.729	0.41	1.0 at 0.025s	0.022	0.00821	83.33
DC bus voltage source (C_{rotor})	0.994 at 2000s	871.00	489.00	1.0 at 2000s	11.12	3.00	0.60
Grid AC current source (C_{grid})	0.488 at 450s	183.00	103.00s	1.0 at 450s	9.45	2.67	51.20
Rotor-side DC current source (C_{rotor})	1.0 at 9.0s	3.71	2.09	1.0 at 9.0s	2.55	1.10	0.00

3.5 Implementation of Control Strategies

The converter is used for power control. The composite ac-ac converter consists of two converters, namely, ac-dc (rotor side) and dc-ac (grid side) converters.

3.5.1 Power and pitch control systems

The pitch angle is maintained constant at zero degree until the speed reaches point D of the tracking characteristic. After point D, the pitch angle is proportional to the speed deviation from point D speed. The control system is shown in Fig. 3.35.

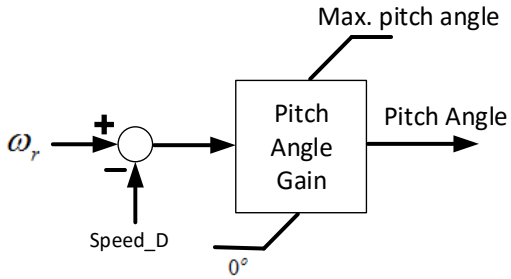

Fig. 3.35. Pitch angle control system

The power is controlled so as to follow a pre-defined characteristic, called power-speed characteristic, as shown in Fig. 3.36.

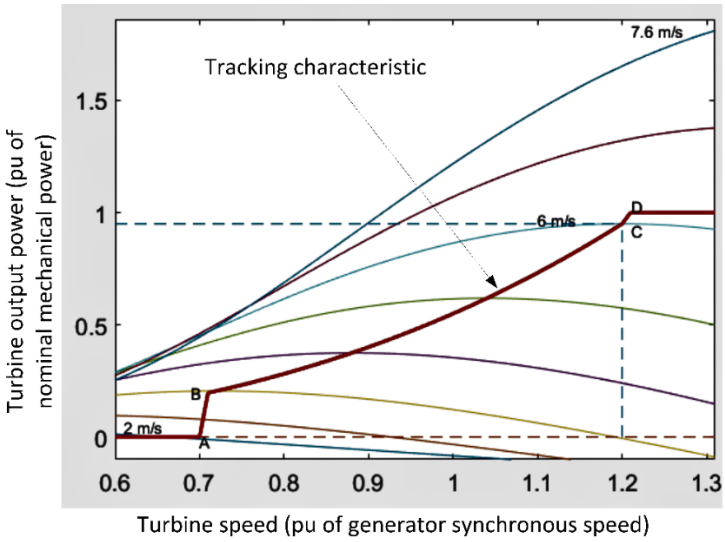

Fig. 3.36. Turbine power characteristics (pitch angle $\beta = 0$)

3.5.2 Rotor-side converter control system

The rotor-side converter is used to control the wind turbine output power and the voltage (or reactive power) measured at the grid terminals, as shown in Fig. 3.37.

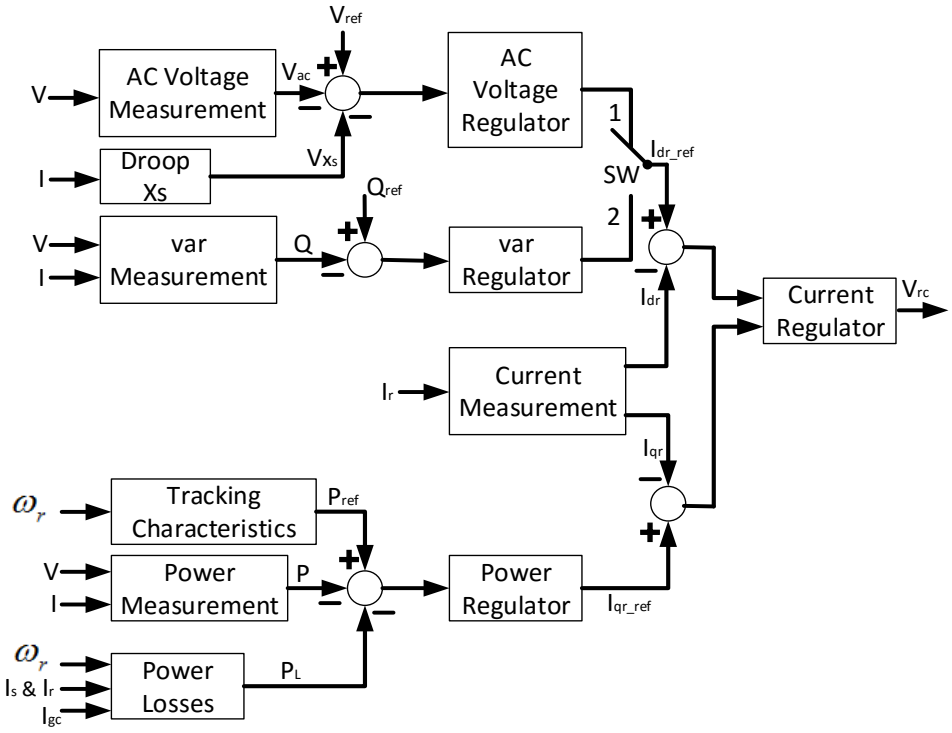

Fig. 3.37. Rotor-side converter voltage and reactive power control systems

3.5.3 Grid-side converter control system

Fig. 3.38 depicts the grid-side converter. The converter is used to inject or absorb reactive power and to regulate the voltage of the dc bus capacitor.

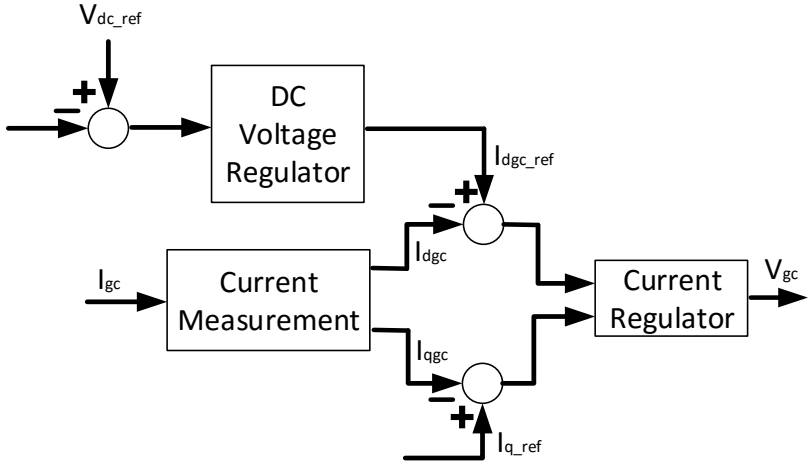

Fig. 3.38. Grid-side converter dc bus voltage and reactive power control systems

3.6 Results and Discussion

The generator open-loop unit step response shown in Fig. 3.20 is indicative of a stable system with poor response. A PI feedback regulator is therefore tuned to improve its response while

retaining its stability, as shown in Fig. 3.21. Fig. 3.22 depicts the closed-loop step response of the active power regulator in time and frequency domains. Each of the regulators in this report has been designed to improve the response of its plant while ensuring that the plant remains stable, as shown in Table 3.5.

The wind energy captured by the wind turbine is converted into electrical power by the induction generator. The generated power is wheeled to the grid via the stator and rotor windings. In order to control the wind turbine mechanical power, the designed pitch angle control system generates the *pitch angle command* (Fig. 3.35) to control the turbine blade. The power is controlled to follow a predefined power-speed characteristic, called tracking characteristic. The power-speed characteristic used is depicted in Fig. 3.36. It shows the tracking characteristic (ABCD) superimposed on the mechanical power characteristics of the turbine at different wind speeds. For the power control loop (Fig. 3.37), the actual speed of the turbine ω_r is measured and the corresponding mechanical power of the tracking characteristic is computed and used as reference power. The error obtained from the reference power (P_{ref}), measured power *(P)* and power losses *(P_L)* is used to generate the rotor-side converter voltage command. The governing control strategy is exclusively PV or PQ control and it is determined by the position of switch SW shown in the figure. When SW is in position 1, PV control is selected. When in position 2, PQ control prevails. The AC/DC/AC converter has been realized in two stages: the rotor-side converter (C_{rotor}) and the grid-side converter (C_{grid}). C_{rotor} and C_{grid} are Voltage-Sourced Converters which use forced-commutated power electronic devices (IGBTs) for voltage synthesis. A capacitor is linked to the dc bus to serve as dc voltage source. C_{grid} is integrated to the grid via a coupling inductor. The capacitance of the capacitor and the inductance of the inductor are realized from the design of converter voltage and current regulators, respectively. In order to control the dc bus voltage and the reactive power (or the voltage) at the grid terminals, the rotor-side converter control system generates the *voltage command* V_{rc} (Fig. 3.37) to control C_{rotor}, while the grid-side converter control system generates the *voltage command* V_{gc} (Fig. 3.38) to control C_{grid}.

3.7 Conclusion

In summary, this chapter has discussed mathematical modeling of the machines in the system under study and the control systems designed. The machines in the utility and micro-grid sides of the test bed have been modeled and presented. The controllers consist of active power management systems, reactive power management system, voltage management systems and converter current management systems. The regulators are combined to implement two mutually exclusive control regimes: the active power-voltage (PV or V) control and the active-reactive

power (PQ or Q) control, as presented in chapter three. In order to validate the system under study, short circuit dynamic analysis has been performed in grid-connected mode and presented in the next chapter.

Chapter 4: Short Circuit Dynamic Analysis in Grid-Connected Mode

This chapter presents grid-connected short circuit dynamic analysis as a technical validation of the test bed developed in the previous chapter. While the micro-grid is grid-connected and under V and Q controls, short circuit faults are applied at different locations in utility and micro-grid. The fault is applied at 30.00 s and withdrawn at 32.00s, while dynamic response of the network for 50 seconds in terms of four parameters (active power, reactive power, voltage and current) are obtained and plotted. The short circuits applied are single line-to-ground, line-to-line, three phase bolted short circuit, and cross-country at requisite micro-sources and feeders.

4.1 Characterization of Three Phase Short Circuit

A power system operates successfully under normal (and abnormal) conditions if certain requirements are satisfied. These requirements include ensuring that power generation meets power demand and losses; bus voltage magnitudes remain close to their nominal values, generators operate within specific real and reactive power limits; and transmission lines, feeders and transformers are not overloaded [35]. The load flow is therefore performed to ensure that above requirements are satisfied by computing bus voltage magnitude and angle under balanced steady-state conditions. These steady-state bus conditions are then used for dynamic analysis as initial conditions. In Chapters 4, 5 and 6, measurements are based on three phase quantities as explained in Sections 4.3 and 6.1.

In a generator, fault current is initially around 8 time's full-load current. It decays rapidly to around 5 times full-load current before decaying less rapidly to less than full-load current value. These three stages of fault current envelop in the direct axis are called sub-transient $(X_d^{''})$, transient $(X_d^{'})$ and steady-state (X_d) respectively. At no load, the electromagnetic force (e.m.f.) is same as the system voltage, *V*, which at the nominal value is 1.0 pu. At any other load the e.m.f. is greater than at no load and given by (4.1) to (4.3). Consequently, in increasing magnitude, the direct-axis reactances are $(X_d^{''}) < (X_d^{'}) < (X_d)$ [77].

$$E'' = [(V + X_d'' I \sin\phi)^2 + (X_d'' I \cos\phi)^2]^{\frac{1}{2}} \quad (4.1)$$

$$E' = [(V + X_d' I \sin\phi)^2 + (X_d' I \cos\phi)^2]^{\frac{1}{2}} \quad (4.2)$$

$$E = [(V + X_d I \sin\phi)^2 + (X_d I \cos\phi)^2]^{\frac{1}{2}} \quad (4.3)$$

While the current associated with (4.3) is a steady value, the currents associated with (4.1) and (4.2) are initial values at the onset of short circuit. The sub-transient value decays in a fraction of a second while the transient value takes several seconds to decay. The open-circuit sub-transient time constant (T_{d0}'') and transient time constant (T_{d0}') are typically 0.1s and 5.0s, respectively [61, 68, 78, 79].

The initial bus condition showing the steady-state response of the index test bed developed in this project is shown in Appendix C4. Note that the steady-state (load flow) solution process achieved convergence as shown in Appendix C4. A summary of the result of steady-state analysis is shown in Appendix C5. Note that the result shown excludes the state of each element in the test bed; it only shows the basic measurements for simplicity. In line 34 to 36, observe the three phase voltage of the synchronous machine (SM) which is linked to the system's slack bus. After load flow, the per phase rms voltages of the bus are $8126.86\angle 0^o$, $8126.86\angle 120^o$ and $8126.86\angle -120^o$. Its rms line-to-line no-load voltage is 13.8kV. These steady-state values are then used as initial conditions for the short circuit dynamic analysis presented in the subsequent sections of this Chapter and in Chapter 5.

4.2 Short Circuit in a Power System

In Fig. 4.1, assuming the power system shown is in steady-state condition and consider a three phase-to-earth short circuit at point F2. G1 and G2 are generators. T and L are transformer and load, respectively.

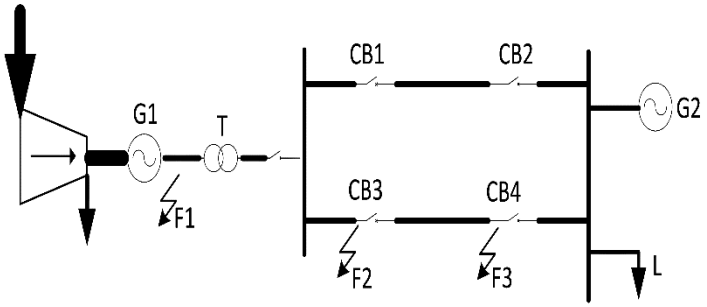

Fig. 4.1. Typical power system with short-circuit points F1, F2 and F3

It is accurate to view fault F2 as a modified generator fault which includes the effect of transformer. In order to obtain effective reactance, $x_d^{"}$ (or $x_d' \; or \; x_d$), the transformer reactance, X_T, is added to the reactance $X_d^{"}$, $X_d^{'}$ or X_d as given in (4.4), (4.5) and (4.6) [61, 68].

$$x_d^{"} = X_d^{"} + X_T \tag{4.4}$$

$$x_d^{'} = X_d^{'} + X_T \tag{4.5}$$

$$x_d = X_d + X_T \tag{4.6}$$

The amplitude of the ac fault current in the sub-transient state, $i_m^{"}$, transient state, $i_m^{'}$, and steady state, i_m^{∞}, is presented in (4.7), (4.8) and (4.9), respectively.

$$i_m^{"} = \frac{E_{fm}}{x_d^{"}} \tag{4.7}$$

$$i_m^{'} = \frac{E_{fm}}{x_d^{'}} \tag{4.8}$$

$$i_m^{\infty} = \frac{E_{fm}}{x_d} \tag{4.9}$$

Addition of X_T attenuates the magnitude of the currents given in (4.7), (4.8) and (4.9). Secondly, the transformer resistance, R_T, speeds up the rate of dissipation of the stored magnetic energy so that the short circuit current (dc component) decays more rapidly. Thirdly, the transformer reactance increases the time constants as given in (4.10) and (4.11) [80-86].

$$T_{d(network)}^{"} = T_d^{"}\left(\frac{X_d^{'}}{X_d^{"}}\right)\left(\frac{X_d^{"} + X_T}{X_d^{'} + X_T}\right) \tag{4.10}$$

$$T_{d(network)}^{'} = T_d^{'}\left(\frac{X_d}{X_d^{'}}\right)\left(\frac{X_d^{'} + X_T}{X_d + X_T}\right) \tag{4.11}$$

In order to simplify instrumentation, the power-invariant right-handed *dq0* transform [87] is applied to the micro-source's stator voltage as presented in (4.12).

$$V_{dq0} = \sqrt{\tfrac{2}{3}}\begin{bmatrix} \cos(\theta) & \cos\left(\theta - \frac{2\pi}{3}\right) & \cos\left(\theta + \frac{2\pi}{3}\right) \\ -\sin(\theta) & -\sin\left(\theta - \frac{2\pi}{3}\right) & -\sin\left(\theta + \frac{2\pi}{3}\right) \\ \frac{\sqrt{2}}{2} & \frac{\sqrt{2}}{2} & \frac{\sqrt{2}}{2} \end{bmatrix} * \begin{bmatrix} V_a \\ V_b \\ V_c \end{bmatrix} \tag{4.12}$$

where,

V_{dq0} represents the per unit (p.u.) voltages in the *dq0* axes.

V_a, V_b and V_c represent the p.u. voltages in the abc reference frame.

For instrumentation purpose, the sequence voltages and currents are measured using (4.13).

$$V_{012} = A^{-1} * V_{abc} \tag{4.13}$$

where,

$V_{012} = \begin{bmatrix} V_0 \\ V_1 \\ V_2 \end{bmatrix}$ and represents the p.u. zero-, positive- and negative-sequence voltages.

$V_{abc} = \begin{bmatrix} V_a \\ V_b \\ V_c \end{bmatrix}$ and represents the p.u. voltages in the abc reference frame.

$$A = \begin{bmatrix} 1 & 1 & 1 \\ 1 & \alpha^2 & \alpha \\ 1 & \alpha & \alpha^2 \end{bmatrix} \tag{4.14}$$

$$\alpha = 1.0 \angle 120^0$$

Equations (4.13) and (4.14) are used to develop the Clarke-transformed voltages shown in the figures contained in Chapters Four and Five.

4.3 Validating System Response to Three Phase Short Circuit using Dynamic Analysis (Grid-connected Mode)

The test bed presented in this report was developed as a working platform for a study which seeks to propose a new relay for micro-grid. The anticipated protective system would be based on measurement of three phase power. Therefore, three phase nominal active and reactive power is investigated and presented in this Chapter and in Chapter Five. In Fig. 4.1 to Fig. 4.11, X represents the horizontal axis while Y represents the vertical axis.

Fig. 4.2 shows the response of the micro-grid during normal operation under V and Q controls. From the results of the simulation, each of the micro-sources in the micro-grid generates 85.15% of its nominal rating when the system is free of stress as shown. Also, when operating conditions are normal, the micro-source absorbs more reactive power from the external reactive power compensator under V control than Q control - indicating reactive support from its converter dc

bus under Q control. However, this is not sustainable for continuous operation as this support is limited to the small capacity of the converter capacitor linked to its dc bus [88].

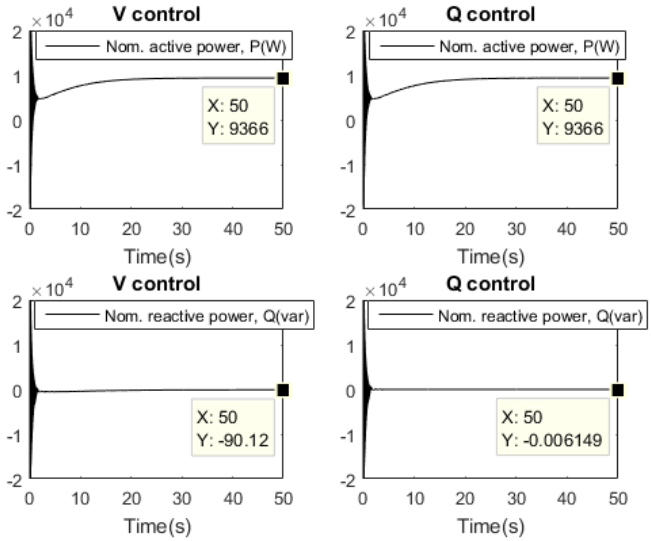

Fig. 4.2. Grid-connected response of micro-grid under normal operation in V and Q controls

In grid-connected mode, three phase-to-earth bolted short circuit fault is applied at 30.00s and withdrawn at 32.00s. The duration of 2-second is sufficient to allow the micro-grid respond to external stress. The stress is also introduced at a time that the micro-sources have achieved steady-state. Dynamic simulation of the test bed (synch. generator, micro-grid feeders and DFIG) under short circuit is performed for 50.00 simulation seconds. The responses of the test bed for different fault locations and DFIG controller in voltage, V, and reactive power, Q, control are obtained and presented in Fig. 4.3 to Fig. 4.11. In the figures, (a) depicts V control while (b) depicts Q control. The responses of MS1 and feeder-a to faults at the terminals of utility generator are presented in Fig. 4.3 and Fig. 4.4, respectively. At 50.0s, under V control (Fig. 4.3(a)), MS1 generates 9.356kW and contributes 2.577kvar to the fault at utility generator terminals with increasing instability. Under Q control, it generates 9.374kW and contributes only 3.972var to the same fault (Fig. 4.3(b)) with superior stability. This is consistent with the power management capability of DFIG as published by Moayed Moghbel et al. in [88] and in [89-91]. Because the utility is tied to the micro-grid, the high-magnitude utility fault results in post-fault voltage oscillation in the micro-sources and power instability in the feeders, as shown in Fig. 4.3 to Fig. 4.6. Post-fault instability is a major challenge of micro-grid, as published in [22, 92].

Observe that the responses of the feeder in Fig. 4.4(a) and Fig. 4.4(b) are same. This is indicative of the passive nature of the feeder which makes it unable to offer distinct responses under both V and Q controls.

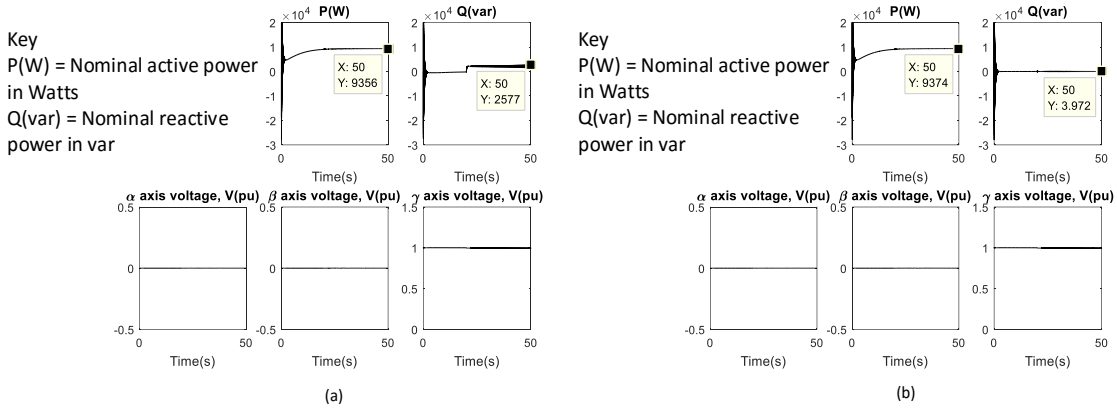

Fig. 4.3. Response of MS1 when utility generator terminals are short-circuited at 20s to 22s - V and Q controls

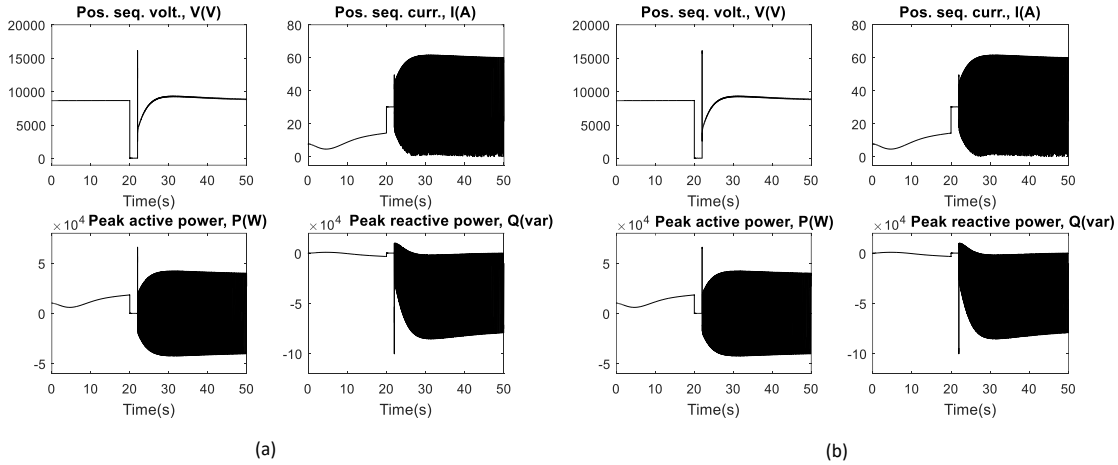

Fig. 4.4. Response of feeder-a when utility generator terminals are short-circuited at 20s to 22s – V and Q controls

The responses of MS1 and feeder-a to faults at the ends of transmission lines (closer to the micro-grid) are presented in Fig. 4.5 and Fig. 4.6, respectively. At 50.0s, under V control (Fig. 4.5(a)), MS1 generates 9.352kW and contributes 2.699kvar to utility fault at the end of transmission lines. Under Q control, it generates 9.372kW and contributes only 4.189var to the same fault (Fig. 4.5(b)). This shows superior reactive power management capability of DFIG under Q control as published by Moayed Moghbel et al. in [88] and in [93, 94]. Because the micro-grid is grid-connected, the high-magnitude utility fault provokes post-fault voltage oscillation in the micro-sources and power instability in the feeders, as shown in Fig. 4.5 and Fig. 4.6. This is a major challenge of micro-grid operation, as published in [26, 95, 96].

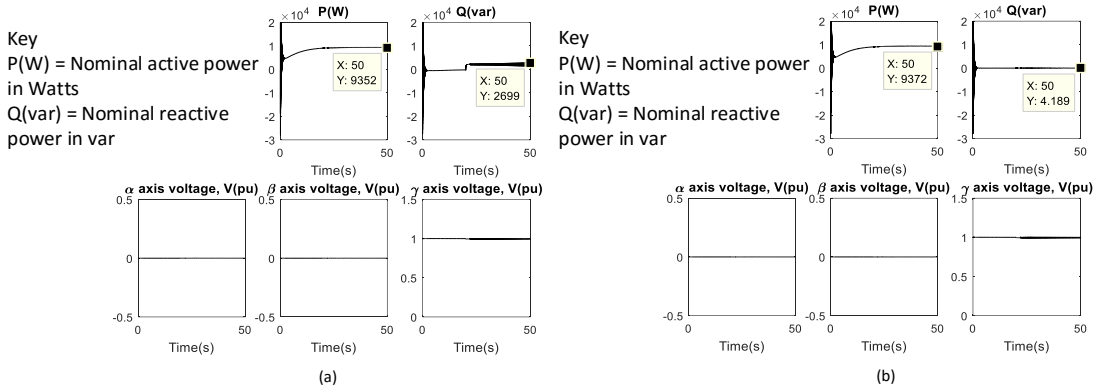

Fig. 4.5. Response of MS1 when ends of transmission lines are short-circuited at 20s to 22s – V and Q controls

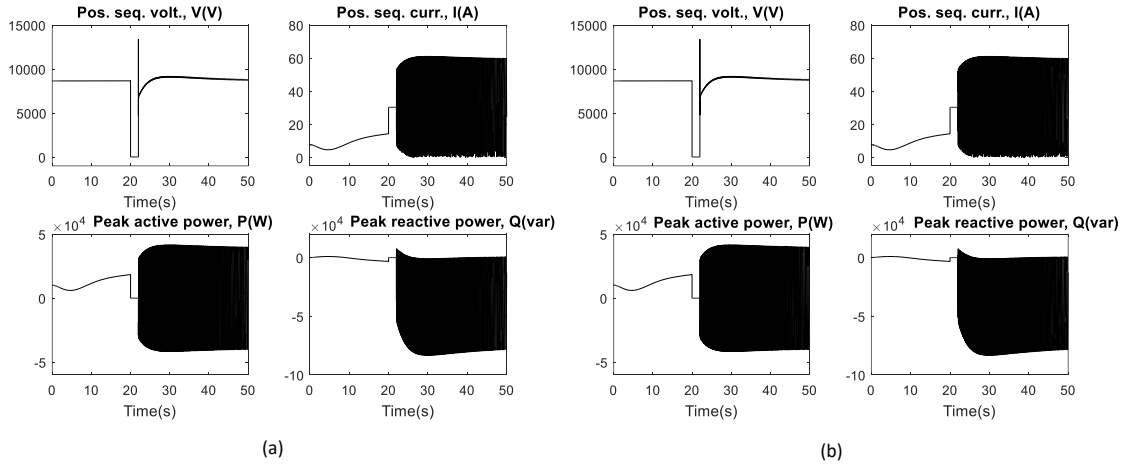

Fig. 4.6. Response of feeder-a when ends of transmission lines are short-circuited at 20s to 22s – V and Q controls

The responses of MS1, MS2 and feeder-a to micro-grid fault at the terminals of MS1 in grid-connected mode are presented in Fig. 4.7, Fig. 4.8 and Fig. 4.9, respectively. At 50.0s, under V control (Fig. 4.7(a)), MS1 generates 7.696kW while it absorbs 0.1209kvar from both sources when three phase bolted short circuit fault is applied at its terminals. This active power it generates represents 69.96 % of its nominal rating. For the same fault condition under Q control, it generates 9.347kW which represents 84.97 % of its nominal rating but absorbs only 0.08177var from both sources (Fig. 4.7(b)). This validates the reactive power management capability of DFIG as reported by Moayed Moghbel et al. in [88] and in [89-91]. Because the simulated fault is a three phase bolted short circuit, it provokes post-fault voltage and power instability in the micro-grid, as shown in Fig. 4.7 to Fig. 4.9. However, because it is a micro-grid fault (not utility fault), severity of resultant voltage oscillation is not as virulent as obtainable in utility fault (Fig. 4.3 to Fig. 4.6).

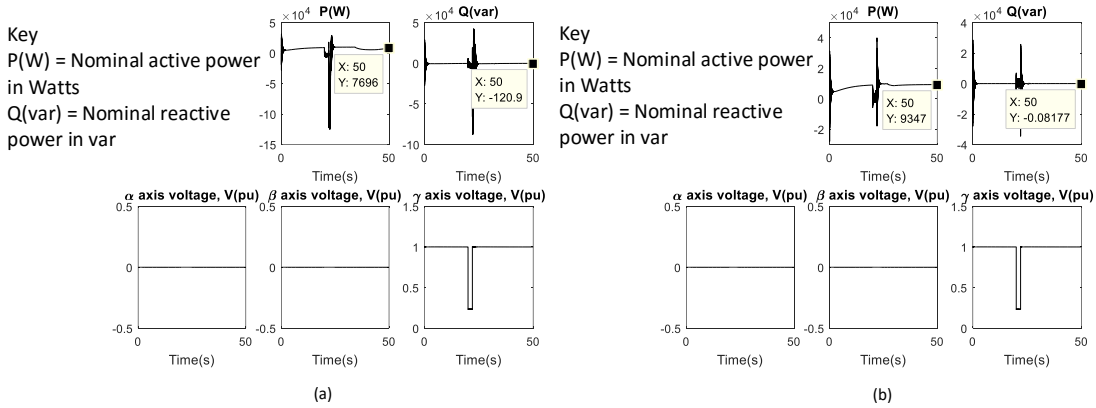

Fig. 4.7. Response of MS1 when its terminals are short-circuited at 20s to 22s – V and Q controls

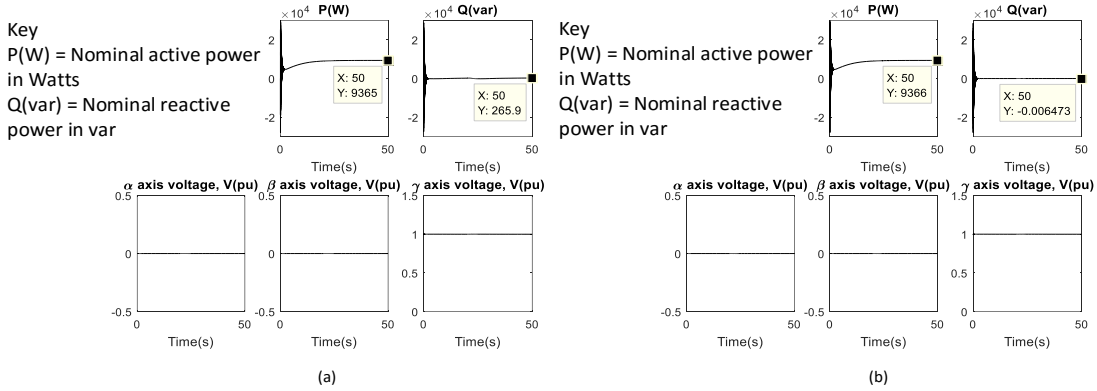

Fig. 4.8. Response of MS2 when terminals of MS1 are short-circuited at 20s to 22s – V and Q controls

From Fig. 4.9((a) and (b)), observe that the peak active power reverses to negative 6.853kW during the fault, indicative of bidirectional power flow on the feeder as reported by Miranda et al. in [97].

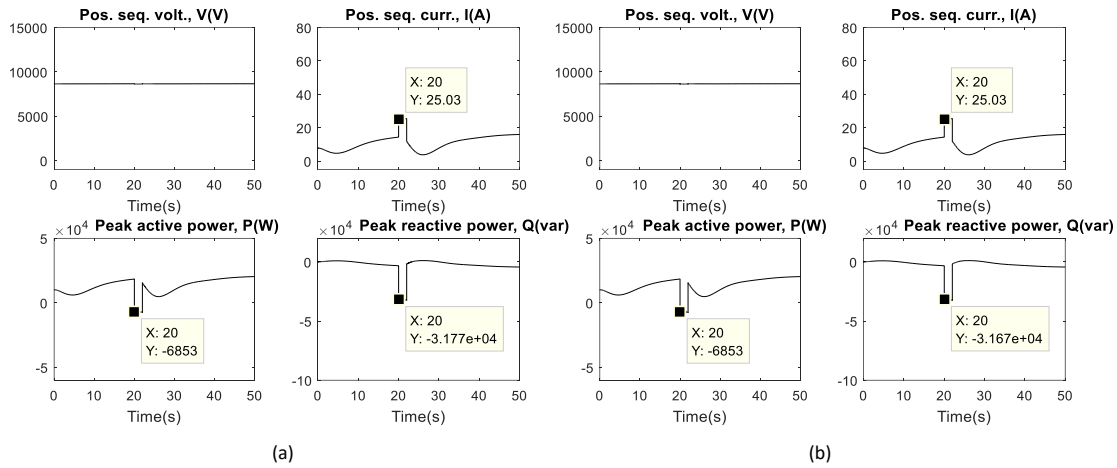

Fig. 4.9. Response of feeder-a when terminals of MS1 are short-circuited at 20s to 22s – V and Q controls

The response of MS1 to cross-country fault at terminals of both MS1 and utility generator is presented in Fig. 4.10. Similarly, the response of feeder-a to cross-country fault at terminals of both MS1 and utility generator is presented in Fig. 4.11. At 50.0s, under V control (Fig. 4.10(a)), MS1 generates 7.579kW and supports the system with 2.564kvar when the system experiences cross-country three phase bolted short circuit. The active power of 7.579kW represents 68.90% of the nominal power rating of MS1. Under Q control, it generates 9.355kW and contributes only 3.962var to the same fault (Fig. 4.10(b)). This is consistent with the power management capability of DFIG as published by Moayed Moghbel et al. in [88] and in [89-91]. Note that the nominal active power generated by MS1 is severely compromised to the vicinity of -12.5kW shortly after the fault under V control. This indicates absorption of active power by MS1 from MS2, a measure of bidirectional flow of active power and power management capability of DFIG, as reported by Miranda et al. in [97].

Because the simulated fault is a cross-country three phase bolted short circuit, it provokes virulent post-fault voltage and power instability in the micro-grid, as shown in Fig. 4.10 and Fig. 4.11.

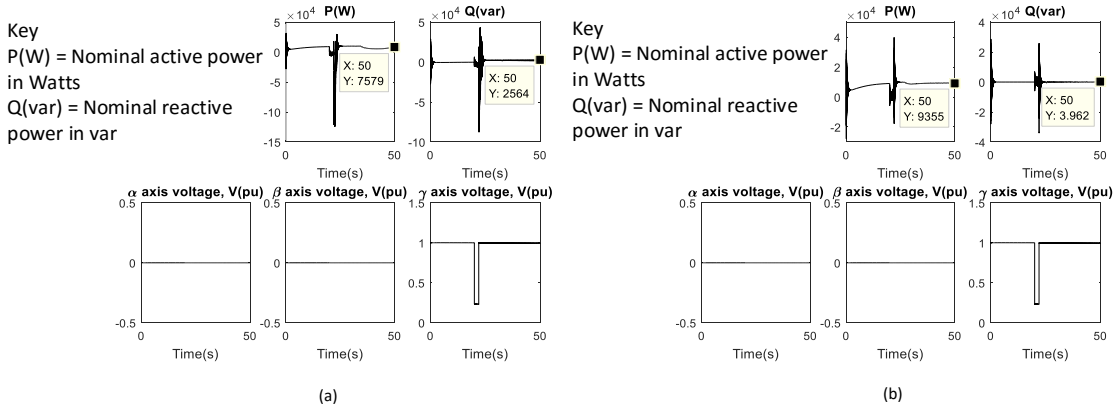

Fig. 4.10. Response of MS1 to a cross-country short circuit at its terminals and terminals of utility generator at 20s to 22s – V and Q controls

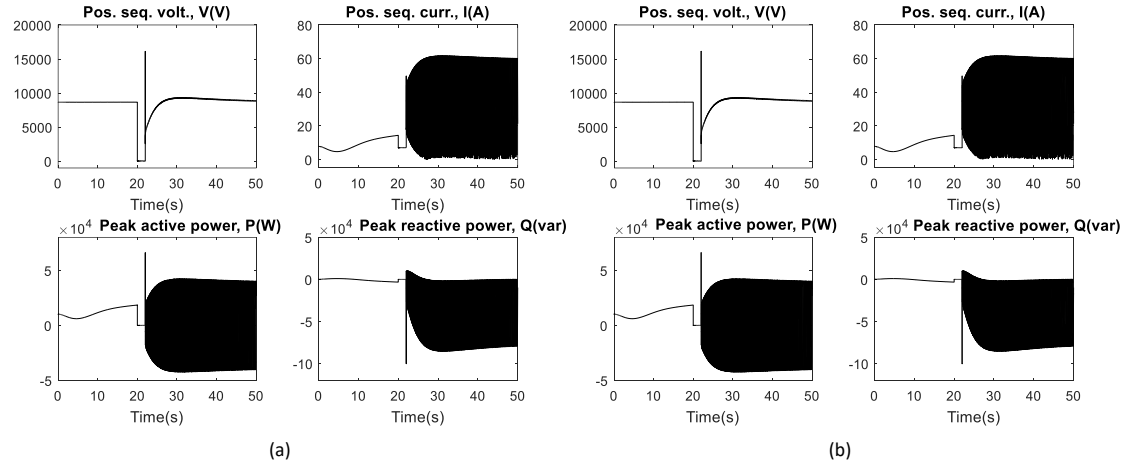

Fig. 4.11. Response of feeder-a to a cross-country short circuit at MS1 terminals and terminals of utility generator at 20s to 22s – V and Q controls

4.4 Conclusion

In conclusion, the system under study has been validated in grid-connected mode under voltage and reactive power controls using short circuit dynamic analysis and presented in this chapter. In this mode, the effect of the utility has been explored and documented. The results of the validation confirm the system's response to three phase bolted short circuit fault to be consistent with established short circuit theory. Since the micro-grid is capable of islanding, the system's response under islanded mode has also been investigated. Its response to short circuit in islanded mode under both control regimes have been simulated and presented in the succeeding chapter.

Chapter 5: Short Circuit Dynamic Analysis in Islanded Mode

This chapter presents dynamic short circuit analysis of the test bed as a technical validation in islanded mode. While the micro-grid is islanded by disconnecting the Point of Common Coupling, three phase bolted short circuit (SC), line-to-line SC and line-to-ground SC are applied to the micro-grid and the response of the network is investigated and presented in this chapter. In Fig. 5.1 to Fig. 5.19, X represents the horizontal axis while Y represents the vertical axis.

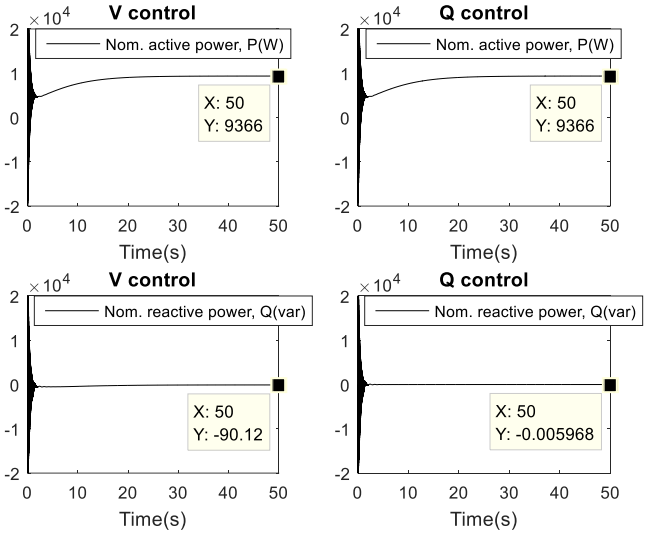

Fig. 5.1. Response of micro-grid under normal operation in V and Q controls

Fig. 5.1 shows islanded mode response of the micro-grid during normal operation under V and Q controls. From the results of the simulation, either of the micro-sources in the micro-grid generates 85.15% of its nominal rating when the system is free of stress as shown. Also, when operating conditions are normal, the micro-source absorbs more reactive power from the external reactive power compensator under V control than Q control - indicating reactive support from its converter dc bus under Q control. However, this is not sustainable for continuous operation as this support is limited to the small capacity of the converter capacitor linked to its dc bus.

Note the similarity between grid-connected normal response (Fig. 4.2) and islanded normal response (Fig. 5.1). The only difference is in the reactive power absorbed under Q control. Under grid-connected mode, the micro-source absorbs 0.006149var which is slightly more than 0.005968var it absorbs under islanded mode. This is indicative of reactive demand from the utility components.

5.1 Validating islanded mode system response to Three Phase Bolted Short Circuit using Dynamic Analysis

In islanded mode, three phase-to-earth bolted short circuit fault is applied at 30.00s and withdrawn at 32.00s. The duration of 2-second is sufficient to allow the micro-grid respond to external stress. The stress is also introduced at a time that the micro-sources have achieved steady-state. Dynamic simulation of the test bed (synch. generator, micro-grid feeders and DFIG) under short circuit is performed for 50.00s. The responses of the test bed for different fault locations and DFIG controller in voltage, V, and reactive power, Q, control are obtained and presented in Fig. 5.2 to Fig. 5.7.

At 50.0s and under V control (Fig. 5.2(a)) when three phase bolted short circuit is applied at its terminals, MS1 generates 5.628kW and absorbs 0.655kvar from its reactive var compensator and that of MS2. This active power represents 51.16% of its nominal rating. This is in contrast with Q control (Fig. 5.2(b)) where MS1 generates 9.241kW and absorbs only 0.4586var from the network at 50.00s. The active power of 9.241kW under Q control represents 84.00% of its nominal rating, indicating superior performance of the micro-source under Q control and system stress. This validates reactive power management capability of DFIG as published by Moayed Moghbel et al. in [88] and in [98-100].

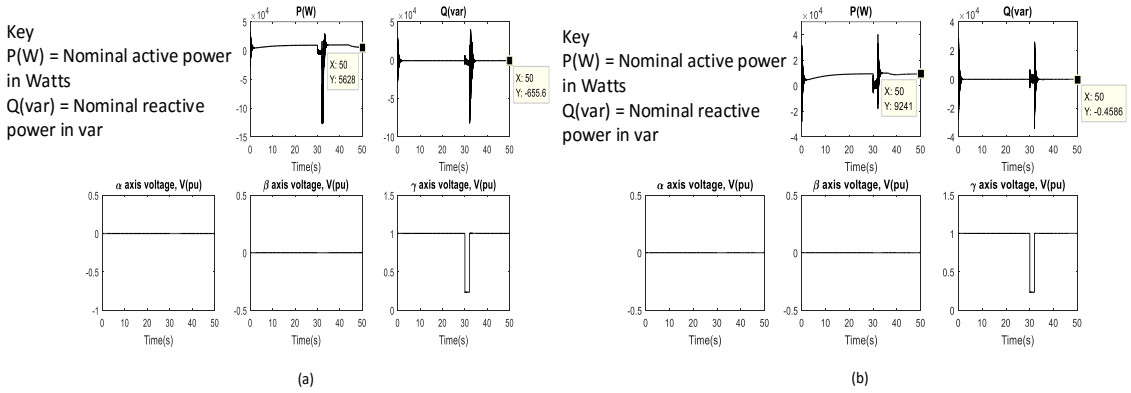

Fig. 5.2. Response of MS1 to three phase bolted short circuit – V and Q controls

In Fig. 5.3, the peak active power of feeder-a rises to 4.356kW in a direction opposite the nominal active power flow direction during the fault, indicating active power support from MS2 and feeder-b to feed the fault point in feeder-a. Similarly, reactive power flow on feeder-a rises to 8.586kvar in an opposite direction during the fault. Feeder-a experiences drop from 8.987kV to 4.658kV in positive sequence voltage during the fault, while positive sequence current rises from 0.2603A to 13.78A during the fault. This response is consistent with well-established short circuit theory on the effect of balanced SC on positive sequence quantities as published by Jan Machowski in [61].

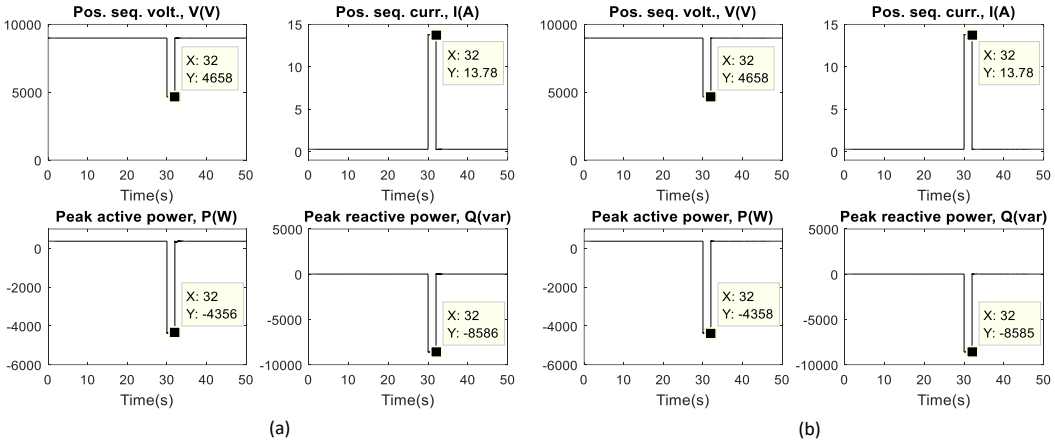

Fig. 5.3. Response of feeder-a to three phase bolted short circuit at terminals of MS1 – V and Q controls

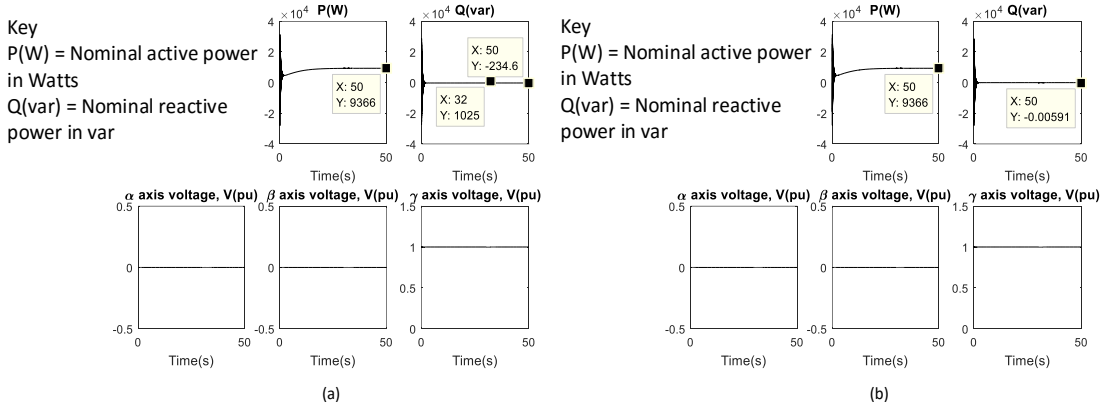

Fig. 5.4. Response of MS2 to three phase bolted short circuit at terminals of MS1 – V and Q controls

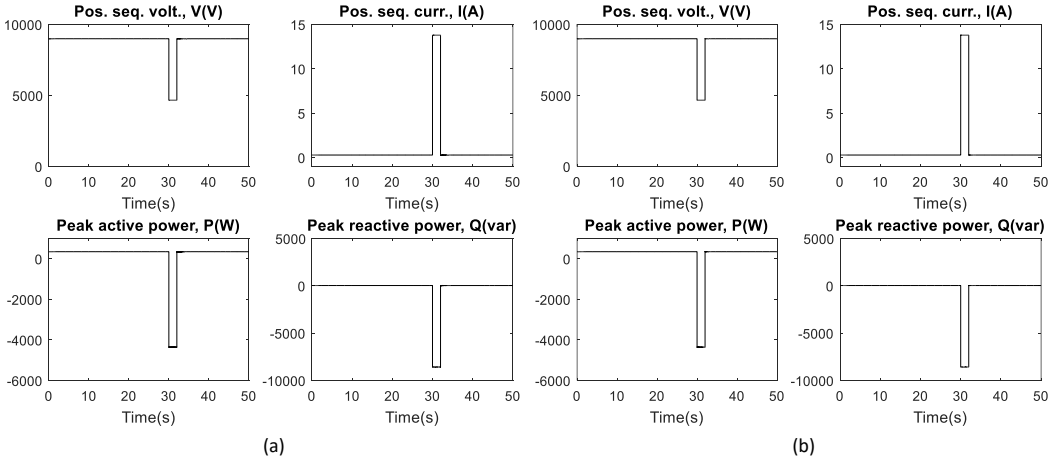

Fig. 5.5. Response of feeder-b to three phase bolted short circuit at terminals of MS1 – V and Q controls

Fig. 5.4((a) and (b)) shows that when MS1 is faulted, MS2 is undisturbed and generates active power to support the network in both V and Q control regimes. On the other hand, Fig. 5.5 ((a) and (b)) depicts the response of feeder-b under same SC condition. Since feeder-b is a passive element, it can be seen that its positive sequence voltage, positive sequence current, active power and reactive power are affected by the SC in both control regimes.

When both micro-sources experience three phase bolted cross-country SC at their terminals, under V control MS1 generates 5.615kW and absorbs 0.6556kvar at 50.00s, as shown in Fig. 5.6(a). The active power represents 51.05% of its nominal rating and is severely compromised during the fault.

At 50.00s and under Q control (Fig. 5.6(b)), during three phase cross-country SC, MS1 generates 9.237kW and absorbs only 0.4722 var. The active power represents 83.97% of its nominal rating, indicating superior DFIG's performance under Q control.

The feeder response to three phase cross-country SC is shown in Fig. 5.7. Observe the drop in the positive sequence voltage from 8.987kV to 2.093kV, this is consistent with established SC theory. Specially observe the drop in positive sequence current from 0.2744A to 0.06232A during the fault and compare this response with the rise in positive sequence current of Fig. 5.5 when only MS1 is short-circuited. The drop in positive sequence current of Fig. 5.7 is explained by the fact that under cross-country three phase SC, both micro-sources are stressed therefore the feeder cannot support its current since it is a passive element. As a passive element, the feeder lacks power generation or energy storage capability. Therefore, the feeder is neither able to provide long term energy support typical of a power generator nor short term energy support typical of an energy storage system. In addition, the currents from the micro-sources feed the fault points at their terminals, considering their small short circuit capabilities.

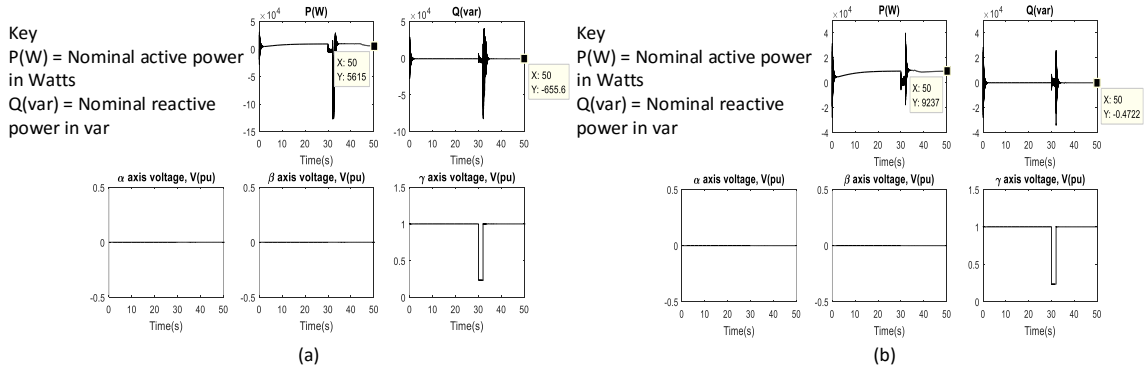

Fig. 5.6. Response of MS1 to three phase bolted cross-country short circuit at terminals of MS1 and MS2 – V and Q controls

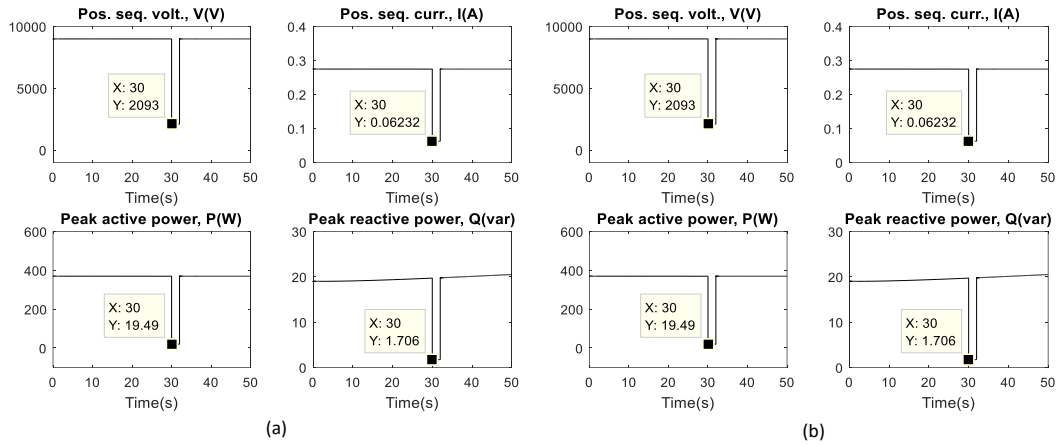

Fig. 5.7. Response of feeder-a to three phase bolted cross-country short circuit at terminals of MS1 and MS2 – V and Q controls

5.2 Validating Islanded Mode System Response to Line-to-Line Short Circuit using Dynamic Analysis

In islanded mode, line-to-line short circuit fault is applied between phase B and phase C at 30.00s and withdrawn at 32.00s. Under this short circuit, system's (micro-grid feeders and DFIG) dynamics are simulated for 50.00s. The test bed's responses for different fault locations and DFIG controller in voltage, V, and reactive power, Q, control are obtained and presented in Fig. 5.8 to Fig. 5.13.

At 50.0s and under V control (Fig. 5.8(a)) when line-to-line short circuit is applied at its terminals, MS1 generates 9.168kW and absorbs 0.6586kvar from its reactive var compensator and that of MS2. This active power represents 83.35% of its nominal rating. This is in contrast with Q control (Fig. 5.8(b)) where MS1 generates 9.367kW and absorbs only 0.001391var from the network at 50.00s. The active power of 9.367kW under Q control represents 85.15% of its nominal rating, indicating superior performance of the micro-source under Q control and system stress. This validates reactive power management capability of DFIG as published by Moayed Moghbel et al. in [88] and in [98-100].

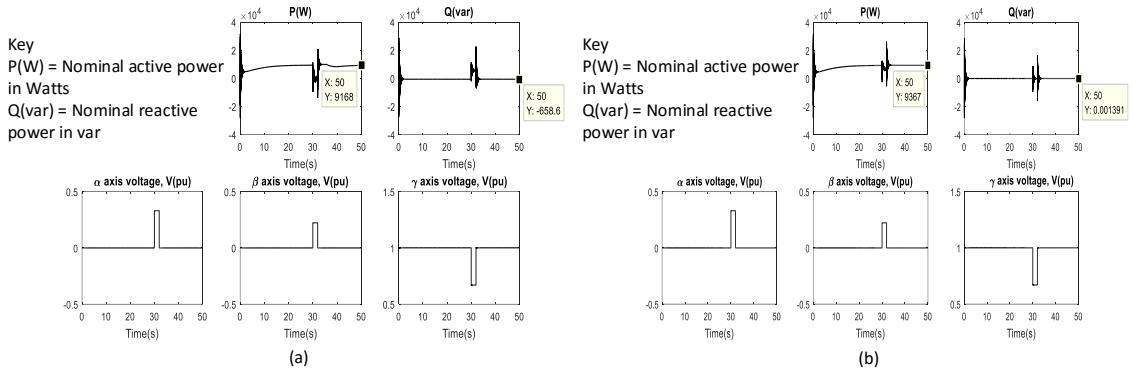

Fig. 5.8. Response of MS1 to L-L short circuit – V and Q controls

In Fig. 5.9, the peak active power of feeder-a changes to 1.994kW in a direction opposite the nominal active power flow direction during the fault, indicating active power support from MS2 and feeder-b to feed the fault point at MS1. Similarly, reactive power flow on feeder-a rises to 4.283kvar in an opposite direction during the fault. Observe the existence of negative sequence voltage and current of 2.299kV and 6.93A respectively during the fault. This is consistent with well-established short circuit theory on the effect of unbalanced SC on negative sequence quantities as published by Jan Machowski in [61].

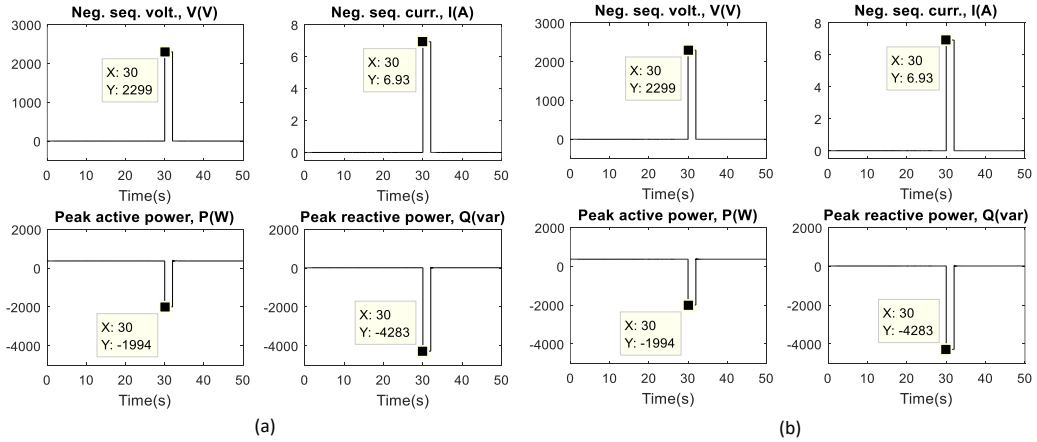

Fig. 5.9. Response of feeder-a to L-L short circuit at terminals of MS1– V and Q controls

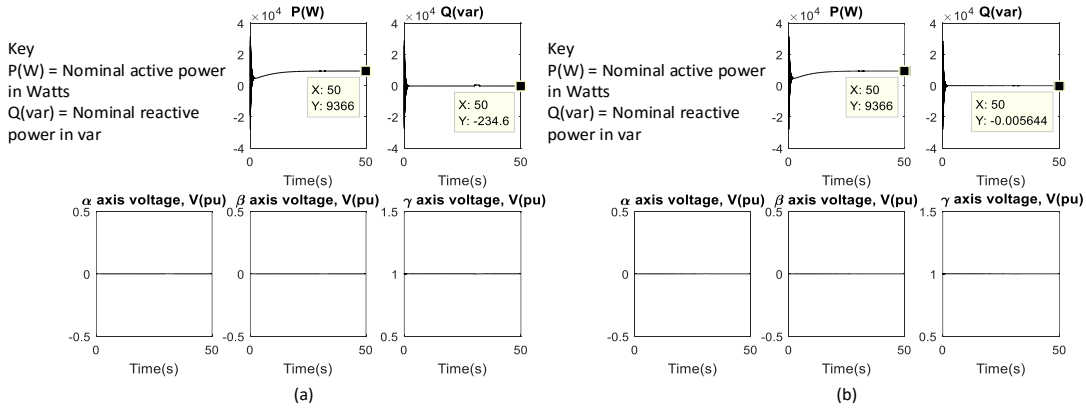

Fig. 5.10. Response of MS2 to L-L short circuit at terminals of MS1– V and Q controls

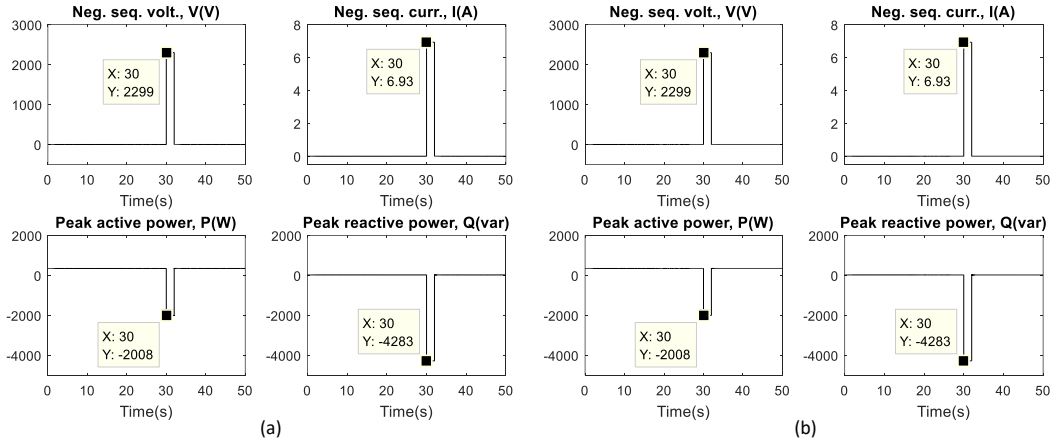

Fig. 5.11. Response of feeder-b to L-L short circuit at terminals of MS1– V and Q controls

Fig. 5.10((a) and (b)) shows that when MS1 is faulted, MS2 is undisturbed and generates active power to support the network in both V and Q control regimes. On the other hand, Fig. 5.11 ((a) and (b)) depicts the response of feeder-b under same line-to-line SC condition. Since feeder-b is a passive element, it can be seen that its negative sequence voltage, negative sequence current, active power and reactive power are affected by the SC in both control regimes.

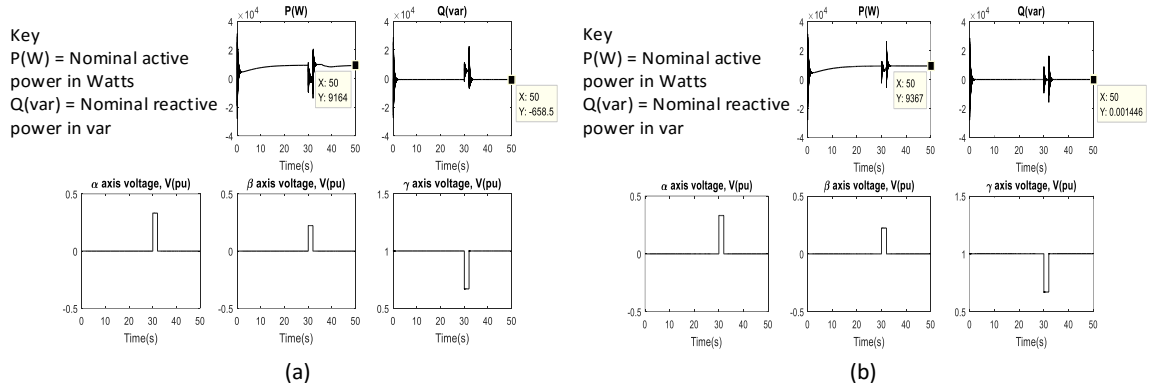

Fig. 5.12. Response of MS1 to L-L cross-country short circuit at terminals of MS1 and MS2 – V and Q controls

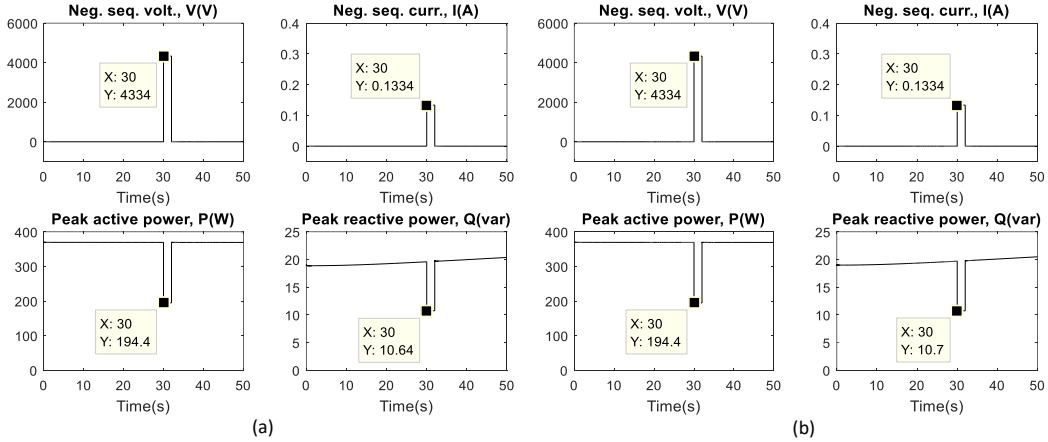

Fig. 5.13. Response of feeder-a to L-L cross-country short circuit at terminals of MS1 and MS2 – V and Q controls

When both micro-sources experience line-to-line cross-country SC at their terminals, under V control MS1 generates 9.164kW and absorbs 0.6585kvar at 50.00s, as shown in Fig. 5.12(a). The active power represents 83.31% of its nominal rating.

At 50.00s and under Q control (Fig. 5.12(b)), during line-to-line cross-country SC, MS1 generates 9.367kW and absorbs only 0.001446var. The active power represents 85.15% of its nominal rating, indicating superior DFIG's performance under Q control.

The feeder response to line-to-line cross-country SC is shown in Fig. 5.13. Observe the negative sequence voltage and current of 4.334kV and 0.1334A, respectively, during the fault. This is consistent with established SC theory.

5.3 Validating Islanded Mode System Response to Single Line-to-Ground Short Circuit using Dynamic Analysis

In islanded mode, single line-to-ground short circuit fault is applied to phase A at 30.00s and withdrawn at 32.00s. Dynamic simulation of the test bed under short circuit is performed for 50.00s. The responses of the test bed for different fault locations and DFIG controller in voltage, V, and reactive power, Q, control are obtained and presented in Fig. 5.14 to Fig. 5.19.

At 50.0s and under V control (Fig. 5.14(a)) when line-to-ground short circuit is applied at its terminals, MS1 generates 9.366kW and absorbs 0.6579kvar from the reactive var compensators. This active power represents 85.15% of its nominal rating. Since the fault is an L-G short circuit with relatively minimal impact, MS1 generates same amount of active power under Q control but absorbs only 0.006496var from the network at 50.00s. Minimal absorption of reactive power under Q control is a measure of superior performance under this control regime and system stress. This validates reactive power management capability of DFIG as published by Moayed Moghbel et al. in [88] and in [101-103].

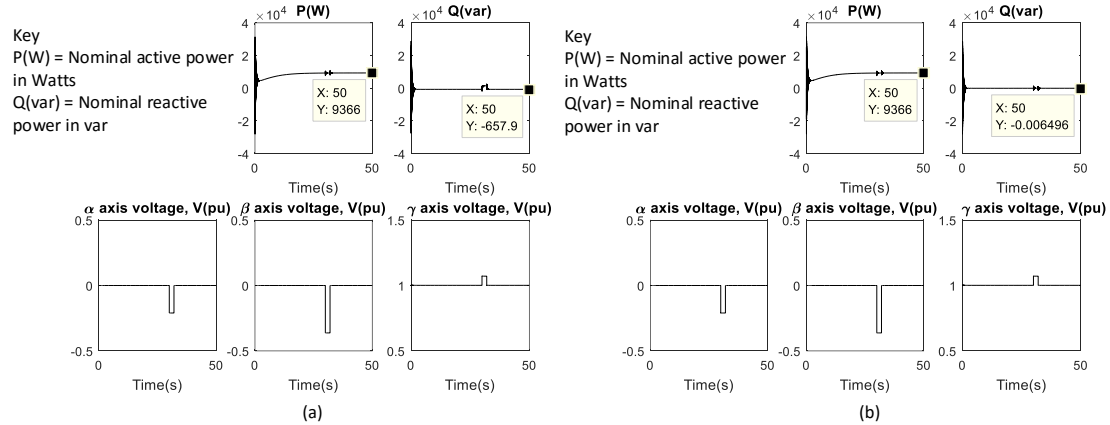

Fig. 5.14. Response of MS1 to single L-G short circuit – V and Q controls

In Fig. 5.15, the peak active power of feeder-a drops to 0.2048kW without any change in direction, indicating minimal impact of the SC on the feeder active power since it is an L-G short circuit fault. On the other hand, reactive power flow on feeder-a rises to 0.1346kvar in the normal flow direction during the fault. The rise in reactive power on the feeder indicates that the var compensators are able to provide requisite var for low voltage fault ride through. Observe the existence of zero sequence voltage and current of 2.254kV and 1.938A respectively during the fault. This response is consistent with well-established short circuit theory on the effect of unbalanced SC on zero sequence quantities as published by Jan Machowski in [61]. Note that because the feeder does not absorb (or inject) active or reactive power, the response of the SC is same under both control strategies.

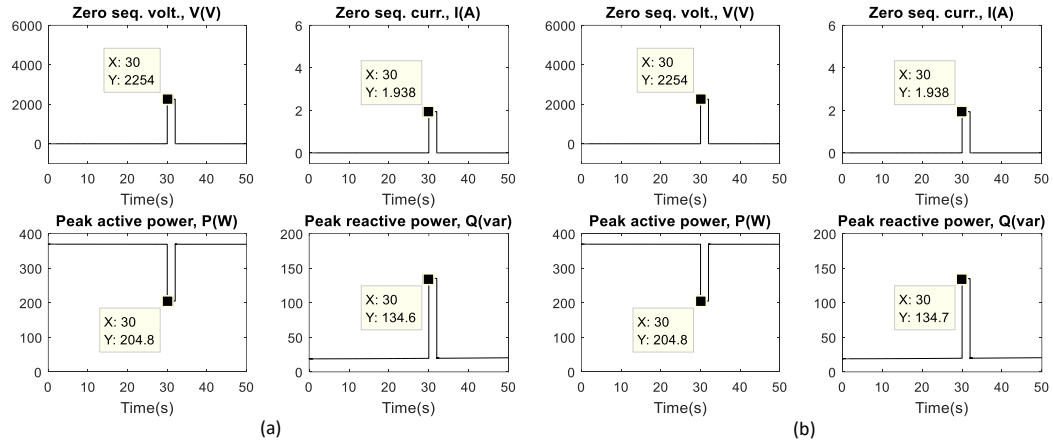

Fig. 5.15. Response of feeder-a to L-G short circuit at terminals of MS1– V and Q controls

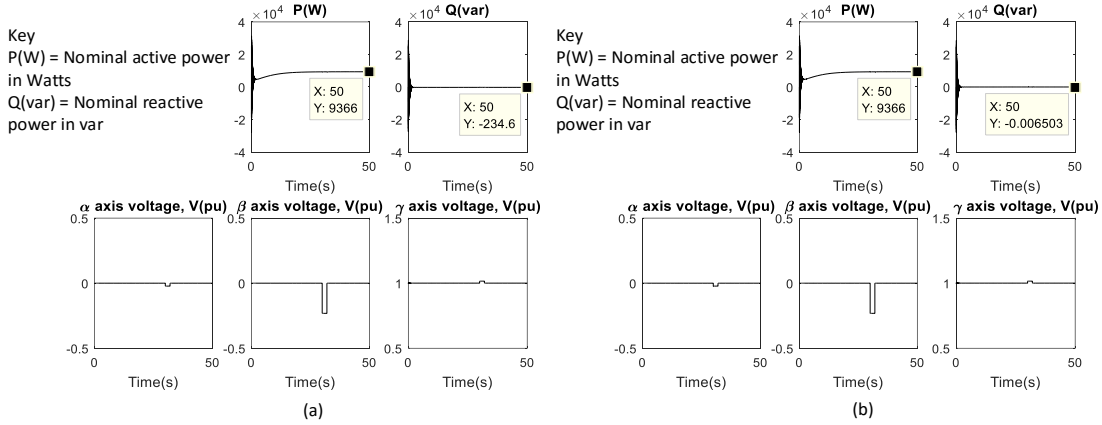

Fig. 5.16. Response of MS2 to L-G short circuit at terminals of MS1– V and Q controls

Fig. 5.16((a) and (b)) shows that when MS1 is faulted, MS2 is undisturbed and generates active power to support the network in both V and Q control regimes. On the other hand, Fig. 5.17 ((a) and (b)) depicts the response of feeder-b under same line-to-ground SC condition. Since feeder-b is a passive element, it can be seen that its zero sequence voltage, zero sequence current, active power and reactive power are affected by the SC in both control regimes.

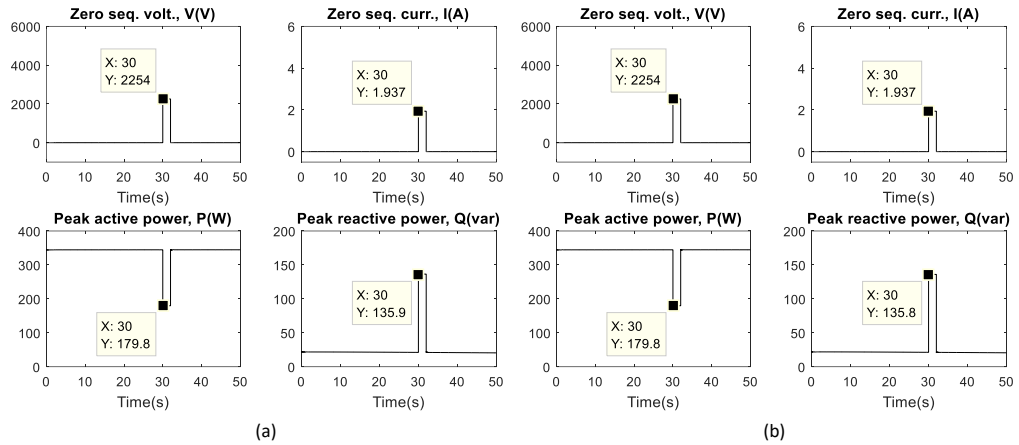

Fig. 5.17. Response of feeder-b to L-G short circuit at terminals of MS1– V and Q controls

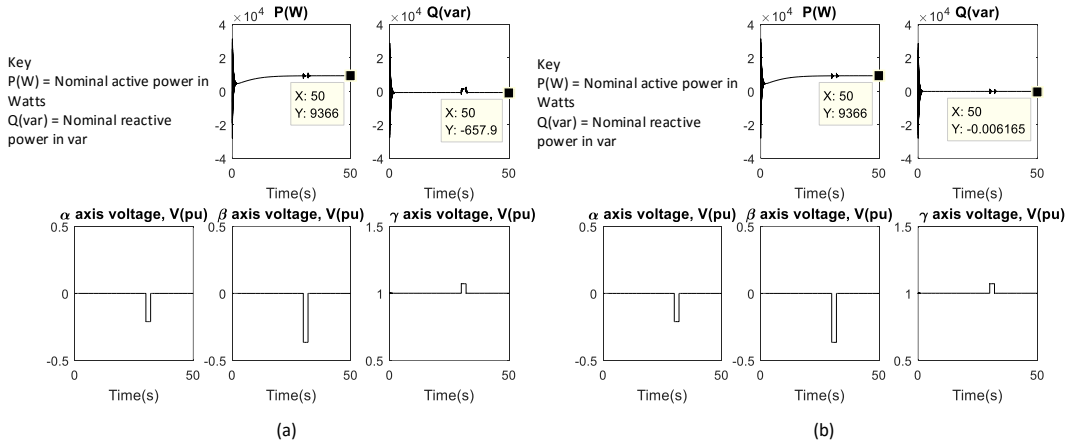

Fig. 5.18. Response of MS1 to L-G cross-country short circuit at terminals of MS1 and MS2 – V and Q controls

When both micro-sources experience line-to-ground cross-country SC at their terminals, under V control MS1 generates 9.366kW and absorbs 0.6579kvar at 50.00s, as shown in Fig. 5.18(a). The active power represents 85.15% of its nominal rating.

At 50.00s and under Q control (Fig. 5.18(b)), during line-to-ground cross-country SC, MS1 generates same amount of active power as obtained under V control but absorbs only 0.006165var, indicating superior DFIG's performance under Q control.

The feeder response to line-to-ground cross-country SC is shown in Fig. 5.19. Observe the zero sequence voltage and current of 3.081kV and 0.2128A, respectively, during the fault. This is consistent with established SC theory.

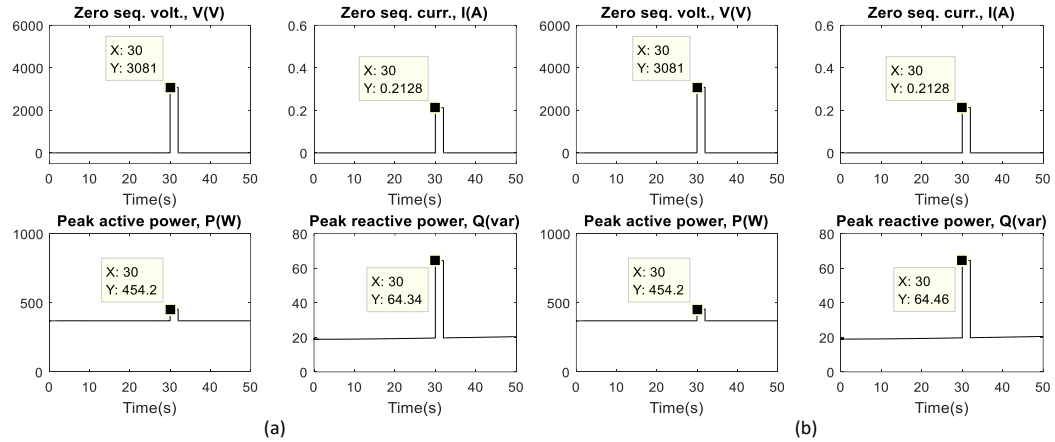

Fig. 5.19. Response of feeder-a to L-G cross-country short circuit at terminals of MS1 and MS2 – V and Q controls

5.4 Conclusion

This chapter discussed technical validation of the test bed under study using dynamic short circuit analysis. The results of the investigation show that the test bed's response to balanced and unbalanced short circuit fault is consistent with established SC theory as well as theories on micro-grid operation and stability. It has been established that the magnitude of impact on the response of the test bed decreases with decrease in the severity of short circuit. Since the crux of this report is presentation of a new protective relay for micro-grid, the rules which engage some of the critical variables of the test bed have been framed and employed to develop a new relay for ac micro-grid, as presented in the succeeding Chapter.

Chapter 6: Proposed Micro-Grid Protection

In this chapter, the proposed multivariable fuzzy rule-based (MFR) relay for short circuits in ac micro-grids is developed and presented. Using a combination of experience, IEC standards, trial and error, and optimization, the rules which govern the interaction of the four parameters are framed. Using the framed rules fuzzy logic controllers are designed for micro-source and feeder sub-relays. The hardware is realized using software combinational logic components. Offline and online response tests of the proposed relay show that it provides reliable detection and protection of the micro-grid against different short circuits in both islanded and grid-connected modes under both control regimes. Its implementation supports the plug-and-play and peer-to-peer features of micro-grids. The proposed relay is a departure from classical short circuit protection wherein protection is based on a certain short circuit capacity. In the proposed MFR relay, protection is based on parameters of micro-sources and feeders.

6.1 Micro-source and Feeder Parameters

The proposed MFR relay consists of two sub-relays: micro-source sub-relay and feeder sub-relay. The rated micro-source voltage, current, active power and reactive power are given in (6.1) to (6.4). The sub-relays detect onset of short circuits by comparing actual micro-source and feeder flows with their rated capacities plus allowable tolerance in terms of voltage, current, active power and reactive power.

6.1.1 Micro-source

The rated rotor and stator voltages of the micro-source are provided in (6.1).

$$\left.\begin{aligned}
\begin{bmatrix} v_{as} \\ v_{bs} \\ v_{cs} \end{bmatrix} &= R_s \begin{bmatrix} i_{as} \\ i_{bs} \\ i_{cs} \end{bmatrix} + \frac{d}{dt}\begin{bmatrix} \phi_{as} \\ \phi_{bs} \\ \phi_{cs} \end{bmatrix} \\
\begin{bmatrix} v_{ar} \\ v_{br} \\ v_{cr} \end{bmatrix} &= R_r \begin{bmatrix} i_{ar} \\ i_{br} \\ i_{cr} \end{bmatrix} + \frac{d}{dt}\begin{bmatrix} \phi_{ar} \\ \phi_{br} \\ \phi_{cr} \end{bmatrix} \\
v_{\alpha\beta\gamma} &= \frac{2}{3}\begin{vmatrix} 1 & -\frac{1}{2} & -\frac{1}{2} \\ 0 & \frac{\sqrt{3}}{2} & -\frac{\sqrt{3}}{2} \\ \frac{1}{2} & \frac{1}{2} & \frac{1}{2} \end{vmatrix}\begin{vmatrix} v_a \\ v_b \\ v_c \end{vmatrix} \\
v_m &= v_\alpha
\end{aligned}\right\} \tag{6.1}$$

where,

v, i and ϕ represent phase voltage, current and flux linkages, respectively.

Subscripts *a*, *b* and *c* represent phases a, b and c, respectively.

Subscripts *r*, *s* and *m* represent rotor, stator and micro-source quantities, respectively.

The rated current expected to flow from the micro-source to the grid is given in (6.2).

$$\left.\begin{aligned}
i_s &= \frac{E' - v_s}{jX'} \\
i_r &= \frac{1}{X_m X'}\left[jv_s\left(X' - X_s\right) + jX_s E'\right] \\
I_m &= i_s + i_r
\end{aligned}\right\} \tag{6.2}$$

where,

E', X', X_m and I_m are fictitious voltage, reactance associated to the fictitious voltage source, rotor-stator mutual reactance and micro-source current, respectively.

The rated active power flowing between the micro-source and the grid is given in (6.3).

$$\left.\begin{aligned}
P_m &= P_s + P_r \\
P_m &= -\frac{v_s E_{eq}}{X_{eq}}\sin\left(\theta - \delta\right)
\end{aligned}\right\} \tag{6.3}$$

where,

P_m, P_s and P_r are active powers of micro-source, stator and rotor, respectively.

E_{eq}, X_{eq}, θ and δ are controllable voltage magnitude, reactance associated to the controllable voltage, rotor angle and controllable voltage angle, respectively.

The rated reactive power exchange between the micro-source's reactive var source and the grid is given in (6.4).

$$\left.\begin{aligned} Q_m &= Q_s \\ Q_m &= \frac{v_s E_{eq}}{X_{eq}} \cos(\theta - \delta) - \frac{v_s^2}{X_{eq}} \end{aligned}\right\} \quad (6.4)$$

where,

Q_m and Q_s are respectively reactive powers in micro-source and stator [61].

A description of the parameters used for micro-source sub-relay is provided as follows:

- P_m = Nominal three phase active power from micro-source, obtained by summing the three phase components via a summing circuit.
- Q_m = A defined three phase reactive var of micro-sources obtained during normal operation.
- V_α = Alpha axis voltage obtained using Clarke's transformation.
- I_m = Absolute value of the vector sum of the complex stator current in *abc* reference frame.

6.1.2 Feeder

The rated feeder current, voltage, active power and reactive power are given in (6.6) to (6.8). The feeder voltages and currents in *abc* reference frame are transformed to their symmetrical components using (6.5).

$$\left.\begin{aligned} A^{-1} &= \tfrac{1}{3}\begin{bmatrix} 1 & 1 & 1 \\ 1 & \alpha & \alpha^2 \\ 1 & \alpha^2 & \alpha \end{bmatrix} \\ \alpha &= 1\angle 120^o \end{aligned}\right\} \quad (6.5)$$

The feeder current I_f is given in (6.6).

$$\left.\begin{aligned} I_f &= \frac{1}{\sqrt{3}v_f}\left(P_f + jQ_f\right) \\ \begin{vmatrix} I^o \\ I^+ \\ I^- \end{vmatrix} &= A^{-1}\begin{vmatrix} i_a \\ i_b \\ i_c \end{vmatrix} \\ I_2 &= I^- \end{aligned}\right\} \tag{6.6}$$

where,

I^o, I^+ and I^- are zero-, positive- and negative-sequence currents, respectively.

The voltages associated to the feeder are described in (6.7).

$$\left.\begin{aligned} \begin{vmatrix} V^o \\ V^+ \\ V^- \end{vmatrix} &= A^{-1}\begin{vmatrix} v_a \\ v_b \\ v_c \end{vmatrix} \\ V_1 &= V^+ \end{aligned}\right\} \tag{6.7}$$

where,

V^o, V^+ and V^- are zero-, positive- and negative-sequence voltages, respectively.

The active and reactive powers in a feeder are described in (6.8).

$$P_f + jQ_f = \tfrac{1}{2}\left(v_a i_a^* + v_b i_b^* + v_c i_c^*\right) \tag{6.8}$$

where,

i_a^*, i_b^* and i_c^* are the complex conjugates of i_a, i_b and i_c, respectively [68].

A description of the parameters used for feeder sub-relay is provided as follows:

- P_f = Three phase active power rating of the feeder.
- Q_f = Three phase reactive power rating of the feeder.
- V_1 = Positive sequence feeder voltage.
- I_2 = Negative sequence feeder current.

Using (6.1) to (6.8), the attributes of both micro-source and feeder under simulated short circuits are developed and presented in Section 6.2.

6.2 System Under Study

From the results of simulation performed on the index test bed of Fig. 3.1 and by using (6.1) to (6.8) for measurement, characteristics of the four parameters are summarized and presented in both grid-connected and islanded modes of micro-grid operation under V and Q controls during short circuits.

6.2.1 Grid-connected mode

Under grid-connected mode, the attributes of the four parameters associated with a micro-source during utility and micro-source short circuits are summarized and presented in Table 6.1.

Table 6.1. Summary of micro-source parameters during utility and micro-grid short circuits in grid-connected mode

Utility SC		**Micro-grid SC**	
Parameter	Behavior (summary)	Parameter	Behavior (summary)
P	$\rightarrow$	*P*	$\downarrow\sim$
Q	$\uparrow_V, \rightarrow_Q$	*Q*	$\uparrow\sim$
V	$\downarrow\sim$	*V*	$\downarrow\sim$
I	$\uparrow\sim$	*I*	$\uparrow\sim$

In the grid-connected mode, the active power generated by the micro-source steadies during utility short circuit while it drops during micro-grid short circuit. This is because the contribution of the micro-grid to utility short circuits is minimal relative to micro-grid as a result of large impedance between the utility and micro-source, good fault-ride-through capability of utility, power electronic-interfacing of micro-source and its smaller short circuit capacity. In both cases, severe post-fault oscillation is observed in the micro-source due to relatively smaller inertia, as shown in Table 6.1.

Under grid-connected mode, the attributes of the four parameters associated with a feeder during utility and micro-source short circuits are summarized and presented in Table 6.2. Further note on these Tables is provided in Section 6.8.

Table 6.2. Summary of feeder parameters during utility and micro-grid short circuits in grid-connected mode

Utility SC		**Micro-grid SC**	
Parameter	Behavior (summary)	Parameter	Behavior (summary)
P	↓~	*P*	↓~
Q	↑ ~	*Q*	↓~
V	↓	*V*	↓~
I	↑	*I*	↑ ~

6.2.2 Islanded mode

In islanded mode, the attributes of the four parameters associated with a micro-source and a feeder under micro-grid short circuits are summarized and presented in Table 6.3.

Table 6.3. Summary of micro-source and feeder parameters during micro-grid short circuits in islanded mode

Micro-source		**Feeder**	
Parameter	Behavior (summary)	Parameter	Behavior (summary)
P	↓~	*P*	↓
Q	↑ ~	*Q*	↓
V	↓	*V*	↓
I	↑	*I*	↑

From the simulation results and as published in [25], it is obvious that in a micro-grid capable of grid-connection, the difference between normal operating parameters and abnormal operating parameters is not crisp. Typically, a short circuit current magnitude in a grid-connected micro-grid could be so small that it is a normal condition in the utility and the utility protection becomes blinded [27]. On the other hand, a utility short circuit could be a normal operating condition in a grid-connected micro-grid due to the limiting effect of the converters in the micro-grid. This lack of clear separation of normal and abnormal operating boundaries in a micro-grid capable of utility connection is better described using fuzzy logic theory. Therefore, variation of the critical parameters to short circuit under different conditions (islanded or grid-connected, V or Q control) is not crisp but fuzzy. This fuzziness in the boundaries of these parameters challenges use of existing protection such as overcurrent devices as published by Ustun et al. in [20].

6.3 Basics of Fuzzy Logic

In 1965, Professor Lotfi Zadeh introduced the concept of Fuzzy Logic in his paper Fuzzy Set Theory [104]. The pre-eminence of Fuzzy Logic was put forward in the 1920s as the *Infinite-*

valued Logic. In *Classical logic* (also called *Boolean logic*), the truth value of a variable is called its *crisp value* and it is either 0 or 1. Contrary to Boolean logic, Fuzzy Logic is a form of *many-valued logic* where the truth value of a variable is any real number between 0 and 1. While Boolean logic deals with applications where the truth values range between complete truth and complete false, fuzzy logic handles scenarios where the truth values range between partial truth and partial false [105]. In real life situations, human operations are natively based on fuzzy reasoning.

6.3.1 Fuzzy variables

In mathematics, variables are usually represented by numerical values. In fuzzy logic, variables could be represented by non-numeric values in order to facilitate manifestation of rules and facts. A linguistic variable such as *height* may have a value such as *tall* or its antonym *short*. The value of a linguistic value is associated with a function, called *membership function*. Through the process of fuzzification, the values of a linguistic variable are mapped *into* fuzzy membership functions. The reverse fuzzification, called de-fuzzification, is used to map a fuzzy output membership functions into a crisp output value. The *crisp* output value is used for control or decision making.

The fuzzy process involves three essential processes. These are presented as follows:

- Fuzzification of input variables into membership functions.
- Execution of governing rules in the "rules base" so as to compute the fuzzy output functions.
- De-fuzzification of the output functions to obtain the crisp output values.

6.3.2 Membership Function

Let X be a space of objects (or points), having a generic element X denoted by x. This implies $X = \{x\}$. A *fuzzy set A* in X is characterized by a *membership* (characteristic) function $f_A(x)$ which associates with each object in X a real number in the interval [0,1], where the value of $f_A(x)$ at x representing the "grade of membership" of x in A. Therefore, the nearer the value of $f_A(x)$ to unity, the higher the grade of membership of x in A. In order words, a membership function of 0 means x is not a member of the fuzzy set; a membership function of 1 means x is fully a member of the fuzzy set [105]. All elements belonging to the fuzzy set only partially have membership function values between 0 and 1.

A simple application could illustrate different sub-ranges of a continuous variable. Typically, an anemometer measurement for a wind turbine electromagnetic braking system might have three

separate membership functions defining particular wind speed range needed to control the electromagnetic braking system properly, as shown in Fig. 6.1. Each function maps the same wind speed value to a truth value in the 0 to 1 range. The three truth values are therefore used to determine how the braking system should be controlled.

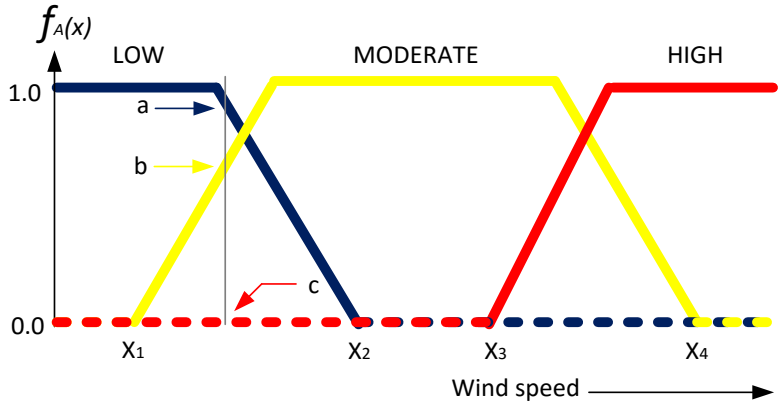

Fig. 6.1. Membership function plots

In Fig. 6.1, the implications of the expressions *LOW*, *MODERATE* and *HIGH* are represented by functions mapping a wind speed scale. A point on the wind speed scale has three "truth values". Each of the three functions has one. The vertical grey line in Fig. 6.1 represents a particular wind speed that the three arrows (truth values) measure. Since the red arrow points to zero (indicated by c), this wind speed could be interpreted as "not HIGH wind speed". The yellow arrow pointing to 0.6 (indicated by b) could be interpreted as "MODERATELY high wind speed" while the blue arrow pointing to 0.9 (indicated by a) is interpreted as "fairly LOW wind speed".

6.3.3 Applications

Fuzzy logic finds application in many engineering systems. Some of such applications include:

- Aircraft flight guidance.
- Road subway controls.
- Fuel consumption for automobiles.
- Controls in consumer electronics such as washing machines and vacuum cleaners.
- Systems for prediction of disasters such as earthquake.
- Economics of power generation such as cost-power optimization.

6.4 Development of Fuzzy Controller for Short Circuit Protection

The fuzzy logic controller inputs are normalized using per unit of the four parameters: active power (*P*), reactive power (*Q*), voltage (*V*) and magnitude of current (*I*). The input parameters are defined in (6.9) to (6.16).

$$\boldsymbol{P_{mn}} = \frac{\boldsymbol{P_{ma}}}{\boldsymbol{P_m}} \tag{6.9}$$

where,

P_{ma} = Actual micro-source active power.

$$Q_{mn} = \frac{Q_{ma}}{Q_m} \tag{6.10}$$

where,

Q_{ma} = Actual micro-source reactive power.

$$V_{\alpha n} = \frac{V_{\propto a}}{V_{\propto}} \tag{6.11}$$

where,

$V_{\alpha a}$ = Actual α-axis micro-source voltage magnitude.

$$I_{mn} = \frac{I_{ma}}{I_m} \tag{6.12}$$

where,

I_{ma} = Actual micro-source current magnitude.

A description of the input parameters for micro-source sub-relay is provided as follows:

- P_{mn} = Nominalized micro-source active power ratio.
- Q_{mn} = Normalized micro-source reactive power ratio.
- $V_{\alpha n}$ = Normalized α-axis micro-source voltage ratio.
- I_{mn} = Normalized micro-source current ratio.

$$P_{fn} = \frac{P_{fa}}{P_f} \tag{6.13}$$

where,

P_{fa} = Actual feeder active power.

$$Q_{fn} = \frac{Q_{fa}}{Q_f} \tag{6.14}$$

where,

Q_{fa} = Actual feeder reactive power.

$$V_{1n} = \frac{V_{1a}}{V_1} \tag{6.15}$$

where,

V_{1a} = Actual feeder positive sequence voltage magnitude.

$$I_{2n} = \frac{I_{2a}}{I_2} \tag{6.16}$$

where,

I_{2a} = Actual feeder negative sequence current magnitude.

A description of the input parameters for feeder sub-relay is provided as follows:

- P_{fn} = Normalized feeder active power ratio.
- Q_{fn} = Normalized feeder reactive power ratio.
- V_{1n} = Normalized feeder positive sequence voltage magnitude ratio.
- I_{2n} = Normalized feeder negative sequence current magnitude ratio.

The output of the fuzzy logic controller is either logic 0 (Close CB) or logic 1 (Open CB). The proposed relay controller consists of two sub-controllers; micro-source sub-controller and feeder sub-controller. Either of the sub-controllers generates a logic response which depends on its input conditions and the rules embedded in it. The rules are developed in Section 6.4.2.

6.4.1 Membership functions

Membership functions are used to fuzzify each of the input parameters of the micro-source as shown in Fig. 6.2. In Simulink Fuzzy Logic Toolbox, Gaussian membership functions are used with three linguistic characteristics for P_{mn}, Q_{mn}, $V_{\alpha n}$, P_{fn}, Q_{fn} and V_{1n} each, while either of I_{mn} and I_{2n} has two linguistic characteristics. In this work, the Gaussian function provided in (6.17) is used.

$$f(x) = ae^{-\frac{(x-b)^2}{2c^2}} \tag{6.17}$$

where,

a is the height of the curve's peak.

b is the position of the center of the curve's peak.

c is the Gaussian rms width which controls the width of the curve.

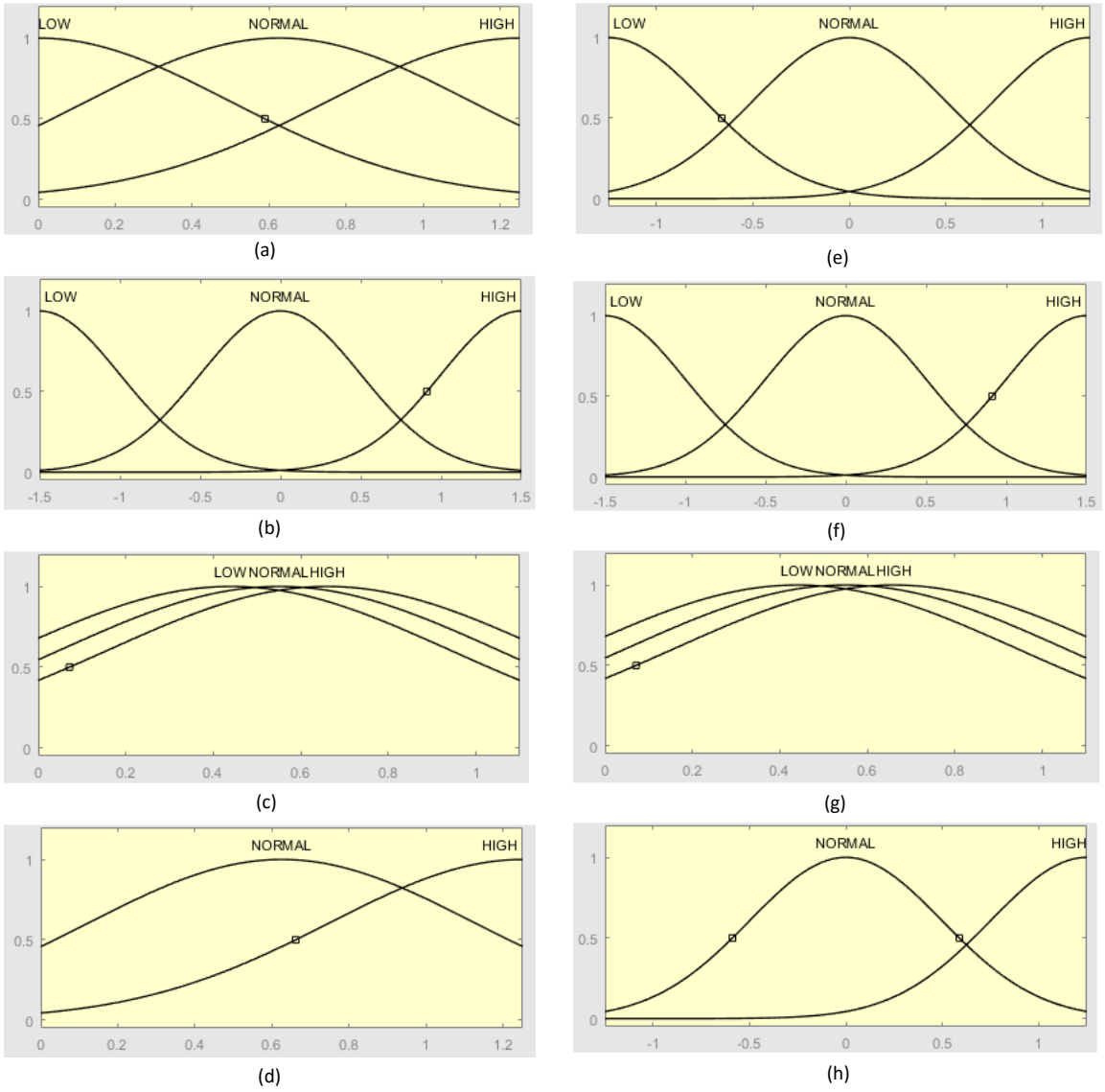

(a) Micro-source active power ratio, P_{mn}.

(b) Micro-source reactive power ratio, Q_{mn}.

(c) Micro-source voltage ratio, $V_{\alpha n}$.

(d) Micro-source current ratio, I_{mn}.

(e) Feeder active power ratio, P_{fn}.

(f) Feeder reactive power ratio, Q_{fn}.

(g) Feeder voltage ratio, V_{1n}.

(h) Feeder current ratio, I_{2n}.

Fig. 6.2. Membership function plots for micro-source sub-relay and feeder sub-relay input parameters

The degree of membership for each input parameter is developed as follows:

Micro-source:

* The micro-source active power ratio (P_{mn}) is described using three linguistic characteristics as shown in Fig. 6.2(a). Active power flow in the micro-source is unidirectional. Using Gaussian function defined in (6.17) and to enable it

generate active power from 0 p.u. to 1.2 p.u. (representing 20% allowable overload) of its rated power, then,

LOW → The Gaussian plot is centered at 0.

NORMAL → The Gaussian plot is centered at 0.6.

HIGH → The Gaussian plot is centered at 1.2.

* The micro-source reactive power ratio (Q_{mn}) is described using three linguistic characteristics as shown in Fig. 6.2(b). Reactive power flow in the micro-source is bidirectional. Using Gaussian function and to allow 50% overload of reactive power flow, then,

  LOW → The Gaussian plot is centered at -1.5.

  NORMAL → The Gaussian plot is centered at 0.

  HIGH → The Gaussian plot is centered at 1.5.

* The micro-source voltage ratio (V_{an}) is described using three linguistic characteristics as shown in Fig. 6.2(c). Using IEC 60038 Standard Voltage which specifies 10% voltage drop at supply side of distribution network for normal operation, then,

  LOW → The Gaussian plot is centered at 0.44.

  NORMAL → The Gaussian plot is centered at 0.55.

  HIGH → The Gaussian plot is centered at 0.66.

* Micro-source current ratio (I_{mn}) is described using two linguistic characteristics as shown in Fig. 6.2(d); NORMAL and HIGH. For 25% overload and using the Gaussian function, then,

  NORMAL → The Gaussian plot is centered at 0.625.

  HIGH → The Gaussian plot is centered at 1.25.

Feeder:

* The feeder active power ratio (P_{fn}) is described using three linguistic characteristics as shown in Fig. 6.2(e). Active power flow in the feeder is bidirectional. Using Gaussian function and to allow 25% overload, then,

  LOW → The Gaussian plot is centered at -1.25.

  NORMAL → The Gaussian plot is centered at 0.

  HIGH → The Gaussian plot is centered at +1.25.

* The feeder reactive power ratio (Q_{fn}) is described using three linguistic characteristics as shown in Fig. 6.2(f). Reactive power flow in the feeder is

bidirectional. Using Gaussian function defined in (6.8a) and to allow 50% overload of reactive power flow, then,

LOW → The Gaussian plot is centered at -1.5.

NORMAL → The Gaussian plot is centered at 0.

HIGH → The Gaussian plot is centered at 1.5.

* The feeder voltage ratio ($V_{\alpha n}$) is described using three linguistic characteristics as shown in Fig. 6.2(g). Using IEC 60038 Standard Voltage which specifies 10% voltage drop at supply side of distribution network for normal operation, then,

  LOW → The Gaussian plot is centered at 0.44.

  NORMAL → The Gaussian plot is centered at 0.55.

  HIGH → The Gaussian plot is centered at 0.66.

* Current flow in the feeder is bidirectional. Micro-source current ratio (I_{mn}) is described using two linguistic characteristics in Fig. 6.2(h); Normal and High. For 25% overload and using the Gaussian function, then,

  NORMAL → The Gaussian plot is centered at 0.

  HIGH → The Gaussian plot is centered at 1.25.

6.4.2 Developing fuzzy rules

Fuzzy logic rules are developed using a combination of experience, IEC standard [106], trial and error until the rules are optimized. This is done in Simulink Fuzzy Logic Toolbox, resulting in three rules for either of micro-source and feeder sub-relays. A total of six rules in the form of "IF-and-Then" are developed for the proposed fuzzy logic controller. Other possible combinations of the input parameters are invalid in the context of the system under study (typically, current magnitude will not fall under any short circuit, control regime or operating mode). The purpose of using Simulink Fuzzy Logic Toolbox in this work is to frame optimized rule set which best describes the four parameters. The response of the fuzzy controller is then simulated and the optimal rule set is extracted. The hardware of extracted rule set is realized using combinational logic devices in SimPowerSystems. The framed optimal rules are given as follows:

Micro-source sub-relay

a. IF P_{mn} is NORMAL AND Q_{mn} is NORMAL AND $V_{\alpha n}$ is NORMAL AND I_{mn} is NORMAL; Then, Close Output (Logic 0).

b. IF $V_{\alpha n}$ is LOW AND I_{mn} is HIGH; Then, Open Output (Logic 1).

c. IF $V_{\alpha n}$ is NORMAL AND I_{mn} is HIGH; Then, Open Output (Logic 1).

Feeder sub-relay

a. IF P_{fn} is NORMAL AND Q_{fn} is NORMAL AND V_{1n} is NORMAL AND I_{2n} is NORMAL; Then, Close Output (Logic 0).

b. IF P_{fn} is LOW AND Q_{fn} is LOW; Then, Open Output (Logic 1).

c. IF P_{fn} is LOW AND Q_{fn} is HIGH; Then, Open Output (Logic 1).

Table 6.4 provides a summary of the membership functions of the input parameters.

Table 6.4. Membership functions associated with micro-source and feeder sub-relays

Micro-source				**Feeder**			
Parameter	Center of Gaussian curve			Parameter	Center of Gaussian curve		
	LOW	NORMAL	HIGH		LOW	NORMAL	HIGH
P_{mn}	0	0.6	1.2	P_{fn}	-1.25	0	1.25
Q_{mn}	-1.5	0	1.5	Q_{fn}	-1.5	0	1.5
$V_{\alpha n}$	0.44	0.55	0.66	V_{1n}	0.44	0.55	0.66
I_{mn}	-	0.625	1.25	I_{2n}	-	0	1.25
Output		CLOSE	OPEN	Output		CLOSE	OPEN
		0	1			0	1

6.4.3 De-fuzzification

The rules are executed in the FIS system and de-fuzzification is performed based on the data acquired during rules evaluation. De-fuzzification is performed using cetroid method in the FIS system. The crisp values are obtained from the de-fuzzification process and the controller takes a decision based on the result of de-fuzzification. Typically, for the micro-source when P_{mn} = 0.8, Q_{mn} = 0.7, V_{am} = 0 and I_{mn} = 1, the output from the de-fuzzification process is 0.923. This is a "HIGH" and is digitally processed to 1. This scenario is shown in Fig. 6.3.

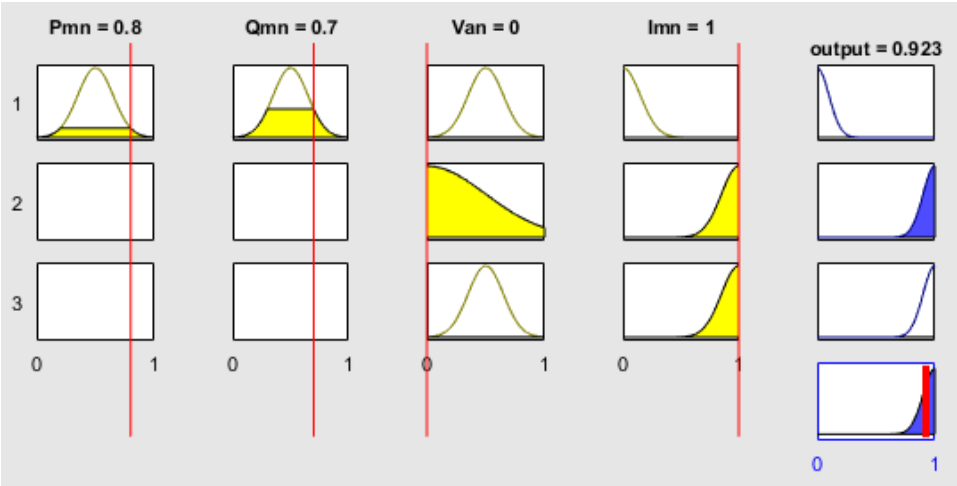

Fig. 6.3. De-fuzzification process

6.4.4 Fuzzy logic controller's response

Using the developed fuzzy logic rules and data-driven modeling, fuzzy logic controllers are designed for both sub-relays. For the micro-source sub-relay, the controller inputs are P_{mn}, Q_{mn}, $V_{\alpha n}$ and I_{mn} while its output is logic 0 (close CB) or logic 1 (open CB). The controller is modeled such that when all inputs are normal, the output remains closed. However, when the input parameters violate the normal operating rule (this is a SC fault), the controller sends a trip signal (logic 1) to the CB. When normal operating rules are fulfilled, the controller recloses the CB. The surface plot for the micro-source controller's response depicting three dimensions is shown in Fig. 6.4.

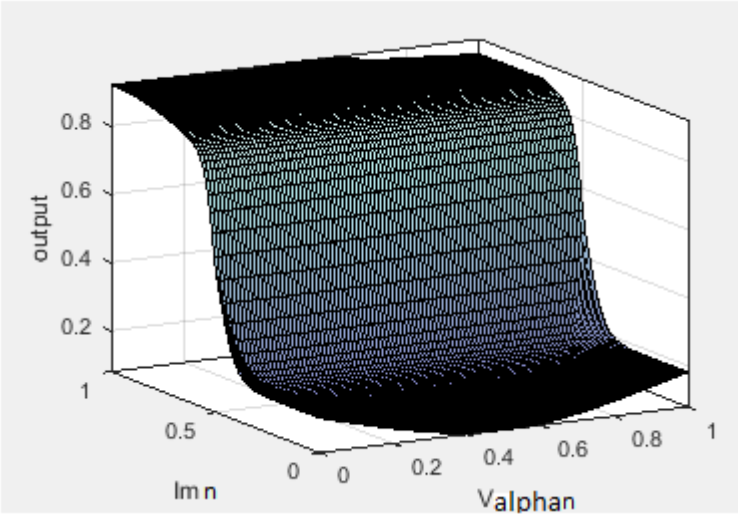

Fig. 6.4. Surface plot of micro-source sub-relay controller's response

For the feeder sub-relay, the controller inputs are P_{fn}, Q_{fn}, I_{2n} and V_{1n}. When all inputs are normal, the output remains closed. However, when any input is not normal, the controller sends a trip signal (logic 1) to the CB. The surface plot for the feeder controller's response depicting three dimensions is shown in Fig. 6.5.

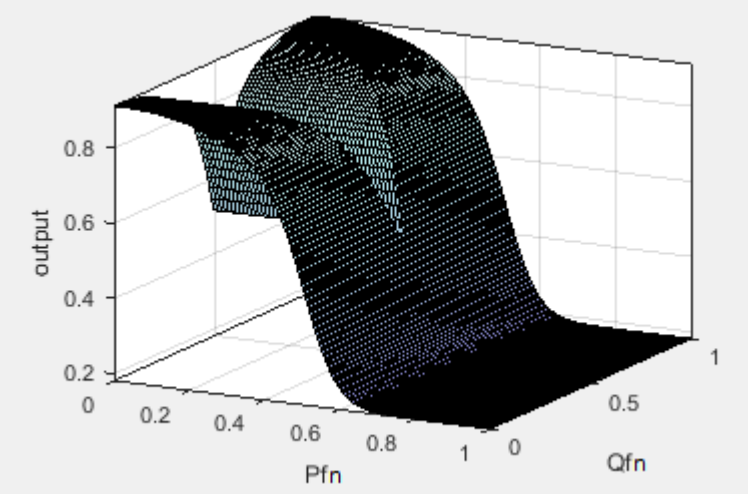

Fig. 6.5. Surface plot of feeder sub-relay controller's response

6.5 Proposed MFR Relay, Connection Schemes and Response Tests

The relay hardware is implemented using software. Its realization is achieved in software implementation of the requisite rules using combinational logic devices. The outputs of the two sub-relays are combined using an OR gate, forming a composite relay for both micro-source and feeder, as shown in Fig. 6.6.

Each sub-relay is implemented using distinct fuzzy rule combination of the four measured parameters such that, regardless of the control regime and operating mode, a micro-source short circuit fault is instantly detected by the micro-source sub-relay while a feeder short circuit fault is instantly detected by the feeder sub-relay. Also, depending on its severity, a utility fault is detected by either feeder sub-relay or both sub-relays.

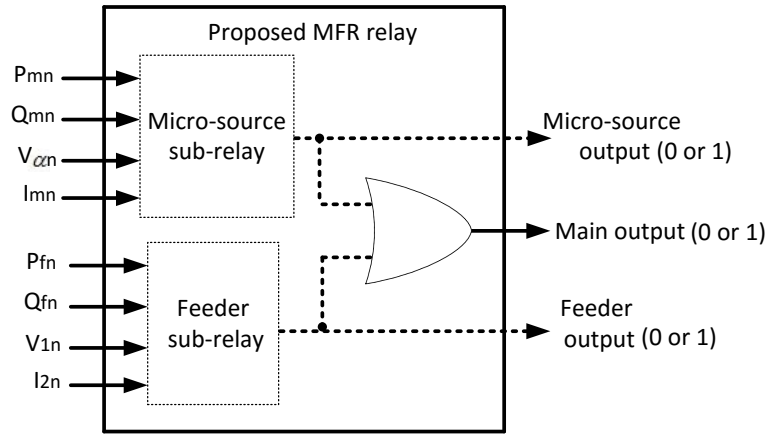

Fig. 6.6. Block diagram showing inputs and outputs of the proposed relay

The proposed MFR relay could be connected in two schemes: the *unit* scheme and the *sub-unit* scheme. In the unit scheme, the outputs of the two sub-relays are combined via an OR gate to output a single logic. This output then controls a dedicated CB such as at the PCC. In the subunit scheme, the output of the micro-source sub-relay controls a CB associated with output terminals of a micro-source. Similarly, the output of the feeder sub-relay controls a CB associated with a feeder. In both schemes, the micro-source sub-relay receives inputs from its associated micro-source while the feeder sub-relay receives its inputs from requisite feeder.

The proposed relay is subjected to offline and online tests at different locations of the test bed. A summary of the online test results is presented in Tables 6.5 and 6.6. The offline test results are similar to the results of online tests presented in the Tables. In the tables, t_f^- = pre-fault time, t_f = fault-on time, t_f^+ = post-fault time.

Table 6.5. Logic response of MFR relay in grid-connected mode

	Logic response of MFR relay					
	V control			Q control		
Nature of SC	t_f^-	t_f	t_f^+	t_f^-	t_f	t_f^+
$1-\phi$	0	1	0	0	1	0
$L-L$	0	1	0	0	1	0
$3-\phi$	0	1	0	0	1	0
$C-C$	0	1	0	0	1	0

Table 6.6. Logic response of MFR relay in islanded mode

	Logic response of MFR relay					
	V control			Q control		
Nature of SC	t_f^-	t_f	t_f^+	t_f^-	t_f	t_f^+
$1-\phi$	0	1	0	0	1	0
$L-L$	0	1	0	0	1	0
$3-\phi$	0	1	0	0	1	0
$C-C$	0	1	0	0	1	0

Fig. 6.7 presents graphical display of parameters of the micro-source (P_m, Q_m, V_α and I_m) during a three phase bolted SC applied at terminals of MS1. The SC is applied at 30s and withdrawn at 32s, in islanded mode V control. Note that the sub-relay outputs logic 1 from 0s to approximately 9s due to the high starting current of the micro-source. This response is expected and indicates proper operation of a protective device. However, if this is undesirable (since desirability is a function of application) it can be avoided if a 10s starting delay is modeled and connected to the

micro-source sub-relay. Also, note that the sub-relay's response to the fault is logic 1 from 30s to 32s, with another oscillatory response from approximately 32s to 33.5s due to post-fault high currents occasioned by instability. After the SC, the sub-relay generates logic 0 to reclose requisite CB.

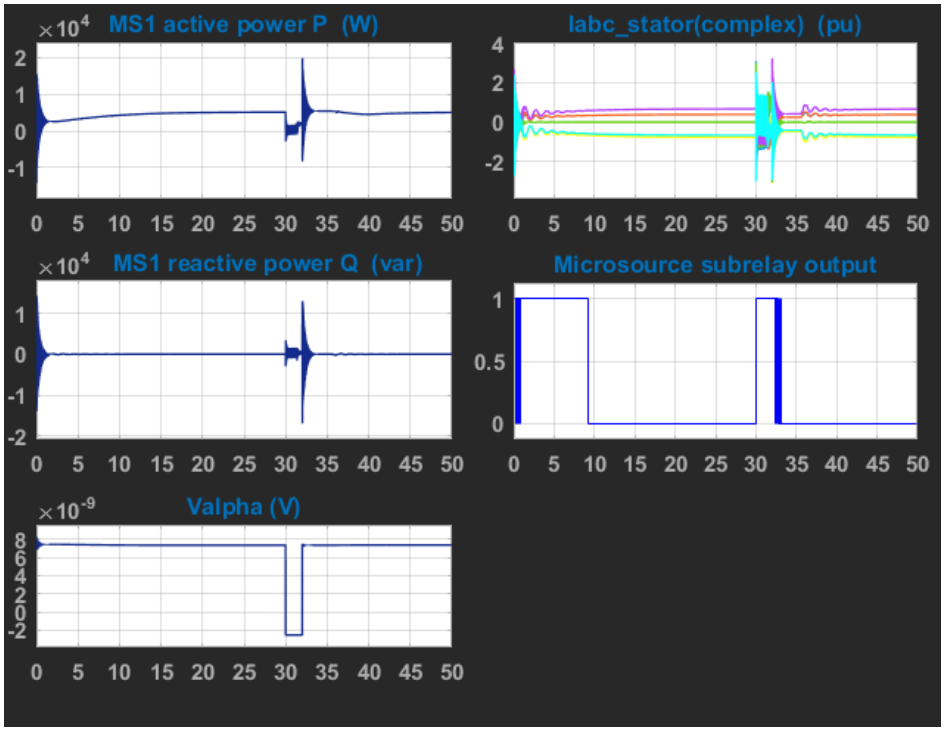

Fig. 6.7. Graphical display of the critical parameters and sub-relay logic output for micro-source

Fig. 6.8 presents graphical display of parameters of the feeder (P_f, Q_f, V_1 and I_2) during a three phase bolted short circuit applied at terminals of feeder-a. The fault is applied at 30s and withdrawn at 32s, in islanded mode V control. Note that the sub-relay's pre-fault response is 0. Its response to the fault is logic 1 from 30s to 32s. After the fault, the sub-relay generates logic 0 to reclose requisite CB.

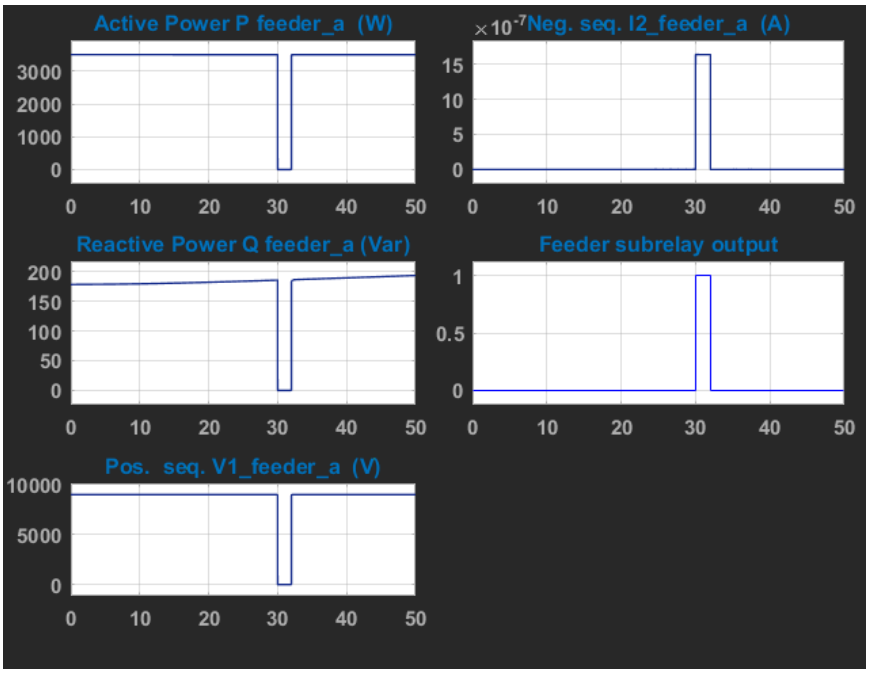

Fig. 6.8. Graphical display of the critical parameters and sub-relay logic output for feeder

6.6 Response of Proposed MFR Relay under Short Circuits

The response of proposed MFR relay to short circuit when embedded in the index test bed is presented in Fig. 6.9 to Fig. 6.24. Short circuit is applied at 30.00s and withdrawn at 32.00s. In the figures, sub-figure (a) displays response under V control while sub-figure (b) displays response under Q control. In either sub-figure, the blue trace in the left-hand-side shows response of the sub-relay linked to micro-source1. The red trace in the center shows response of proposed MFR relay to same short circuit, while the black trace in the right-hand-side shows response of sub-relay linked to feeder-a under same short circuit. The faults applied are single line-to-ground, line-to-line, three phase-to-ground and cross-country short circuits. Note that single line-to-ground SC is applied between phase *A* and neutral while line-to-line SC is applied between phases *A* and *B*. The proposed relay's response to short circuit is split into two: grid-connected responses and islanded responses.

6.6.1 Grid-connected responses

In the grid-connected mode, note that the sub-relays output logic 1 from 0s to approximately 12s in the micro-source sub-relay (and 10s in the feeder sub-relay) due to the high starting current of the micro-source. This response is expected and indicates proper operation of a protective device. However, if this is undesirable (since desirability is a function of application) it can be avoided if a 10s starting delay is modeled and connected to both sub-relays.

MS1 under L-G short circuit

Fig. 6.9 presents responses of MS1 sub-relay, proposed MFR relay and feeder-a sub-relay to single line-to-ground SC applied at the terminals of MS1 in grid-connected mode under V and Q controls.

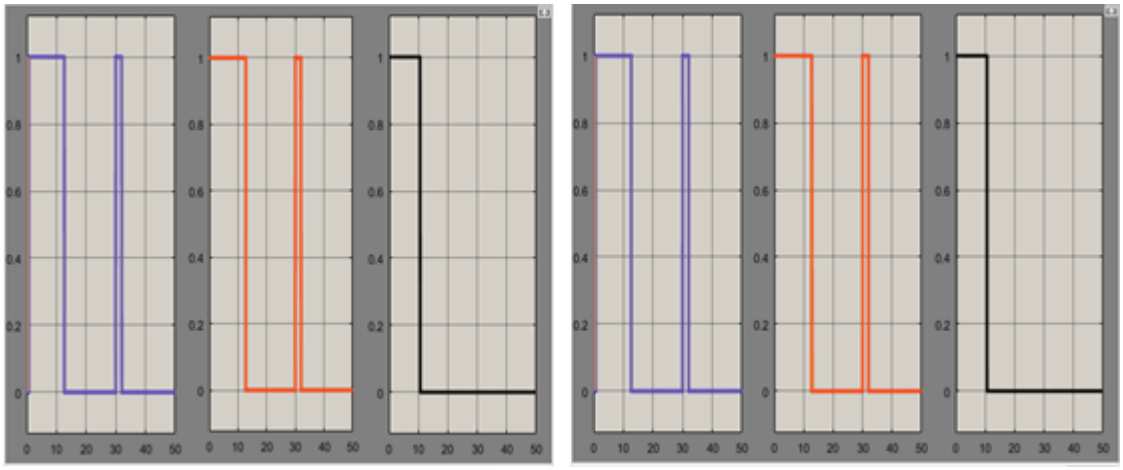

(a) (b)

(a) V control; (b) Q control

Fig. 6.9. MS1 under L-G short circuit

In Fig. 6.9, note that MS1 sub-relay generates logic 0 during pre-fault, logic 1 during fault-on and logic 0 during post-fault, in both control strategies. This triggers the proposed MFR relay to generate logic 0 during pre-fault, logic 1 during fault-on and logic 0 during post-fault, accordingly. As expected, note that response of feeder-a sub-relay is logic 0 during pre-fault, logic 0 during fault-on and logic 0 during post-fault, in both control strategies. This shows that the micro-source sub-relay responds to micro-source short circuit while feeder sub-relay is passive to micro-source short circuit, an indication of selectivity of the proposed MFR relay to ensure minimal supply disruption as required by micro-grid protective system [107].

MS1 under L-L short circuit

Fig. 6.10 presents responses of MS1 sub-relay, proposed MFR relay and feeder-a sub-relay to line-to-line SC applied at the terminals of MS1 in grid-connected mode under V and Q controls.

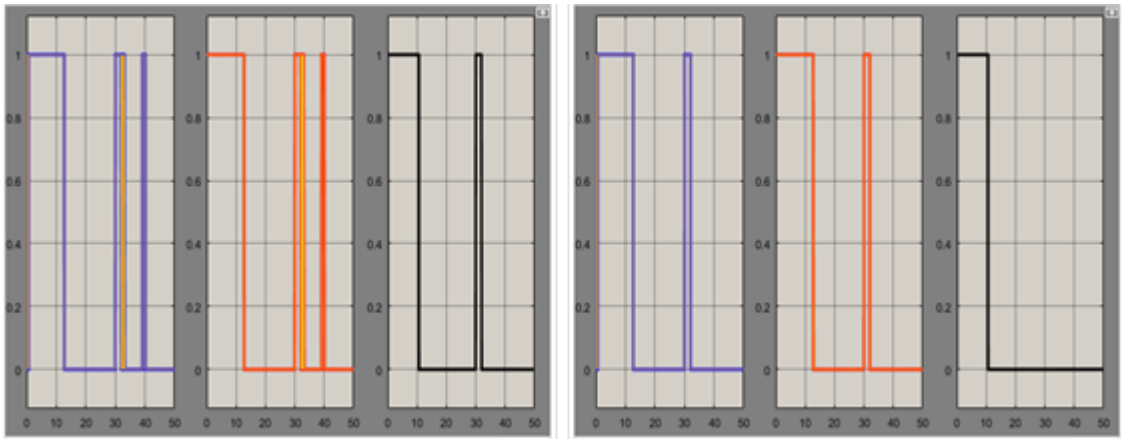

(a) (b)

(a) V control; (b) Q control

Fig. 6.10. MS1 under L-L short circuit

In Fig. 6.10, note that MS1 sub-relay generates logic 0 during pre-fault, logic 1 during fault-on and logic 0 during post-fault, in both control strategies. Due to post-fault un-sustained oscillation occasioned by increased SC severity, MS1 sub-relay is compelled to generate oscillatory 1 and 0 logics during post-fault in V control. This triggers the proposed MFR relay to produce oscillatory 1 and 0 logics during post-fault, before the system attains a new steady-state at approximately 40.00s. Thereafter, the proposed MFR relay produces logic 0 during post-fault. As expected, note that response of feeder-a sub-relay is logic 0 during pre-fault, 0 during fault-on and logic 0 during post-fault, in both control strategies. This shows that the micro-source sub-relay responds to micro-source SC while feeder sub-relay is passive to micro-source SC, an indication of selectivity of the proposed MFR relay to ensure minimal supply disruption as required by micro-grid protective system. It also highlights the need to operate the system under Q control at the onset of short circuits.

MS1 under three phase short circuit

Fig. 6.11 presents responses of MS1 sub-relay, proposed MFR relay and feeder-a sub-relay to three phase-to-ground SC applied at the terminals of MS1 in grid-connected mode under V and Q controls.

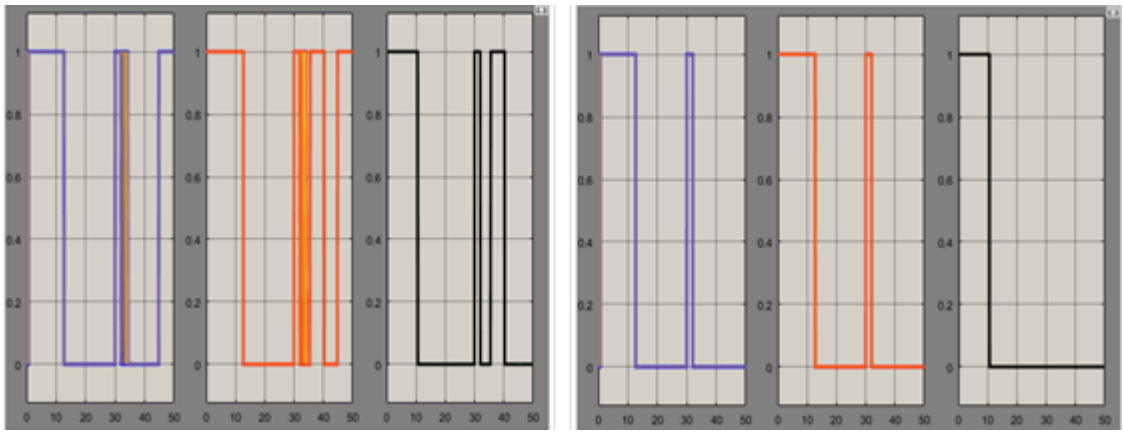

(a) (b)

(a) V control; (b) Q control

Fig. 6.11. MS1 under three phase short circuit

In Fig. 6.11, note that MS1 sub-relay generates logic 0 during pre-fault, logic 1 during fault-on and logic 0 during post-fault, in both control strategies. Due to post-fault sustained oscillation occasioned by increased SC severity, MS1 sub-relay is compelled to generate oscillatory 1 and 0 logics during post-fault in V control. This triggers the proposed MFR relay to produce oscillatory 1 and 0 logics during post-fault. Similarly, for the same reason of very high short circuit severity feeder-a sub-relay is compelled to respond to the SC and produce virulent oscillatory logics during post-fault in V control. Note that in Q control, the proposed MFR relay and its sub-relays produce responses that are consistent with design expectations. This is an indication of superior performance of the proposed MFR relay under requisite control strategy, a further confirmation that control strategies dictate system's characteristics as published by Bikash Pal and Balarko Chaudhuri in [108].

MS2 is under L-G short circuit

Fig. 6.12 presents responses of MS1 sub-relay, proposed MFR relay and feeder-a sub-relay to single line-to-ground SC applied at the terminals of MS2 in grid-connected mode under V and Q controls.

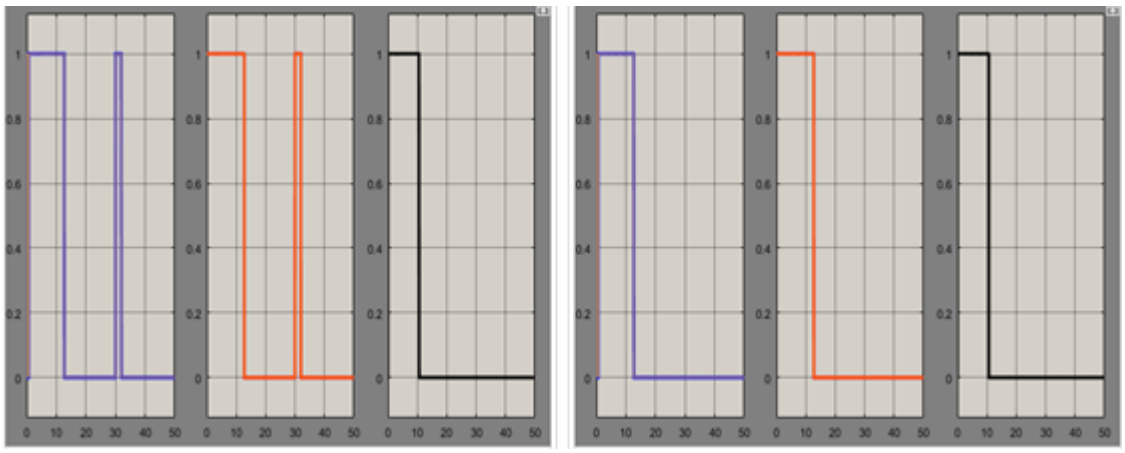

(a) (b)

(a) V control; (b) Q control

Fig. 6.12. MS2 is under L-G short circuit

In Fig. 6.12, note that MS1 sub-relay generates logic 0 during pre-fault, logic 1 during fault-on and logic 0 during post-fault, in V control strategy. It generates logic 0 during pre-fault, fault-on and post-fault in Q control. This triggers the proposed MFR relay to generate corresponding logics during pre-fault, fault-on and post-fault. As expected, note that response of feeder-a sub-relay is logic 0 during pre-fault, logic 0 during fault-on and logic 0 during post-fault, in both control strategies. This further shows that the proposed MFR relay and its sub-relays provide superior performance under Q control.

Feeder-a under L-G short circuit

Fig. 6.13 presents responses of MS1 sub-relay, proposed MFR relay and feeder-a sub-relay to single line-to-ground SC applied at the terminals of feeder-a in grid-connected mode under V and Q controls.

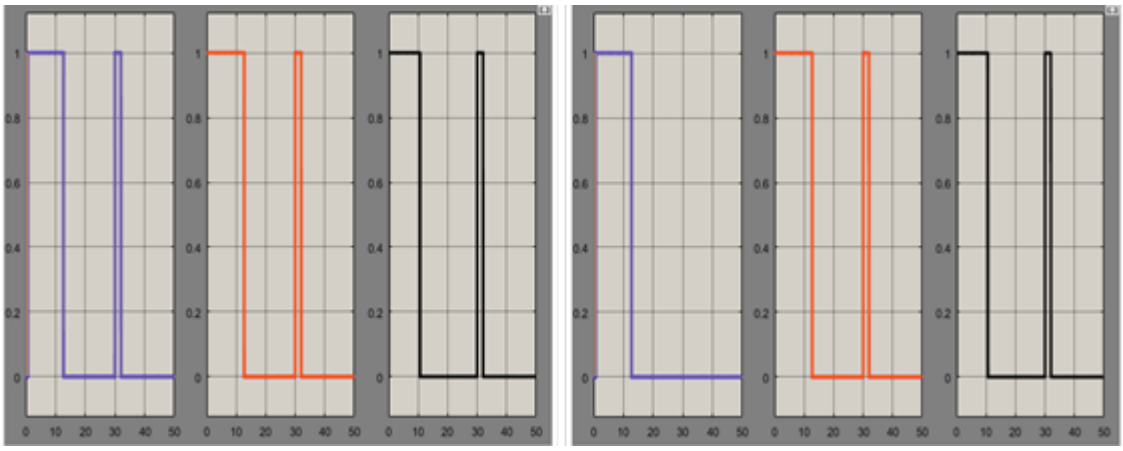

(a) (b)

(a) V control; (b) Q control

Fig. 6.13. Feeder-a under L-G short circuit

In Fig. 6.13, note that feeder-a sub-relay generates logic 0 during pre-fault, logic 1 during fault-on and logic 0 during post-fault, in both control strategies. Note also that due to high current demand on MS1 to support the SC and due to its inability to provide requisite reactive power demand, MS1 sub-relay detects rise in current and drop in voltage, triggering it to produce logic 1 during fault-on under V control. However, observe the response of MS1 under Q control strategy – logic 0. This is consistent with design expectation, indicative of superior performance of the proposed MFR relay under requisite control strategy.

Feeder-a under three phase short circuit

Fig. 6.14 presents responses of MS1 sub-relay, proposed MFR relay and feeder-a sub-relay to three phase-to-ground SC applied at the terminals of feeder-a in grid-connected mode under V and Q controls.

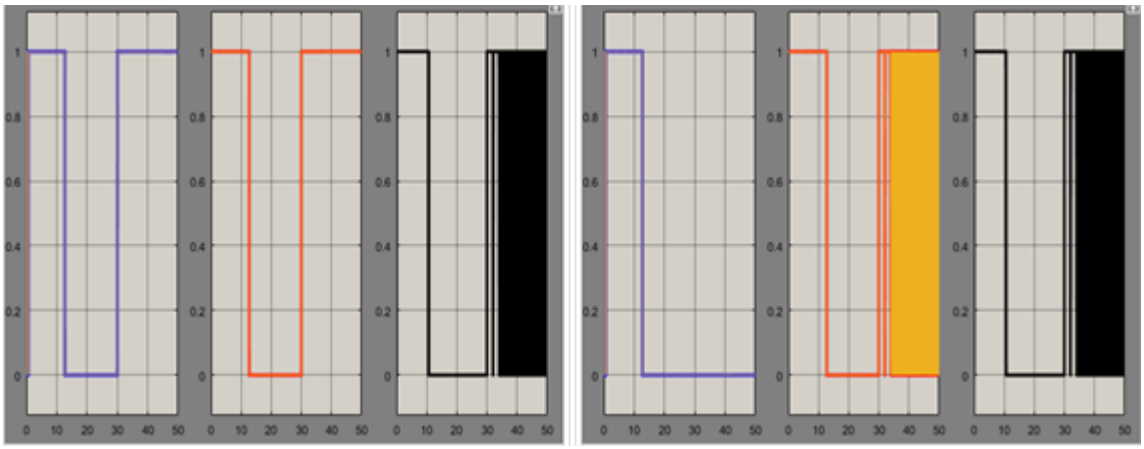

(a) (b)

(a) V control; (b) Q control

Fig. 6.14. Feeder-a under three phase short circuit

In Fig. 6.14, note that feeder-a sub-relay generates logic 0 during pre-fault, logic 1 during fault-on and logic 0 during post-fault, in both control strategies. However, due to very high current demand on MS1 to support the SC and due to its inability to provide requisite reactive power demand, MS1 sub-relay detects rise in current and drop in voltage, triggering it to produce logic 1 during fault-on under V control. Note the response of MS1 under Q control strategy – logic 0. Due to sustained oscillation of active power and voltage in the feeder occasioned by very high short circuit demands in the feeder, feeder-a is compelled to produce oscillatory 0 and 1 logics during post-fault. This triggers the proposed MFR relay to produce oscillatory 0 and 1 logics during post-fault. This situation could be mitigated by incorporating appropriate D-STATCOM at the feeder to support the feeder during such severe stress.

Feeder-b under three phase short circuit

Fig. 6.15 presents responses of MS1 sub-relay, proposed MFR relay and feeder-a sub-relay to three phase-to-ground SC applied at the terminals of feeder-b in grid-connected mode under V and Q controls.

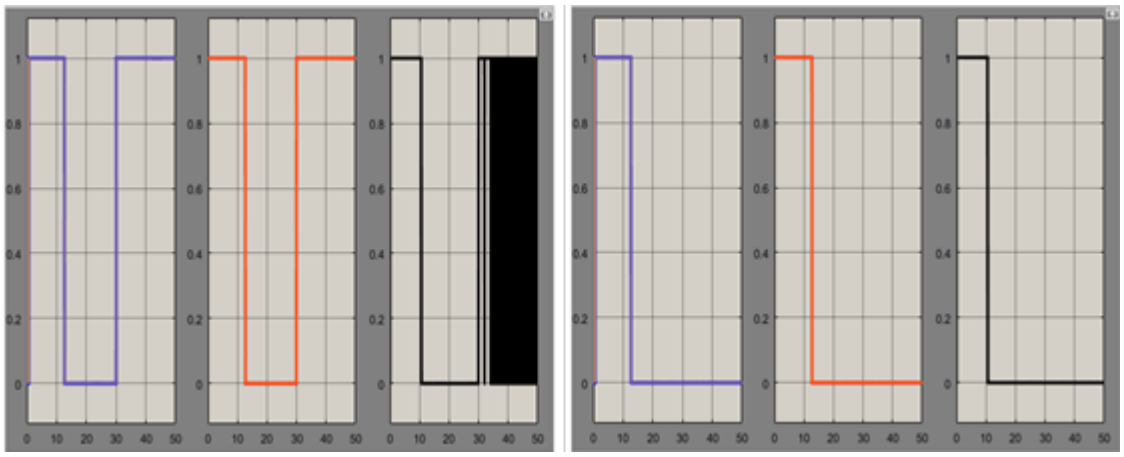

(a) (b)

(a) V control; (b) Q control

Fig. 6.15. Feeder-b under three phase short circuit

In Fig. 6.15, note that feeder-a sub-relay generates logic 0 during pre-fault, logic 1 during fault-on and logic 0 during post-fault, in both control strategies. Note also that due to high SC demand on MS1 its sub-relay produces logic 1 during fault-on and during post-fault in V control strategy. Observe the responses of MS1 and feeder-a under Q control strategy – logic 0. This shows that MS1 sub-relay and feeder-a sub-relay do not exhibit *sympathetic tripping* to SC events of feeder-b. This shows superior performance of the proposed MFR relay in comparison with existing proposals using over-current devices.

Utility generator terminals under L-G short circuit

Fig. 6.16 presents responses of MS1 sub-relay, proposed MFR relay and feeder-a sub-relay to single phase-to-ground SC applied at the terminals of utility generator in grid-connected mode under V and Q controls.

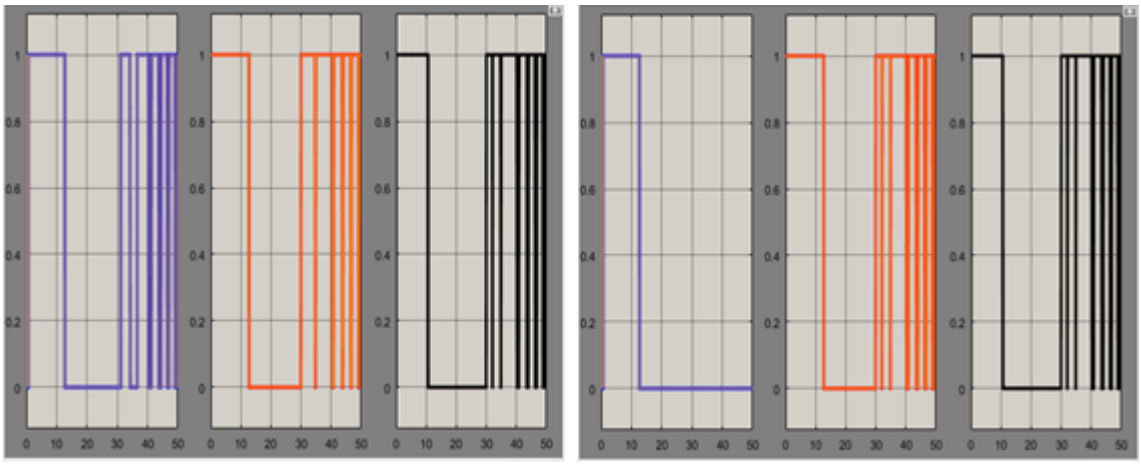

(a) (b)

(a) V control; (b) Q control

Fig. 6.16. Utility generator terminals under L-G short circuit

In Fig. 6.16, note that feeder-a sub-relay generates logic 0 during pre-fault, logic 1 during fault-on and logic 0 during post-fault, in both control strategies. Note also that due to high SC demand on MS1 its sub-relay produces logic 1 during fault-on and during post-fault in V control strategy. Observe the response of MS1 under Q control strategy – logic 0. Also observe the response of feeder-a in both control strategies. The responses under Q control strategy is consistent with design expectation. This is because utility generator is located at the extreme end of the utility, far away from the PCC which is closer to the feeder sub-relay. The distance is accounted for by high impedance between the utility generator and MS1 sub-relay, resulting in passive response of MS1 in Q control. However, due to proximate location of feeder-a sub-relay, it detects the short circuit in the utility. On one hand, this shows that the MS1 sub-relay does not operate sympathetically under Q control. On another hand, it shows that feeder-a sub-relay is not blinded to contribution of micro-grid to short circuit in the utility. This confirms that the proposed MFR relay exhibits capability for use in the *unit scheme* since feeder-a sub-relay detects abnormal flow of current and power occasioned by short circuit effect at the PCC.

Utility and micro-grid cross-country three phase short circuit

Fig. 6.17 presents responses of MS1 sub-relay, proposed MFR relay and feeder-a sub-relay to cross-country three phase-to-ground SC spanning both utility and micro-grid. The short circuit is applied at the terminals of utility generator, transformer *T*, feeder-a, MS1, feeder-b and MS2 in grid-connected mode under V and Q controls.

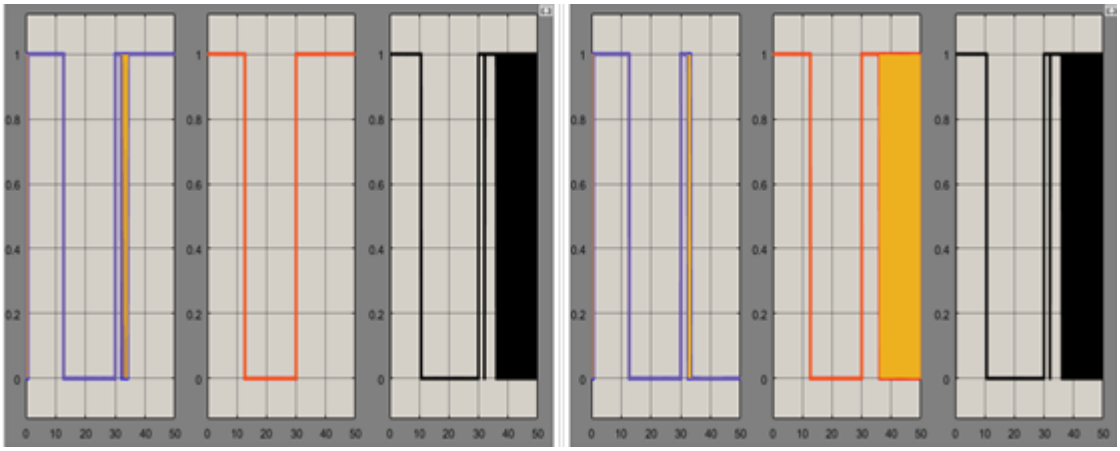

(a) (b)

(a) V control; (b) Q control

Fig. 6.17. Utility and micro-grid cross-country three phase short circuit

In Fig. 6.17, note that feeder-a sub-relay generates logic 0 during pre-fault, logic 1 during fault-on and logic 0 during post-fault, in both control strategies. However, due to extremely high short circuit demand on MS1, MS1 sub-relay produces logic 1 during fault-on and during post-fault (with oscillatory logics during early post-fault) under V control. Under Q control strategy, MS1 produces short oscillatory logics during early post-fault and logic 0 during late post-fault. The oscillation recorded under Q control is triggered by the astronomically high demand on the reactive var compensator. The var compensator supplies reactive power to the system. Under such severe short circuit, the compensator is stretched to its limits since it was designed to have a maximum capacitive reactive power of 100kvar. The short circuit capacity of the utility is sufficiently large to trigger sustained oscillation in the micro-grid. Due to sustained oscillation of active power and voltage in the feeder occasioned by extremely high short circuit demands in the feeder, feeder-a is compelled to produce oscillatory 0 and 1 logics during post-fault. This triggers the proposed MFR relay to produce oscillatory 0 and 1 logics during post-fault. This situation could be mitigated by incorporating appropriate D-STATCOM at the feeder to support the feeder during such uncommon severe stress. Note that the yellow rectangle recorded by response of MFR relay during post-fault under Q control is an indication of continuous and unsuccessful attempt by the MFR relay to switch from logic 1 to logic 0.

6.6.2 Responses in islanded mode

Fig. 6.18 to Fig. 6.25 present the responses of MS1 sub-relay, proposed MFR relay and feeder-a sub-relay to short circuits in both V and Q control strategies in islanded mode of operation. In all

the figures, observe that the response of feeder-a sub-relay does not record the initial high starting current occasioned by starting of micro-sources (wind turbines) obtained in the grid-connected mode. This is a result of combination of the fact that micro-sources are not directly connected downstream of feeder-a (the position where feeder-a sub-relay is linked) on one hand, and the effect of high resistance of the feeder which is typical of distribution feeders, on the other hand. As obtainable in the grid-connected mode, sub-figure (a) shows response under V control while sub-figure (b) shows response under Q control. In either sub-figure, the blue trace in the left-hand-side represents response of MS1 sub-relay. The red trace in the center shows response of proposed MFR relay, while the black trace in the right-hand-side shows response of feeder-a sub-relay. Note also that virulent oscillations are not recorded during micro-grid short circuits in islanded mode largely due to comparatively small short circuit capacity of the system in islanded mode.

MS1 under L-G short circuit

Fig. 6.18 presents response of MS1 sub-relay, proposed MFR relay and feeder-a sub-relay to single phase-to-ground SC in islanded mode under V and Q control strategies. The SC is applied at terminals of MS1.

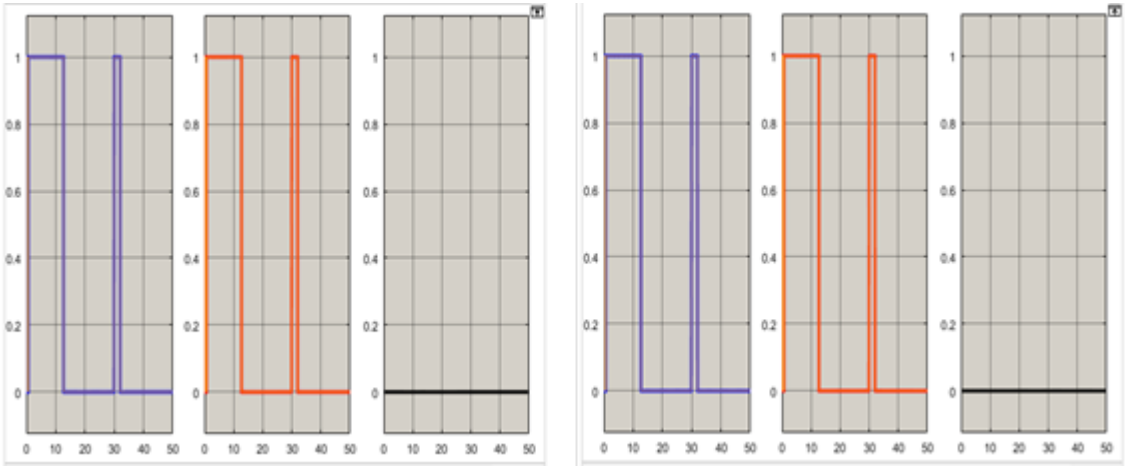

(a) (b)

(a) V control, (b) Q control

Fig. 6.18. MS1 under L-G short circuit

In Fig. 6.18, MS1 sub-relay produces logic 0 during pre-fault, logic 1 during fault-on and logic 0 during post-fault in both control strategies. This triggers the proposed MFR relay to trigger logic 1 only during single line-to-ground short circuit in both control strategies. As expected, the feeder

sub-relay remains passive in both control strategies, indicative of *selectivity* required of a micro-grid protective system.

MS1 under L-L short circuit

Fig. 6.19 presents response of MS1 sub-relay, proposed MFR relay and feeder-a sub-relay to line-to-line SC in islanded mode under V and Q control strategies. The short circuit is applied at terminals of MS1.

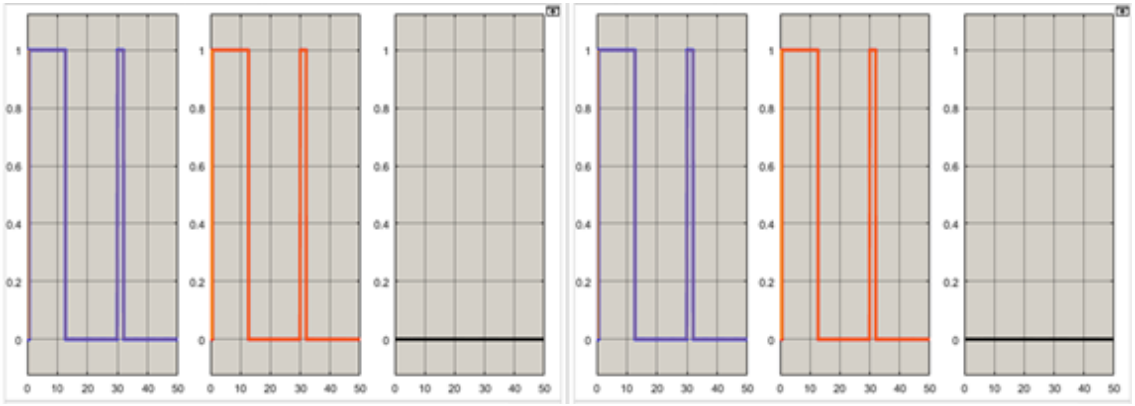

(a) (b)

(a) V control, (b) Q control

Fig. 6.19. MS1 under L-L short circuit

In Fig. 6.19, MS1 sub-relay produces logic 0 during pre-fault, logic 1 during fault-on and logic 0 during post-fault in both control strategies. This triggers the proposed MFR relay to trigger logic 1 only during line-to-line short circuit in both control strategies. As expected, the feeder sub-relay remains passive in both control strategies.

MS1 under three phase short circuit

Fig. 6.20 presents response of MS1 sub-relay, proposed MFR relay and feeder-a sub-relay to three phase-to-ground short circuit in islanded mode under V and Q control strategies. The short circuit is applied at terminals of MS1.

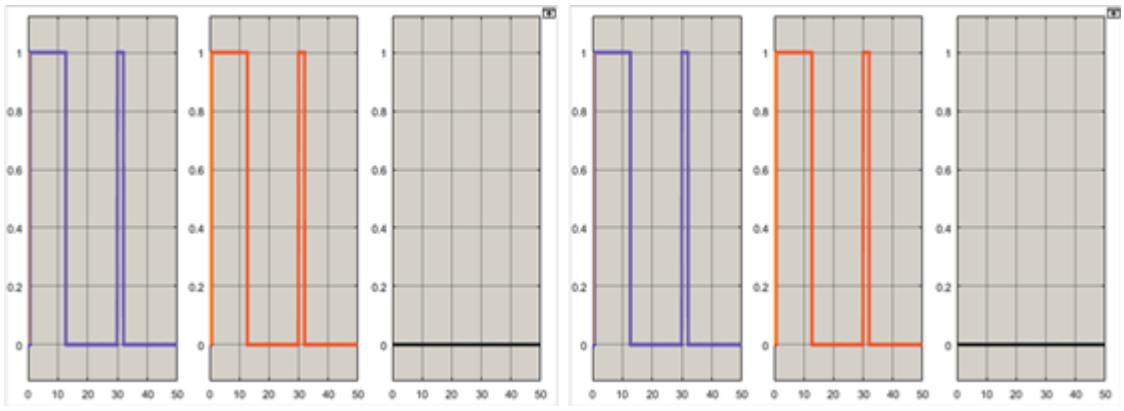

(a) (b)

(a) V control, (b) Q control

Fig. 6.20. MS1 under three phase short circuit

In Fig. 6.20, MS1 sub-relay produces logic 0 during pre-fault, logic 1 during fault-on and logic 0 during post-fault in both control strategies. This triggers the proposed MFR relay to trigger logic 1 only during three phase-to-ground short circuit in both control strategies. As expected, the feeder sub-relay remains passive in both control strategies.

Feeder-a under three phase short circuit

Fig. 6.21 presents response of MS1 sub-relay, proposed MFR relay and feeder-a sub-relay to three phase-to-ground SC in islanded mode under V and Q control strategies. The short circuit is applied at terminals of feeder-a.

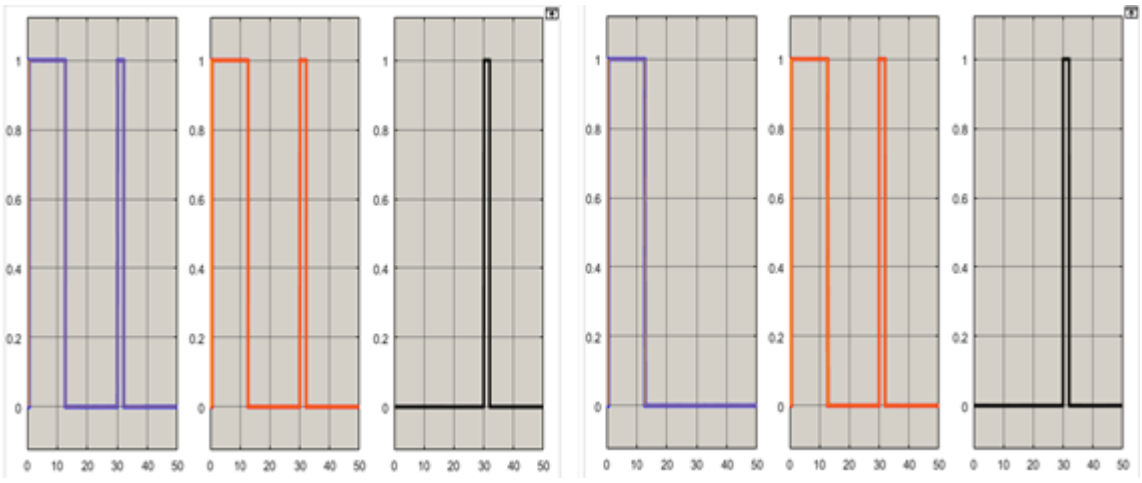

(a) (b)

(a) V control, (b) Q control

Fig. 6.21. Feeder-a under three phase short circuit

In Fig. 6.21, MS1 sub-relay produces logic 0 during pre-fault, logic 1 during fault-on and logic 0 during post-fault under V control. This triggers the proposed MFR relay to trigger logic 1 during three phase-to-ground short circuit under V control. This is undesired and contrary to Q control where, as expected, MS1 sub-relay produces passive response to feeder-a short circuit. Observe with pleasure, the response of feeder-a sub-relay to feeder-a SC. It produces logic 0 during pre-fault, logic 1 during fault-on and logic 0 during post-fault.

Feeder-b under three phase short circuit

Fig. 6.22 presents response of MS1 sub-relay, proposed MFR relay and feeder-a sub-relay to three phase-to-ground SC in islanded mode under V and Q control strategies. The short circuit is applied at terminals of feeder-b.

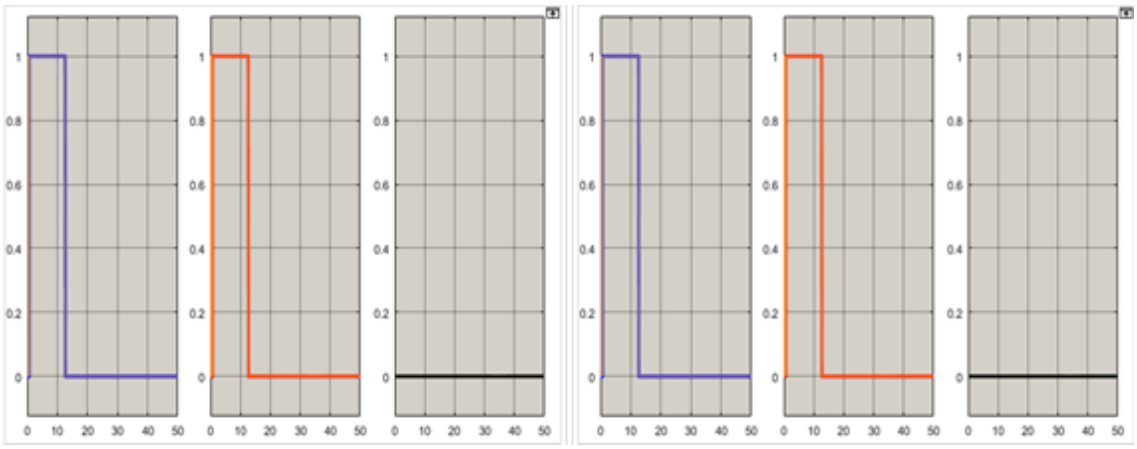

(a) (b)

(a) V control, Q control

Fig. 6.22. Feeder-b under three phase short circuit

In Fig. 6.22, both sub-relays produce passive response to the short circuit. This is because the short circuit is applied at adjacent feeder, indicating lack of *sympathetic tripping* by the proposed MFR relay as obtained in the grid-connected mode. This shows superior performance of the proposed MFR relay over proposals in literature that are based on use of over-current devices for micro-grid protection.

MS2 under three phase short circuit

Fig. 6.23 presents response of MS1 sub-relay, proposed MFR relay and feeder-a sub-relay to three phase-to-ground short circuit in islanded mode under V and Q control strategies. The short circuit is applied at terminals of MS2.

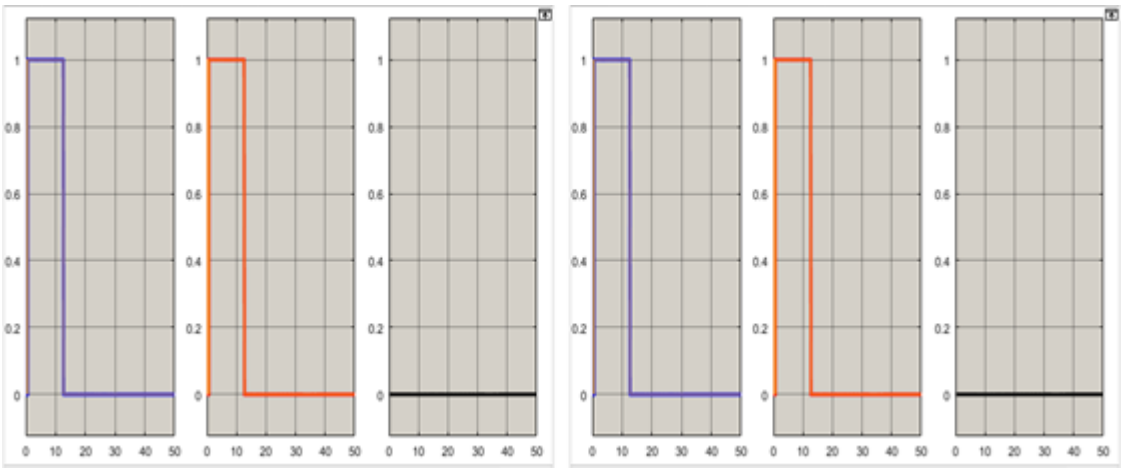

(a) (b)

(a) V control, (b) Q control

Fig. 6.23. MS2 under three phase short circuit

In Fig. 6.23, both sub-relays produce passive response to the short circuit. This is because the short circuit is applied at the terminals of a micro-source linked to adjacent feeder, indicating lack of *sympathetic tripping* by the proposed MFR relay as obtained in the grid-connected mode. This further shows superior performance of the proposed MFR relay over proposals in literature that are based on use of over-current devices for micro-grid protection. This is because the proposals in literature based on use of over-current devices are prone to *sympathetic tripping*.

Micro-grid under cross-country three phase short circuit

Fig. 6.24 presents response of MS1 sub-relay, proposed MFR relay and feeder-a sub-relay to cross-country three phase-to-ground short circuit in islanded mode under V and Q control strategies. The short circuit is applied at terminals of MS1, feeder-a, MS2 and feeder-b.

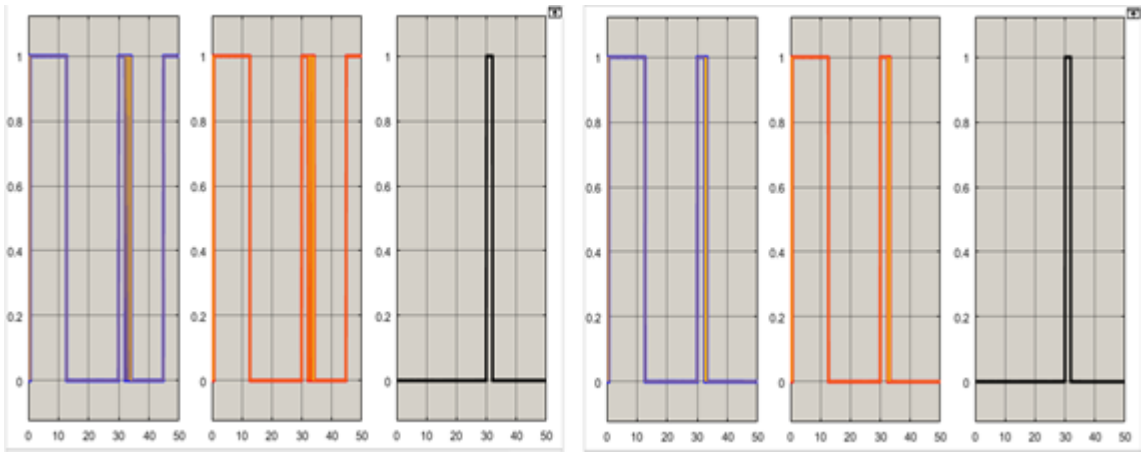

(a) (b)

(a) V control, (b) Q control

Fig. 6.24. Micro-grid (MS1, MS2, feeder-a and feeder-b) under cross-country three phase short circuit

In Fig. 6.24, note that feeder-a sub-relay generates logic 0 during pre-fault, logic 1 during fault-on and logic 0 during post-fault, in both control strategies. However, due to very high short circuit demand on MS1, MS1 sub-relay produces logic 1 during fault-on and during post-fault (with oscillatory logics during early and late post-fault) under V control. Under Q control strategy, MS1 produces short oscillatory logics during early post-fault and logic 0 during late post-fault. The oscillation recorded under Q control is triggered by the very high demand on the reactive var compensator. Feeder-a produces logic 0 during pre-fault, logic 1 during fault-on and then logic 0 during post-fault under both control strategies.

6.7 Alternative Test Beds

In order to establish wide applicability of the proposed MFR relay model, three alternative test beds are developed. A summary of their parameters is provided in Table 6.7.

Table 6.7. Major Parameters of the alternative test beds

	Test bed 2		Test bed 3		Test bed 4	
	Utility	**Micro-grid**	**Utility**	**Micro-grid**	**Utility**	**Micro-grid**
Generator voltage	Utility parameters of test bed 2 are same with utility parameters of the index test bed provided in Section 3.	-	16kV	-	12kV	-
Generated power		-	180MVA	-	60MVA	-
Transmission voltage		-	700kV	-	132kV	-
Transmission length		-	600km	-	65km	-
Micro-source voltage		400 V	-	800V	-	575V
Micro-source power		1.5kW	-	30kW	-	22kW
Demand on micro-grid		1.2kVA	-	24kVA	-	18kVA
Feeder voltage		6kV	-	25kV	-	11kV
Feeder length		0.5km	-	5.5km	-	2.5km

The proposed MFR relay is embedded in each of the three alternative test beds. The system under study is run for 50s under normal operating conditions. The system is also run under SC faults. The pre-fault, fault-on and post-fault output logics of the proposed MFR relay are found to be similar to those of the index test bed as presented in Tables 6.5 and 6.6.

6.7.1 Response of proposed MFR relay in standard test beds

After establishing its response in the developed alternative test beds, the proposed relay is further embedded in each of 24 standard test beds. The standard test beds include the CERTS/AEP Test Bed shown in Fig. 6.25 and The IEEE European Low Voltage Test Feeders.

The CERTS/AEP test bed consists of three feeders (A, B and C) servicing loads (Load-1 to Load-4). It also includes a micro-grid and it is linked to a utility. The micro-grid has three micro-sources (A-1, A-2 and B-1).

Feeder-A and Feeder-B can be islanded from the utility using a static switch. The hardware of the static switch consists of back-to-back thyristors and local implementation of the CERTS micro-grid islanding and re-synchronization techniques.

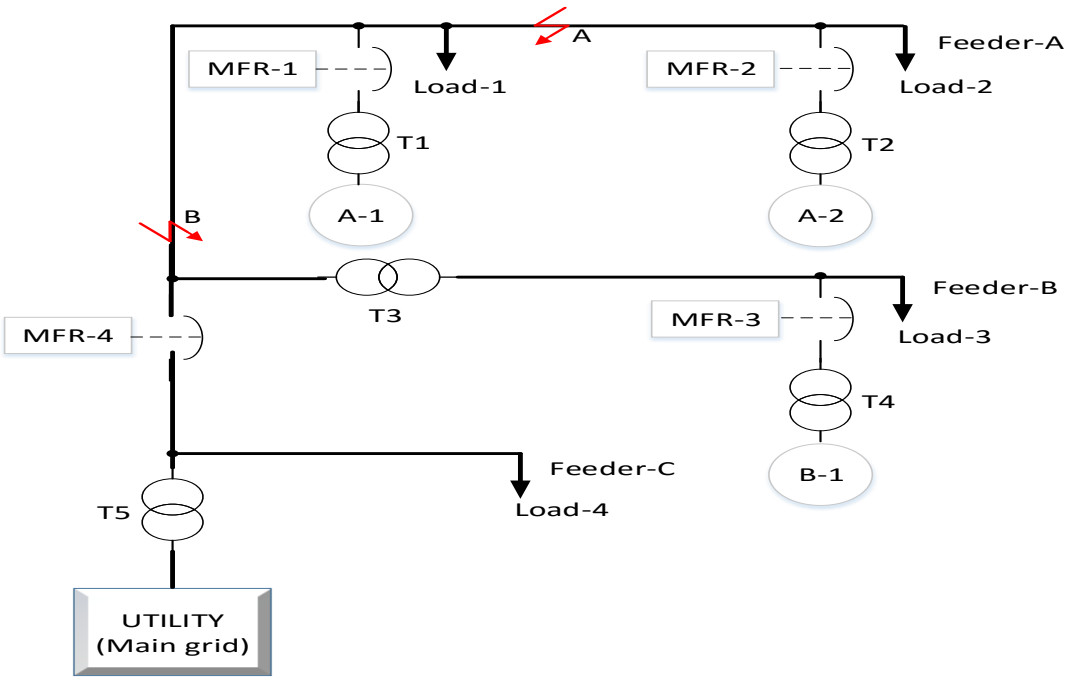

Fig. 6.25. CERTS/AEP micro-grid test bed

Source: CERTS Micro-grid Laboratory Test Bed, IEEE Transactions on Power Delivery, Vol. 26, No. 1, January 2011.

The relay performance is evaluated on the basis of the demerits associated with existing proposals. These demerits include drawbacks of using overcurrent relays in micro-grids - such as blinding of protection and sympathetic tripping.

The response of the proposed MFR relay is found to be devoid of the drawbacks associated with use of overcurrent relays in micro-grids, specifically blinding of protection and sympathetic tripping.

6.8 Results and Discussion

In grid-connected mode and under reactive power control regime, the micro-source maintains steady reactive power during utility fault. The reactive power rises under voltage control, indicative of reactive support from the utility as shown in Table 6.1. In the same mode, the micro-source consumes more reactive power from the utility and its reactive var compensator during micro-grid fault. In grid-connected mode, the micro-source voltage drops during both utility and micro-grid faults. The current rises during the fault. Active power, reactive power, voltage and current experience severe post-fault oscillations.

In grid-connected mode, active power in the feeder drops with severe post-fault oscillations during both utility and micro-grid faults as shown in Table 6.2. Feeder reactive power rises during

utility fault in grid-connected mode, justifying high reactive power supply from utility to support the network voltage. Table 6.2 shows that the feeder reactive power drops during micro-grid fault and records severe post-fault oscillation, indicative of limited reactive supply from the var sources to provide good LVRT. This is a major drawback of micro-grid operation, as published by Olivares et al. in [22] and Zamora in [26]. Feeder voltage drops while current rises during fault, as shown in Table 6.2, and recording severe post-fault oscillations.

In islanded mode, the micro-source and feeder active power drops during short circuit fault with virulent post-fault oscillations (recorded in the micro-source), as shown in Table 6.3. While micro-source reactive power rises during short circuit in the same mode, feeder reactive power falls. The feeder is a passive element which lacks capacity to slack reactive demand. As a passive element, the feeder lacks power generation or energy storage capability. Therefore, the feeder is neither able to provide long term energy support typical of a power generator nor short term energy support typical of an energy storage system. This is an indication of reactive power management capability of DFIG, as published by Moayed Moghbel et al. in [88] and in [89, 91]. Both micro-source and feeder voltages drop during the fault, while their currents rise during same fault.

The surface plot of micro-source sub-relay controller's response (Fig. 6.4) shows that it outputs Logic 1 whenever micro-source current is HIGH AND micro-source voltage is NORMAL (or LOW). Under other feasible combinations of P_{mn}, Q_{mn}, $V_{\alpha n}$ and I_{mn}, the controller outputs a non-unity response which is digitally processed to Logic 0 using logic gates.

The surface plot of feeder sub-relay controller's response (Fig. 6.5) shows that it outputs Logic 1 whenever feeder active power is LOW AND feeder reactive power is LOW (or HIGH). Under other feasible combinations of P_{fn}, Q_{fn}, V_{1n} and I_{2n} the controller, in combination with logic gates, outputs Logic 0.

6.9 Conclusion

In this chapter, a new protective relay has been developed and presented. Using a combination of requisite equations and extensive simulation of the test bed, the rules which engage four variables have been framed in fuzzy form. Using the framed rules, fuzzy logic controllers have been designed for micro-source and feeder sub-relays. The hardware has been realized using software combinational logic components, making it cost-effective. Offline and online response tests of the relay have been investigated and they show that it provides reliable detection and protection of the micro-grid against different short circuits in both islanded and grid-connected modes under both control regimes. It has been shown that the proposed relay does not suffer from blinding and

sympathetic tripping. Its implementation facilitates the plug-and-play and peer-to-peer requirements of micro-grid protection, as presented in this Chapter. The succeeding chapter presents overall summary, conclusion and future works for this project.

Chapter 7: Conclusion and Future Works

This thesis presents an attempt to propose a new protective relay for ac micro-grids. The relay is based on fault detection and fuzzy logic combination of four parameters (active power, reactive power, voltage and current). It consists of two sub-relays, namely; micro-source sub-relay and feeder sub-relay. Performance of the proposed rely is evaluated through extensive simulation analyses on a test bed consisting of 100MVA utility and an 11kW micro-grid. The test bed was developed using first principle modeling in SimPowerSystems ® software. Small signal analysis was performed on the test bed to establish its stability and response. Requisite regulators were designed using data-driven modeling and closed-loop feedback topology in Simulink Control Design® and PID Tuner®. The regulators were combined to implement two mutually exclusive control regimes; the active power-voltage (PV or V) control and the active-reactive power (PQ or Q) control. Short circuit faults were simulated on the studied micro-grid system and the dynamic response of the system was analyzed and utilized to develop fuzzy logic rules that govern the proposed relay performance. Each sub-relay has been implemented using distinct fuzzy rule combination of the four measured parameters such that, regardless of the control regime and operating mode, a micro-source short circuit fault is instantly detected by the micro-source sub-relay while a feeder short circuit fault is instantly detected by the feeder sub-relay. The proposed relay is reliable, easy to implement and cost-effective in comparison with other micro-grid relay topologies in literature. Moreover, the proposed relay facilitates the plug-and-play and peer-to-peer features of micro-grid protection. Consequently, a new protective relay for short circuits in ac micro-grids is proposed.

7.1 Research Contributions

a. This research has proposed a new relay for short circuit faults in ac micro-grids. Design of quality and cost-effective protective system is one of the challenges bedeviling full-scale deployment of micro-grids.
b. This research has also proposed two connection schemes for the new relay. Depending on application, the proposed relay could be connected in unit or sub-unit scheme.
c. This study has developed a system for studying micro-grid interaction with utility in terms of steady-state and dynamic stability when the micro-grid is in grid-connected and islanded operating modes.
d. This research has performed power system study which investigated and validated literary theories on micro-grid and utility short circuits when the micro-grid is in grid-connected and islanded modes, under two mutually exclusive control regimes.

e. This study provides an addition to the retinue of devices available for investigations which seek to enhance resilience, quality and sustainability of future power systems.

7.2 Conclusion

In this work, an attempt has been made to develop a utility-connected micro-grid test bed. The utility includes a steam turbine, excitation system, power system stabilizer, synchronous generator, STATCOM, loads and transmission lines. The micro-grid includes DFIGs as micro-sources, feeders, loads and var compensators. The micro-grid is capable of PV and PQ controls. Response of the test bed to standard short circuits has been investigated and presented in this report. Formulation of fuzzy rules that engage four parameters has also been presented. Responses of modeled fuzzy logic controllers have been demonstrated and availed in this report. The controllers have been realized in a soft hardware implementation and briefly articulated. The response of the relay hardware and proper connection schemes have also been summarized in this thesis. Consequently, a new multivariable fuzzy rule-based relay for short circuits in ac micro-grids is proposed. The proposed relay presents improved reliability for detection of short circuits in both grid-connected and islanded modes.

7.3 Comparison of Proposed MFR Relay with Proposals in Literature

Table 7.1 provides a summarized comparison of the proposed MFR relay with proposals reported in literature. In the Table, the symbol F implies that the proposal(s) fully satisfies the measure; P implies that the proposal(s) partially satisfies the measure; and X implies the proposal(s) fails to satisfy the measure.

Table 7.1. Comparison of proposed MFR relay with those reported in literature

Measure	Proposal(s) in Literature	Proposed MFR Relay
Plug-and-play	𝒫	𝓕
Peer-to-peer	𝒫	𝓕
Simulated controls	𝒳	𝓕
Dual mode operation	𝒫	𝓕
Balanced and unbalanced short circuits	𝒫	𝓕
Use of Fuzzy Logic for unit protection	𝓕	𝓕
Use of Fuzzy Logic for integrated system protection	𝒳	𝓕

7.4 Future Works

The following is a highlight of the activities that are recommended for further investigation in order to improve understanding, validity and performance of this research work:

a. Thorough investigation of the effect of type, severity and location of short circuit on the operating modes of DFIGs in the test beds with the aim of improving them.
b. Further technical validation of the test bed using key performance indices such as system stiffness and operating efficiency with the aim of improving them where necessary.
c. Investigations which could lead to a new control algorithm which offers enhanced micro-grid performance even under the severest short circuit fault.
d. Further development of the proposed relay to determine adequacy of its response time and possibly develop a Time-MFR relay for time-dependent protection.
e. Investigation which seeks to determine the effects of incorporating other active micro-sources such as solar PV, active loads and energy storage to the test bed.

7.5 List of Publications

M. A. Aminu, "Design of Reactive Power and Voltage Controllers for Converter-interfaced ac Microgrids", British Journal of Applied Science & Technology, Vol. 17, 2016.

Maruf A. Aminu. Validating Response of ac Micro-grid to Three Phase Short Circuit in Grid-Connected Mode Using Dynamic Analysis. *International Journal of Electrical Components and Energy Conversion Vol. 2, No. 4, 2016, pp. 21-34. doi: 10.11648/j.ijecec.20160204.11*

APPENDICES

Appendix A1. Parameters of excitation system

S/N0.	Variable	Description	Data
1.	$T_R(s)$	Low-pass filter time constant in seconds [first-order system representing the stator terminal voltage transducer]	$20x10^{-3}$
2.	$T_B(s), T_C(s)$	Time constants in seconds for transient gain reduction [first-order system representing a lead-lag compensator]	0, 0
3.	$K_A, T_A(s)$	Regulator gain, time constant in seconds [first-order system representing the main regulator]	300, 0.001
4.	$E_{f_{\min}}(pu), E_{f_{\max}}(pu), K_p$	Regulator output limits in p.u. and gain. The upper limit can be a constant and equal to $E_{f_{\max}}$. It can also be variable and equal to the rectified stator terminal voltage V_{tf} times a proportional gain K_p. If K_p is set to 0, the former applies. If K_p is set to a positive value, the latter applies.	-11.5, 11.5, 0
5.	$K_E, T_E(s)$	Exciter gain, time constant in seconds [first-order system representing the exciter]	1, 0
6.	$K_f, T_f(s)$	Damping filter gain and time constant in seconds [first-order system representing a derivative feedback]	0.001, 0.1
7.	$V_{t_o}(pu), V_{f_o}(pu)$	Initial values of terminal voltage and field voltage in p.u.. They are correctly set to start the simulation in steady state. They are automatically updated by the load flow solution process.	1.0, 1.25

Appendix A2. Parameters of synchronous generator

S/N0.	Variable	Description	Data
1.	$S_n(VA), V_{rms}(V), f_n(Hz)$	Nominal power in Volt-Ampere, RMS line-to-line voltage in Volt, nominal frequency in Hertz.	100 X 106, 13800, 50
2.	H, K_d, p	Inertia *H* in seconds (or *J* in kg.m^2), damping factor and pole pair. The damping	3.5, 0, 20

		factor is specified in (p.u of torque)/(p.u. of speed).	
3.	$Z = R + jX$ p.u.	Per phase generator internal impedance (sum of resistance, *R*, and reactance, *X*, in p.u.).	*R*=0.02, *X*=0.3
4.	$\Delta\omega(\%); \delta(^o); i_a, i_b, i_c (p.u.); \phi_a, \phi_b, \phi_c (^o)$	Initial conditions (per cent initial speed deviation from nominal value, power angle in degrees, per unit line current magnitudes, phase angles in degrees).	0; 0; 0, 0, 0; 0, 0, 0.

Appendix A3. Electrical parameters of synchronous generator

S/N0.	**Variable**	**Description**	**Data**
1.	$R_s; L_l; L_{md}; L_{mq}$	Stator resistance, leakage inductance, *d*-axis magnetizing inductance and *q*-axis magnetizing inductance. All in p.u..	[$2.85\,x10^{-3}$; 0.112; 1.20; 0.30] p.u.
2.	$R_f^{'}; L_{lfd}^{'}$	Per unit field resistance and leakage inductance, both referred to the stator.	[$5.8\,x10^{-4}$; 0.112]p.u.
3.	$R_{kd}^{'}; L_{lkd}^{'}; R_{kq1}^{'}; L_{lkq1}^{'}$	Damper parameters – d-axis resistance ($R_{kd}^{'}$), leakage inductance (L_{lkd}^{1}), q-axis resistance ($R_{kq1}^{'}$) and leakage inductance ($L_{lkq1}^{'}$). All in p.u. and referred to the stator.	[$1.15\,x10^{-2}$; 0.18; 1.97 $x10^{-2}$; 0.385] p.u.
4.	$H(s); F(p.u.); p$	Inertia *H* in seconds (or *J* in kg.m^2), friction factor *F* in N.m.s and pole pair. Friction torque T_f is proportional to rotor speed ω . $T_f = F\omega$, T_f is expressed in N.m, ω in rads^{-1}, and *F* in N.m.s.	3.5; 0; 20
5.	$\Delta\omega(\%); \delta(^o); i_a, i_b, i_c (p.u.); \phi_a, \phi_b, \phi_c (^o); V_f (p.u.)$	Initial conditions (per cent initial speed deviation from nominal value, power angle in degrees, per unit line current magnitudes, phase angles in degrees, and initial field voltage in p.u.).	0; 0; 0, 0, 0; 0, 0, 0; 1.0.

Appendix B1. Parameters of three phase reactive var source

S/N0.	Variable	Description	Data
1.	$V_{base}; f; S_{sc}; X/R$	**Voltage source** Phase-to-phase base voltage in Volt; nominal source frequency in Hz; three phase short circuit level of source at base voltage in VA; and X/R ratio at nominal source frequency.	25kV; 50; $3x10^6$; 10.
2.	$S_n; f_n; [V_1, R_1, L_1]; [V_2, R_2, L_2]; [R_m, L_m]$	**Transformer** Nominal power in VA; nominal frequency in Hz; winding 1 parameters (V_1 in V_{rms}, R_1 in p.u., L_1 in p.u.); winding 2 parameters (V_2 in V_{rms}, R_2 in p.u., L_2 in p.u.); magnetization resistance and inductance (R_m and L_m, both in p.u.).	$500x10^3$; 50; [$25x10^3$, 0.003456, 0.11526]; [575, 0.003456, 0.11526]; [500, 500].
3.	$V_n; f_n; Q_c$	**Capacitive load** The nominal line-to-line voltage of the load, in Volt rms; the nominal frequency in Hz; the three phase capacitive reactive power in var.	575; 50; $100x10^3$.

Appendix B2. Parameters of wind turbine-generator system

S/N0.	Variable	Description	Data
1.	$P_m; [Speed\_A ... Speed\_D]; P_{\_c}; v_{w\_c}; K_p; \beta_{\max}; \dot{\beta}_{\max}$	**Wind turbine** The nominal wind turbine mechanical output power in Watts; tracking characteristic speeds (speed_A in p.u. … speed_D in p.u.); power at point C (p.u. of mechanical power); wind speed at point C (in ms^{-1}); pitch angle regulator gain (K_p); maximum pitch angle in degrees ($\beta \geq 0$); maximum rate of	$12x10^3$, [0.7, 0.71, 1.2, 1.21]; 0.95; 6.0; 479; 45; 2.

		change of pitch angle in degs^{-1}.	
2.	$S_n; V_n; f_n; R_s, L_{ls}; R_r^{'}, L_{lr}^{'};$ $L_m; H; F; p;$ Initial conditions $[s, \theta, I_s, \phi_s, I_r, \phi_r]$	**<u>Induction generator</u>** Nominal generator apparent power in VA; RMS line-to-line voltage in V; nominal frequency in Hz; stator resistance R_s and leakage inductance L_{ls} in p.u.; rotor resistance $R_r^{'}$ and leakage inductance $L_{lr}^{'}$ in p.u., both referred to stator, magnetizing inductance in p.u.; combined machine and load inertia constant in p.u.; combined viscous friction coefficient in p.u.; pole pair; Initial conditions [slip, electrical angle in degree, stator current magnitude in p.u., stator current phase angle in degree, rotor current magnitude in p.u., rotor current phase angle in degree].	$11x10^3$; 575; 50; 0.004843, 0.1248; 0.004377, 0.1791; 6.77; 5.04; 0.01; 2; [-0.01, 0,0,0,0,0].

Appendix B3. Parameters of VSI

IGBT	**Ron (Ohm)**				
	0.001				
Modulator (Pulse Generator)	**Amplitude**	**Period (seconds)**	**Duty Cycle (50%)**	**Phase Delay (second)**	**Frequency (Hz)**
	10	0.02	50.00	See Table 3.3	50.00

Appendix C1. Index test bed showing utility and micro-grid as sub-systems

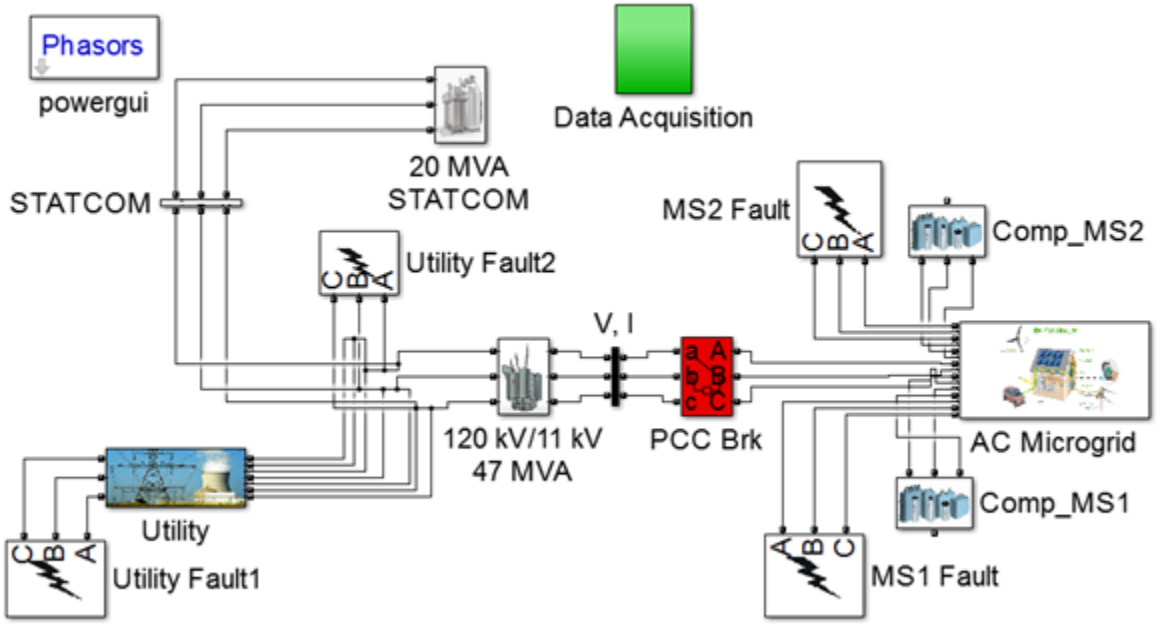

Appendix C2. Utility as a sub-system of the index test bed

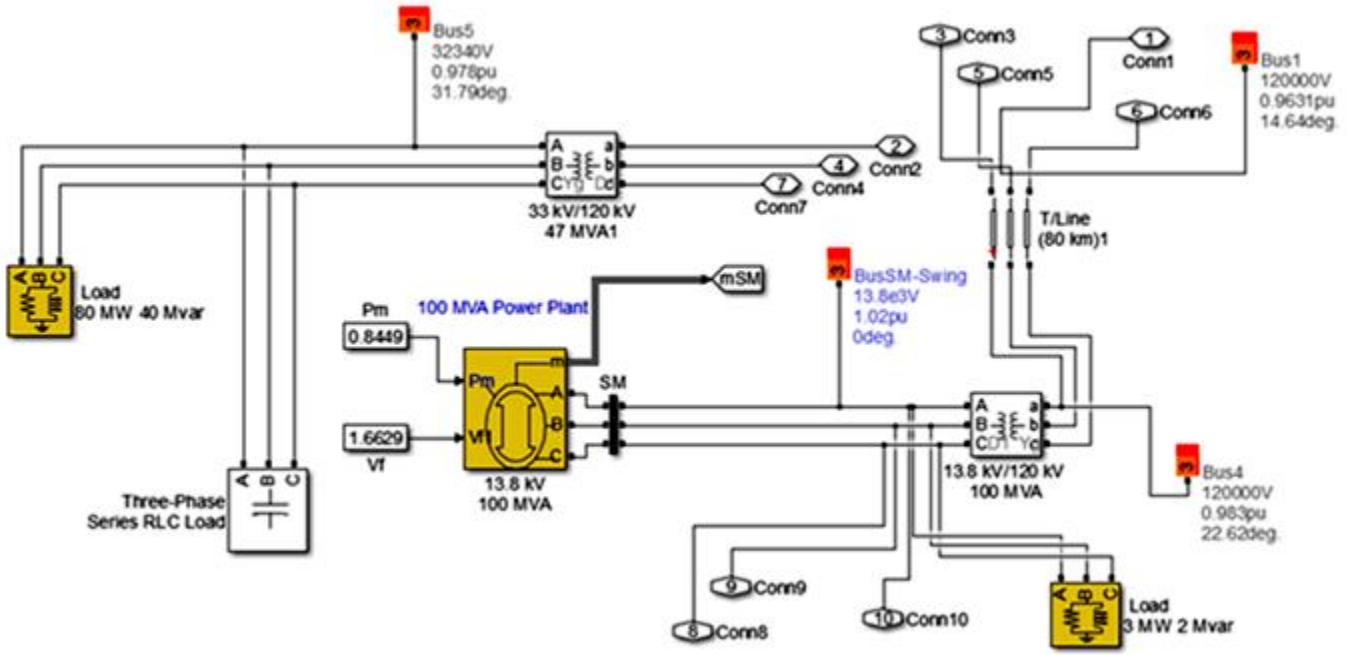

Appendix C3. Reactive power source as a sub-system of the index test bed

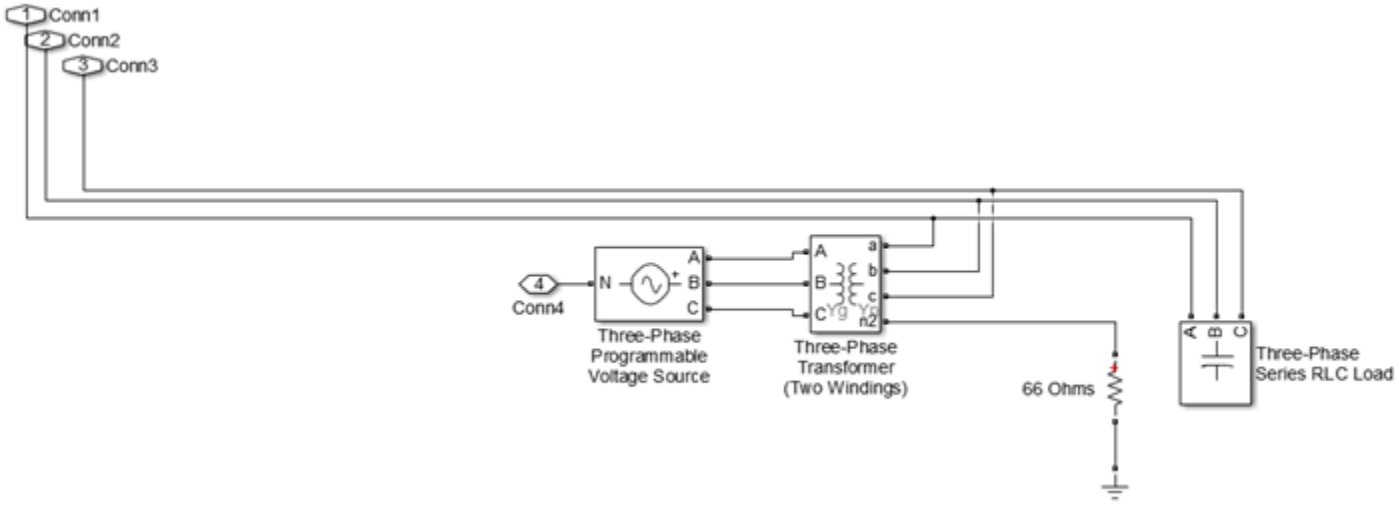

Appendix C4. Steady-state response of the index test bed

	Block type	Bus type	Bus ID	Vbase (kV)	Vref (pu)	Vangle (deg)	P (MW)	Q (Mv...	Qmin (Mvar)	Qmax (Mvar)	V_LF (pu)	Vangle_LF (deg)	P_LF (MW)	Q_LF (Mvar)	Block Name
1	RLC load	Z	Bus7	11.00	1	0.00	0.01	0.00	-Inf	Inf	1.0001	-1.37	0.01	0.00	AC Microgrid/6.4 kW 0.30 kvar
2	Bus	-	Bus2	11.00	1	0.00	0.00	0.00	0.00	0.00	1.0006	-0.91	0.00	0.00	AC Microgrid/Load Flow Bus2
3	RLC load	Z	Bus3	11.00	1	0.00	0.01	0.00	-Inf	Inf	1.0011	-0.43	0.01	0.00	AC Microgrid/3 kW 0.125 kvar
4	RLC load	Z	WT3Bus1	0.58	1	0.00	0.00	-0.10	-Inf	Inf	1.0012	-0.07	0.00	-0.10	Comp_MS1/Three-Phase Series RL...
5	RLC load	Z	WT3Bus2	0.58	1	0.00	0.00	-0.04	-Inf	Inf	1.0004	-0.08	0.00	-0.04	Comp_MS2/Three-Phase Series RL...
6	Bus	-	Bus1	120.00	1	0.00	0.00	0.00	0.00	0.00	0.9631	14.64	0.00	0.00	Utility/Bus*1*
7	Bus	-	Bus4	120.00	1	0.00	0.00	0.00	0.00	0.00	0.9830	22.62	0.00	0.00	Utility/Bus*2*
8	RLC load	Z	Bus5	32.34	1	0.00	0.00	-50.00	-Inf	Inf	0.9780	31.79	0.00	-50.00	Utility/Three-Phase Series RLC...
9	RLC load	PQ	Bus5	32.34	1	0.00	80.00	40.00	-Inf	Inf	0.9780	31.79	80.00	40.00	Utility/ Load 80 MW 40 Mvar
10	SM	swing	BusSM-...	13.80	1.0200	0.00	12.00	2.00	0.00	Inf	1.0200	0.00	84.26	28.83	Utility/13.8 kV 100 MVA
11	RLC load	PQ	BusSM-...	13.80	1.0200	0.00	3.00	2.00	-Inf	Inf	1.0200	0.00	3.00	2.00	Utility/ Load 3 MW 2 Mvar
12	Vprog	swing	*1*	25.00	1	0.00	0.00	0.40	-Inf	Inf	1	0.00	0.11	-0.04	Comp_MS2/Three-Phase Programma...
13	Vprog	swing	*2*	25.00	1	0.00	0.00	0.40	-Inf	Inf	1	0.00	0.10	-0.10	Comp_MS1/Three-Phase Programma...
14	Bus	-	*3*	11.00	1	0.00	0.00	0.00	0.00	0.00	0.9630	-15.37	0.00	0.00	120 kV//11 kV 47 MVA/120 kV//1...

Appendix C5. Basic measurements obtained from steady-state analysis

MEASUREMENTS:
1: 'U A: STATCOM ' = 66727.69 Vrms 14.64°
2: 'U B: STATCOM ' = 66728.10 Vrms -105.36°
3: 'U C: STATCOM ' = 66728.10 Vrms 134.64°
4: 'U A: Bus1 ' = 66727.69 Vrms 14.64°
5: 'U B: Bus1 ' = 66728.10 Vrms -105.36°
6: 'U C: Bus1 ' = 66728.10 Vrms 134.64°
7: 'U A: B575a
' = 332.37 Vrms -0.07°
8: 'U B: B575a
' = 332.37 Vrms -120.07°
9: 'U C: B575a
' = 332.37 Vrms 119.93°
10: 'U A: B575b ' = 332.12 Vrms -0.08°
11: 'U B: B575b ' = 332.12 Vrms -120.08°
12: 'U C: B575b ' = 332.12 Vrms 119.92°
13: 'U A: B1 ' = 332.37 Vrms -0.07°
14: 'U B: B1 ' = 332.37 Vrms -120.07°
15: 'U C: B1 ' = 332.37 Vrms 119.93°
16: 'U A: B1 ' = 332.12 Vrms -0.08°
17: 'U B: B1 ' = 332.12 Vrms -120.08°
18: 'U C: B1 ' = 332.12 Vrms 119.92°
19: 'U A: fa
' = 6354.72 Vrms -0.91°
20: 'U B: fa

21: 'U C: fa
' = 6354.72 Vrms 119.09°
22: 'U A: fa
1 ' = 6354.72 Vrms -0.91°
23: 'U B: fa
1 ' = 6354.72 Vrms -120.91°
24: 'U C: fa
1 ' = 6354.72 Vrms 119.09°
25: 'U A: fa_pu ' = 6354.72 Vrms -0.91°
26: 'U B: fa_pu ' = 6354.72 Vrms -120.91°
27: 'U C: fa_pu ' = 6354.72 Vrms 119.09°
28: 'U A: fb ' = 6354.72 Vrms -0.91°
29: 'U B: fb ' = 6354.72 Vrms -120.91°
30: 'U C: fb ' = 6354.72 Vrms 119.09°
31: 'U A: fb_pu ' = 6354.72 Vrms -0.91°
32: 'U B: fb_pu ' = 6354.72 Vrms -120.91°
33: 'U C: fb_pu ' = 6354.72 Vrms 119.09°
34: 'U A:
SM ' = 8126.86 Vrms 120.00°
35: 'U B:
SM ' = 8126.81 Vrms -120.00°
36: 'U C:
SM ' = 8126.81 Vrms 0.00°
37: 'U AB: V, I ' = 10593.13 Vrms 14.63°
38: 'U BC: V, I ' = 10593.19 Vrms -105.37°
39: 'U CA: V, I ' = 10593.19 Vrms 134.63°
40: 'I A: STATCOM ' = 0.00 Arms 95.19°

REFERENCES

[1] UN, "World Population Prospects - The 2015 Revision," Department of Economic and Social Affairs - Population Division Ney York 2015.

[2] NREL, "DG Power Quality, Protection and Reliability Case Studies Report," New York NREL/SR-560-34635 2003.

[3] Z. Akhtar and M. A. Saqib, "Microgrids formed by renewable energy integration into power grids pose electrical protection challenges," *Renewable Energy,* vol. 99, pp. 148-157, 12// 2016.

[4] B. Kroposki and G. Martin, "Hybrid renewable energy and microgrid research work at NREL," in *2010 IEEE Power and Energy Society General Meeting*, 2010, pp. 1-4.

[5] N. Hatziargyriou, H. Asano, R. Iravani, and C. Marnay, "Microgrids," *IEEE Power and Energy Magazine,* vol. 5, pp. 78-94, 2007.

[6] C. Schwaegerl and L. Tao, "The Microgrids Concept," ed: John Wiley and Sons Ltd, 2013, pp. 1-24.

[7] M. Barnes, J. Kondoh, H. Asano, J. Oyarzabal, G. Ventakaramanan, R. Lasseter*, et al.*, "Real-World MicroGrids-An Overview," in *IEEE International Conference on System of Systems Engineering, 2007. SoSE '07.* , 2007, pp. 1-8.

[8] T. S. Ustun, C. Ozansoy, and A. Zayegh, "Recent developments in microgrids and example cases around the world—A review," *Renewable and Sustainable Energy Reviews,* vol. 15, pp. 4030-4041, 2011.

[9] M. Schäfer, N. Kebir, and K. Neumann, "Research needs for meeting the challenge of decentralized energy supply in developing countries," *Energy for Sustainable Development,* vol. 15, pp. 324-329, 2011.

[10] P. Piagi and R. H. Lasseter, "Autonomous control of microgrids," in *2006 IEEE Power Engineering Society General Meeting*, 2006, p. 8

[11] G. Strbac, P. Djapić, T. Bopp, and N. Jenkins, "Benefits of Active Management of Distribution Systems," in *Wind Power in Power Systems*, ed: John Wiley & Sons, Ltd, 2012, pp. 935-950.

[12] G. J. Kish and P. W. Lehn, "Microgrid Design Considerations for Next Generation Grid Codes," in *2012 IEEE Power and Energy Society General Meeting*, 2012, pp. 1-8.

[13] A. Oudalov, T. Degner, F. V. Overbeeke, and J. M. Yarza, "Microgrid Protection," in *Microgrids*, ed: John Wiley and Sons Ltd, 2013, pp. 117-164.

[14] M. Y. Vaziri, S. Vadhva, C. J. Hoffman, and K. K. Yagnik, "Re-use of existing system protection concerns and interconnection rules for integration of future Distributed Generation," in *2010 IEEE International Conference on Information Reuse and Integration (IRI)*, 2010, pp. 388-393.

[15] M. R. Miveh, M. Gandomkar, S. Mirsaeidi, and M. R. Gharibdoost, "A review on protection challenges in microgrids," in *Electrical Power Distribution Networks (EPDC), 2012 Proceedings of 17th Conference on*, 2012, pp. 1-5.

[16] A. K. Tiwari, S. R. Mohanty, and R. K. Singh, "Review on protection issues with penetration of distributed generation in distribution system," in *Electrical Engineering Congress (iEECON), 2014 International*, 2014, pp. 1-4.

[17] M. Dewadasa, A. Ghosh, and G. Ledwich, "Protection of Microgrids using Differential Relays," in *2011 21st Australasian Universities Power Engineering Conference (AUPEC)*, 2011, pp. 1-6.

[18] SGiP, "Guidelines for Smart Grid Cyber Security," T. S. G. I. P. C. S. W. Group, Ed., ed. Washington: US DOE, 2010.

[19] R. Mattioli and K. Moulinos, "Communication network interdependencies in smart grids," E. U. A. F. N. A. I. Security, Ed., ed. EU: ENISA, 2015.

[20] T. S. Ustun, C. Ozansoy, and A. Zayegh, "A microgrid protection system with central protection unit and extensive communication," in *2011 10th International Conference on Environment and Electrical Engineering (EEEIC)*, 2011, pp. 1-4.

[21] L. Hernandez, C. Baladron, J. M. Aguiar, B. Carro, A. J. Sanchez-Esguevillas, J. Lloret*, et al.*, "A Survey on Electric Power Demand Forecasting: Future Trends in Smart Grids, Microgrids and Smart Buildings," *IEEE Communications Surveys & Tutorials,* vol. 16, pp. 1460-1495, 2014.

[22] D. E. Olivares, A. Mehrizi-Sani, A. H. Etemadi, C. A. Canizares, R. Iravani, M. Kazerani*, et al.*, "Trends in Microgrid Control," *IEEE Transactions on Smart Grid,* vol. 5, pp. 1905-1919, 2014.

[23] Y. L. Goh, A. K. Ramasamy, F. H. Nagi, and A. A. Z. Abidin, "Digital Signal Processor Based Over-current Relay Using Fuzzy Logic Controller," *Electric Power Components and Systems,* vol. 39, pp. 1437-1451, 2011/08/24 2011.

[24] M. A. Aminu, "Design of Reactive Power and Voltage Controllers for Converter-interfaced ac Microgrids," *British Journal of Applied Science & Technology,* vol. 17, 2016.

[25] M. Vaziri, S. Vadhva, T. Oneal, and M. Johnson, "Smart grid, Distributed Generation, and standards," in *Power and Energy Society General Meeting, 2011 IEEE*, 2011, pp. 1-8.

[26] R. Zamora and A. K. Srivastava, "Controls for microgrids with storage: Review, challenges, and research needs," *Renewable and Sustainable Energy Reviews,* vol. 14, pp. 2009-2018, 2010.

[27] M. Vaziri, S. Vadhva, T. Oneal, and M. Johnson, "Distributed generation issues and standards," in *2011 IEEE International Conference on Information Reuse and Integration (IRI)*, 2011, pp. 439-443.

[28] H. J. Laaksonen, "Protection Principles for Future Microgrids," *IEEE Transactions on Power Electronics,* vol. 25, 2010.

[29] N. Hassan and L. H. Robert, "Microgrid Protection," in *2007 IEEE Power Engineering Society General Meeting*, 2007, pp. 1-6.

[30] N. Hassan and L. H. Robert, "Microgrid Fault Protection Based on Symmetrical and Differential Current Components," C. E. Commission, Ed., ed. California, 2006.

[31] R. J. Best, D. J. Morrow, and P. A. Crossley, "Communication assisted protection selectivity for reconfigurable and islanded power networks," in *Universities Power Engineering Conference (UPEC), 2009 Proceedings of the 44th International*, 2009, pp. 1-5.

[32] M. A. Zamani, A. Yazdani, and T. S. Sidhu, "A Communication-Assisted Protection Strategy for Inverter-Based Medium-Voltage Microgrids," *Smart Grid, IEEE Transactions on,* vol. 3, pp. 2088-2099, 2012.

[33] H. Al-Nasseri, M. A. Redfern and F, Li, "A Voltage based Protection for Micro-grids containing Power Electronic Converters," presented at the IEEE Power Engineering Society General Meeting, 2006.

[34] T. Loix, T. Wijnhoven, and G. Deconinck, "Protection of microgrids with a high penetration of inverter-coupled energy sources," in *Integration of Wide-Scale Renewable Resources Into the Power Delivery System, 2009 CIGRE/IEEE PES Joint Symposium*, 2009, pp. 1-6.

[35] S. M. S. Glover D J, *Power system analysis and design*. USA: Books Cole, 2002.

[36] H. H. Zeineldin, E. F. El-Saadany, and M. M. A. Salama, "Distributed Generation Micro-Grid Operation: Control and Protection," in *Power Systems Conference: Advanced Metering, Protection, Control, Communication, and Distributed Resources, 2006. PS '06*, 2006, pp. 105-111.

[37] S. Conti, L. Raffa, and U. Vagliasindi, "Innovative solutions for protection schemes in autonomous MV micro-grids," in *Clean Electrical Power, 2009 International Conference on*, 2009, pp. 647-654.

[38] E. Sortomme, S. S. Venkata, and J. Mitra, "Microgrid Protection Using Communication-Assisted Digital Relays," *Power Delivery, IEEE Transactions on,* vol. 25, pp. 2789-2796, 2010.

[39] A. Prasai, Y. Du, A. Paquette, E. Buck, R. Harley, and D. Divan, "Protection of meshed microgrids with communication overlay," in *2010 IEEE Energy Conversion Congress and Exposition (ECCE)*, 2010, pp. 64-71.

[40] M. Dewadasa, A. Ghosh, and G. Ledwich, "Protection of microgrids using differential relays," in *Universities Power Engineering Conference (AUPEC), 2011 21st Australasian*, 2011, pp. 1-6.

[41] G. Celli, F. Pilo, and F. Pilo, "An Innovative Transient-Based Protection Scheme for MV Distribution Networks with Distributed Generation," in *Developments in Power System Protection, 2008. DPSP 2008. IET 9th International Conference on*, 2008, pp. 285-290.

[42] P. Mahat, Z. Chen, B. Bak-Jensen, and C. L. Bak, "A Simple Adaptive Overcurrent Protection of Distribution Systems With Distributed Generation," *IEEE Transactions on Smart Grid,* vol. 2, 2011.

[43] R. M. Tumilty, M. Brucoli, G. M. Burt, and T. C. Green, "Approaches to Network Protection for Inverter Dominated Electrical Distribution Systems," in *The 3rd IET International Conference on Power Electronics, Machines and Drives, 2006*, 2006, pp. 622-626.

[44] A. F. Alexandre Oudalov. (2009). *Adaptive Network Protection in Microgrids*. Available: www.microgrids.eu/documents/519.pdf

[45] X. H. Ke Dang, Daqiang Bi, Cunliang Feng, "An Adaptive Protection Method for the Inverter Dominated Microgrid," in *2011 International Conference on Electrical Machines and Systems (ICEMS 2011)*, Beijing, China, 2011.

[46] M. Khederzadeh, "Adaptive setting of protective relays in microgrids in grid-connected and autonomous operation," in *11th International Conference on Developments in Power Systems Protection, 2012. DPSP 2012*, 2012, pp. 1-4.

[47] K.-Y. Lien, D. M. Bui, S.-L. Chen, W.-X. Zhao, Y.-R. Chang, Y.-D. Lee*, et al.*, "A novel fault protection system using communication-assisted digital relays for AC microgrids having a multiple grounding system," *International Journal of Electrical Power & Energy Systems,* vol. 78, pp. 600-625, 6// 2016.

[48] B. S. S. Abinash Singh, "Microgrid- A Review," *International Journal of Research in Engineering and Technology,* vol. 03, pp. 185-198, Feb. 2014 2014.

[49] T. S. Ustun, C. Ozansoy, and A. Zayegh, "A central microgrid protection system for networks with fault current limiters," in *2011 10th International Conference on Environment and Electrical Engineering (EEEIC)*, 2011, pp. 1-4.

[50] T. Ghanbari and E. Farjah, "Development of an Efficient Solid-State Fault Current Limiter for Microgrid," *IEEE Transactions on Power Delivery,* vol. 27, pp. 1829-1834, 2012.

[51] T. Ghanbari and E. Farjah, "Unidirectional Fault Current Limiter: An Efficient Interface Between the Microgrid and Main Network," *IEEE Transactions on Power Systems,* vol. 28, pp. 1591-1598, 2013.

[52] A. Hussain, M. Aslam, and S. M. Arif, "N-version programming-based protection scheme for microgrids: A multi-agent system based approach," *Sustainable Energy, Grids and Networks,* vol. 6, pp. 35-45, 6// 2016.

[53] R. M. Kamel, M. A. Alsaffar, and M. K. Habib, "Novel and simple scheme for Micro-Grid protection by connecting its loads neutral points: A review on Micro-Grid protection techniques," *Renewable and Sustainable Energy Reviews,* vol. 58, pp. 931-942, 5// 2016.

[54] H. A. Abyane, K. Faez, and H. K. Karegar, "A new method for overcurrent relay using neural network and fuzzy logic," in *TENCON '97. IEEE Region 10 Annual Conference. Speech and Image Technologies for Computing and Telecommunications., Proceedings of IEEE*, 1997, pp. 407-410 vol.1.

[55] K. Erenturk and I. H. Altas, "Fault Identification in a Radial Power System using Fuzzy Logic," *Instrumentation Science and Technology,* vol. 32, pp. 641-653, 2004.

[56] IEEE, "Dynamic Models for Steam and Hydro Turbines in Power System Studies," *IEEE Transactions on Power Apparatus and Systems,* vol. PAS-92, pp. 1904-1915, 1973.

[57] S. Sivanagaraju, *Power System Operation and Control*. India: Pearson Education India, 2009.

[58] IEEE, "IEEE Recommended Practice for Excitation System Models for Power System Stability Studies," *IEEE Std 421.5-1992,* p. 0_1, 1992.

[59] N. S. Nise, *Control Systems Engineering*, 6th ed. USA: Joh Wiley & Sons, Inc., 2011.

[60] K. Ogata, *Modern Control Engineering 4th Ed...* 4th ed. New Jersey: Aeeizh, 2002.
[61] Jan Machowski, Janusz W. Bialek, and J. R. Bumby, *Power System Dynamics and Stability*. England: John Wiley & Sons, 1997.
[62] T. Wildi, *Electrical Machines, Drives and Power Systems*, 5th ed. New Jersey: Prentice Hall, 2002.
[63] R. G. H. B. Adkins, *The general theory of alternating current machines: Application to practical problems* USA: Chapman and Hall, 1975.
[64] MATLAB. (R2015b). *Three Phase Programmable Voltage Source* Available: http://www.mathworks.com/help/physmod/sps/powersys/ref/threephaseprogrammablevoltagesource.html?requestedDomain=www.mathworks.com
[65] J. C. Smith, D. Osborn, R. Piwko, R. Zavadil, B. Parsons, L. Coles*, et al.*, "Transmission Planning for Wind Energy in the USA: Status and Prospects," in *Wind Power in Power Systems*, ed: John Wiley & Sons, Ltd, 2012, pp. 413-437.
[66] T. Ackermann, A. Orths, and K. Rudion, "Transmission Systems for Offshore Wind Power Plants and Operation Planning Strategies for Offshore Power Systems," in *Wind Power in Power Systems*, ed: John Wiley & Sons, Ltd, 2012, pp. 293-327.
[67] MATLAB. (R2015b). *Parallel RLC Load*. Available: https://www.mathworks.com/help/physmod/sps/powersys/ref/parallelrlcload.html
[68] A. S. Langsdorf, *Theory of alternating-current machinery*. USA: McGraw-Hill, 1955.
[69] S. Heier, *Grid integration of wind energy conversion systems*. USA: John Wiley & Sons Ltd., 1998.
[70] J. G. Slootweg and T. Ackermann, "Wind Power and the Smart Grid," in *Wind Power in Power Systems*, ed: John Wiley & Sons, Ltd, 2012, pp. 951-973.
[71] H. Knudsen and J. N. Nielsen, "Introduction to the Modelling of Wind Turbines," in *Wind Power in Power Systems*, ed: John Wiley & Sons, Ltd, 2012, pp. 767-797.
[72] V. Akhmatov and B. Andresen, "Modelling of Large Wind Power Plants," in *Wind Power in Power Systems*, ed: John Wiley & Sons, Ltd, 2012, pp. 913-933.
[73] C. A. Gross, "Three-Phase Electric Power Systems," in *Power Electronics and Motor Drives*, B. M. Wilamowski and D. J. Irwin, Eds., ed USA: Taylor and Francis, 2011.
[74] S. Kouro, J. I. León, L. G. Franquelo, J. Rodríguez, and B. Wu, in *Power Electronics and Motor Drives*, B. M. Wilamowski and D. J. Irwin, Eds., ed USA: Taylor and Francis, 2011.
[75] J. Sun, F. Vasca, and L. Iannelli, *Pulse-Width Modulation*. UK: Springer-Verlag, 2012.
[76] ON, "Thyristor Theory and Design Considerations," SCILLC, USA 2005.
[77] T. Davies, *Protection of Industrial Power Systems*. USA: Elsevier, 2006.
[78] R. J. Best, D. J. Morrow, and P. A. Crossley, "Current transients in the small salient-pole alternator during sudden short-circuit and synchronisation events," *IET Electric Power Applications,* vol. 4, pp. 687-700, 2010.
[79] A. Mathur, V. Pant, and B. Das, "Unsymmetrical short-circuit analysis for distribution system considering loads," *International Journal of Electrical Power & Energy Systems,* vol. 70, pp. 27-38, 2015.
[80] A. Bracale, P. Caramia, A. R. Di Fazio, and D. Proto, "Probabilistic short circuit analysis in electric power distribution systems including distributed generation," in *8th Mediterranean Conference on Power Generation, Transmission, Distribution and Energy Conversion (MEDPOWER 2012)*, 2012, pp. 1-6.
[81] T. Jen-Hao, "Unsymmetrical Short-Circuit Fault Analysis for Weakly Meshed Distribution Systems," *IEEE Transactions on Power Systems,* vol. 25, pp. 96-105, 2010.
[82] H. Jinwei, L. Yun Wei, W. Ruiqi, and Z. Chenghui, "Analysis and Mitigation of Resonance Propagation in Grid-Connected and Islanding Microgrids," *Energy Conversion, IEEE Transactions on,* vol. 30, pp. 70-81, 2015.

[83] W. Lidi, W. Guangyu, and H. Weizhe, "Short-Circuit Test Simulation System of Transformer with Shunt Capacitor under Different Frequency Source," *AASRI Procedia,* vol. 3, pp. 646-651, 2012.
[84] J. Ouyang and X. Xiong, "Dynamic behavior of the excitation circuit of a doubly-fed induction generator under a symmetrical voltage drop," *Renewable Energy,* vol. 71, pp. 629-638, 11// 2014.
[85] E. Sorrentino and J. C. Burgos, "Application of 2D linear modeling for computing zero-sequence short-circuit impedances of 3-phase core-type YNynd transformers," *Electric Power Systems Research,* vol. 122, pp. 1-9, 5// 2015.
[86] A. Tomioka, T. Otonari, T. Ogata, M. Iwakuma, H. Okamoto, H. Hayashi*, et al.*, "The short-circuit test results of 6.9 kV/2.3 kV 400 kVA-class YBCO model transformer," *Physica C: Superconductivity,* vol. 471, pp. 1374-1378, 11// 2011.
[87] P. M. A. a. A. A. Fouad, *Power System Control and Stability*. USA: Wiley-IEEE Press, 2002.
[88] M. Moghbel, H. T. Mokui, M. A. S. Masoum, and M. Mohseni, "Reactive power control of DFIG wind power system connected to IEEE 14 bus distribution network," in *Universities Power Engineering Conference (AUPEC), 2012 22nd Australasian*, 2012, pp. 1-7.
[89] A. Mehdi, A. Reama, H. E. Medouce, S. E. Rezgui, and H. Benalla, "Direct active and reactive power control of DFIG based wind energy conversion system," in *2014 International Symposium on Power Electronics, Electrical Drives, Automation and Motion (SPEEDAM)*, 2014, pp. 1128-1133.
[90] S. Pati and S. Samantray, "Decoupled control of active and reactive power in a DFIG based wind energy conversion system with conventional P-I controllers," in *2014 International Conference on Circuit, Power and Computing Technologies (ICCPCT)*, 2014, pp. 898-903.
[91] K. Vinothkumar and M. P. Selvan, "Enhanced fault ride-through scheme and coordinated reactive power control for DFIG," in *2010 IEEE International Conference on Sustainable Energy Technologies (ICSET)*, 2010, pp. 1-5.
[92] N. L. Soultanis and N. D. Hatziargyriou, "Control issues of inverters in the formation of LV microgrids," in *2007 IEEE Power Engineering Society General Meeting*, 2007, pp. 1-7.
[93] S. A. Gopalan, V. Sreeram, and H. H. C. Iu, "A review of coordination strategies and protection schemes for microgrids," *Renewable and Sustainable Energy Reviews,* vol. 32, pp. 222-228, 2014.
[94] E. Planas, A. Gil-de-Muro, J. Andreu, I. Kortabarria, and I. Martínez de Alegría, "General aspects, hierarchical controls and droop methods in microgrids: A review," *Renewable and Sustainable Energy Reviews,* vol. 17, pp. 147-159, 2013.
[95] R. Romo and O. Micheloud, "Power quality of actual grids with plug-in electric vehicles in presence of renewables and microgrids," *Renewable and Sustainable Energy Reviews,* vol. 46, pp. 189-200, 2015.
[96] M. Soshinskaya, W. H. J. Crijns-Graus, J. M. Guerrero, and J. C. Vasquez, "Microgrids: Experiences, barriers and success factors," *Renewable and Sustainable Energy Reviews,* vol. 40, pp. 659-672, 2014.
[97] L. M. Miranda, D. Varaj, x00E, B. d. Santos, R. E. Araujo, C. L. Moreira*, et al.*, "Power flow control with bidirectional dual active bridge battery charger in low-voltage microgrids," in *Power Electronics and Applications (EPE), 2013 15th European Conference on*, 2013, pp. 1-10.
[98] X. Dongliang, X. Zhao, Y. Lihui, J. Ostergaard, X. Yusheng, and W. Kit Po, "A Comprehensive LVRT Control Strategy for DFIG Wind Turbines With Enhanced Reactive Power Support," *IEEE Transactions on Power Systems,* vol. 28, pp. 3302-3310, 2013.
[99] J. Jeong-Ik, K. Young-Sin, and L. Dong-Choon, "Active and Reactive Power Control of DFIG for Wind Energy Conversion under Unbalanced Grid Voltage," in *IEEE 5th International Power Electronics and Motion Control Conference 2006, IPEMC 2006*, 2006, pp. 1-5.
[100] M. Kayikci and J. V. Milanovic, "Reactive Power Control Strategies for DFIG-Based Plants," *IEEE Transactions on Energy Conversion,* vol. 22, pp. 389-396, 2007.

[101] X. Dongliang, X. Zhao, Y. Lihui, J. Ostergaard, X. Yusheng, and W. Kit Po, "A Comprehensive LVRT Control Strategy for DFIG Wind Turbines With Enhanced Reactive Power Support," *Power Systems, IEEE Transactions on,* vol. 28, pp. 3302-3310, 2013.
[102] J. Jeong-Ik, K. Young-Sin, and L. Dong-Choon, "Active and Reactive Power Control of DFIG for Wind Energy Conversion under Unbalanced Grid Voltage," in *Power Electronics and Motion Control Conference, 2006. IPEMC 2006. CES/IEEE 5th International*, 2006, pp. 1-5.
[103] M. Kayikci and J. V. Milanovic, "Reactive Power Control Strategies for DFIG-Based Plants," *Energy Conversion, IEEE Transactions on,* vol. 22, pp. 389-396, 2007.
[104] L. A. Zadeh, "Fuzzy Sets*," *Department of Electrical Engineering and Electronics Research Laboratory*

1965.
[105] T. J. Ross, *Fuzzy Logic with Enginering Applications - 3rd edition*. UK: John Wiley, 2010.
[106] IEC, "INTERNATIONAL STANDARD," in *IEC standard voltages* vol. IEC 60038, ed, 2007.
[107] A. R. Haron, A. Mohamed, and H. Shareef, "A Review on Protection Schemes and Coordination Techniques in Microgrid System," *Journal of Applied Sciences,* vol. 12, pp. 101 - 112, 2012.
[108] B. Pal and B. Chaudhuri, *Robust Control in Power Systems*. USA: Springer, 2005.